QUANTITATIVE ASSESSMENT OF METHODS FOR BACTERIAL AND VIRAL PURIFICATION AND CONCENTRATION

A Thesis
Presented to
The Academic Faculty

by

Nina Sara Fraticelli-Guzmán

In Partial Fulfillment
Of the Requirements for the Degree
Master of Science in
Bioengineering

Georgia Institute of Technology
December 2021

QUANTITATIVE ASSESSMENT OF METHODS FOR BACTERIAL AND VIRAL PURIFICATION AND CONCENTRATION

Approved by:

Professor Craig Forest, Advisor
School of Mechanical Engineering
Georgia Institute of Technology

Professor David Hu
School of Mechanical Engineering
Georgia Institute of Technology

Dr. Michael Farrell
Georgia Tech Research Institute (GTRI)
Georgia Institute of Technology

Date Approved: December 1st, 2021

Dedication

I would like to dedicate this thesis to my amazing parents, Sarah and Osvaldo, for supporting me, guiding me, challenging me, and loving me in everything I do and through every moment of my life, every high and every low. Los amo mucho y no pudiese haber logrado esto sin ustedes. Dios me ha bendecido con los mejores padres. I also want to share this dedication with my family, closest friends, and Jordan. This degree will have my name but there's a piece of it that belongs to each one of you because without you, I would have not made it through.

Acknowledgements

There are so many people to thank for helping complete this project, and I would like to start by thanking Craig and the entire PBL lab for their support and guidance throughout these last two and a half years. Thank you, Craig, for sharing your knowledge and extending your support. To PBL, thank you for the laughs and conversations regarding research and everything in between. To Max, thank you for always being available to answer my questions regarding everything research related, from experimental design to data analysis, and for helping me set-up the automated system. Your insight, knowledge, and willingness to help were an integral part of making this work possible. Thank you as well to Corey and Colby for always being willing to share their senior graduate student knowledge and for helping me debug when my experiments weren't going right. To Mohamed, thank you for helping me plan, execute, and analyze many of the experiments of this last semester, your help was invaluable. To my committee members, Dr. Mike Farrell and Dr. David Hu, thank you for agreeing to be on my committee. Mike, thank you for always believing I could do it and for providing me materials when I needed them.

Outside of my fellow lab members in the Precision Biosystems Lab, I want to thank Dr. Phil Santangelo and his laboratory members, specifically Lorena and Jared, for providing me the resources, space, and assistance to execute my virus experiments. Your expertise and generosity left a great impact on me and made a chapter of this thesis possible. In addition, I want to extend a thank you to Andrew Shaw, Shweta Biliya, and Naima Djeddar from the different core facilities in GT, to Dr. Jie Xu and Stephanie Richter for their help in providing me with all the bacteria I needed, and to Dr. Teresa Snow for her statistical analysis help.

Additionally, I want to thank the support of Laura Paige as well as my friends here at GT through the Bioengineering program and the Fellowship of Christian Graduate Students. And finally, thank you to my friends at home, Jordan, and my wonderful parents, I love you all!

Table of Contents

Acknowledgements iv
List of Tables ix
List of Figures x
Summary xvii
Chapter 1 Introduction 1
1.1 Motivation 1
1.1.1 Use cases 1
1.1.2 Field Effect Transistor 4
1.1.3 Interferents 6
1.1.4 Filtration 9
1.1.5 Organisms studied 9
1.2 Thesis Goals 10
1.3 Overview of methods 10
1.3.1 Handling methods 10
1.3.1.1 Centrifugation 12
1.3.1.2 Immunomagnetic separation (IMS) 13
1.3.1.3 Filtration 14
1.3.1.3.1 Microfluidics 15
1.3.1.3.2 Microfiltration overview 16
1.4 Interferent surrogate 23
1.4.1 Quantification methods 24
1.4.1.1 Quantitative Polymerase Chain Reaction (qPCR) 24
1.4.1.2 Flow cytometry 27
1.4.1.3 Fluorescent microscopy 28
1.4.1.4 Luminescence assay 30
1.4.1.5 Alternate quantification methods 31
1.5 Nomenclature 33
Chapter 2 Bacteria purification and concentration 34
2.1 Bacterial methods 34
2.1.1 E. coli quantification 34
2.1.2 Bead quantification 36

2.1.3 Statistical analysis 37
2.2 Purification Results 37
2.2.1 Filter matrix 37
2.2.2 Individual beads experiment with filters separately 43
2.2.3 Interferents with dual filter filtration 45
2.2.4 Bacteria with interferents with dual filter filtration 50
2.3 Concentration Results 51
2.3.1 Bacteria experiment with 0.22 µm pore size filter 51
2.4 Automation 56
2.4.1 Dual filter filtration system design (DFFS) 56
2.4.2 System control 61
2.4.3 Individual interferents experiment 62
2.4.4 Bacteria control experiment (0.45 µm filter and 5 µm filter) 63
2.4.5 Bacteria control experiment (0.22 µm filter and 5 µm filter) 64
2.4.6 Bacteria with interferents (0.22 µm filter and 5 µm filter) 67
2.5 Discussion 69
2.6 Conclusion 82
Chapter 3 Virus purification and concentration 85
3.1 Viral methods 85
3.1.1 Influenza H1N1 quantification 85
3.1.2 Bead quantification 86
3.1.3 Statistical analysis 87
3.1.4 Virus calibration curve 87
3.2 Virus purification 89
3.3 Virus concentration 94
3.4 Integration of purification and concentration 98
3.5 Automation 104
3.5.1 Design 104
3.6 Discussion 108
3.7 Conclusion 116
Appendix A: Additional quantification methods 119
Appendix B: Flow cytometer vs Fluorescent microscope comparison 128

Appendix C: Viral experiments data.....130
References.....131

List of Tables

Table 1. Differently pore sized PVDF filters 13 mm and 25 mm in diameter tested for E. coli recovery..... 38

Table 2. Pre-purification and post-purification bead count used to assess the purification performance of 0.45 µm filter. The 2 µm and 10 µm were successfully removed (as observed in the 10 µL sample)..... 44

Table 3. Results from the three TFF device runs. The number of presses required to push the sample through the TFF device to collect a volume of less than 1 mL is recorded, along with the final concentrated volume. 97

Table 4. The tables show the results of the system using the 0.45 µm pore size filter or the 5 µm pore size filters. Highlighted are the final volumes the samples were concentrated to for each run and the subsequent volume concentration factor determined by the input volume as compared to the post-filtration volume. The concentration factor based on the luminescence reading is also shown. 130

List of Figures

Figure 1. Cross-section of a FET with a look into the molecular bioreceptor layer on the surface of the chip. 4

Figure 2. The diagram shows the atmospheric particulate matter types and distribution in micrometers. (Source: Particulates-Wikipedia) [38] 7

Figure 3. **S**ize comparisons of particulate matter particles (Source: EPA). [36] 7

Figure 4. Microcentrifuge with 1.5 mL tubes in place. Zoomed in we observe the separation that occurs post-centrifugation where the separation based on mass or density causes a pellet with the target pathogen to form allowing for the supernatant to be removed and the pellet to be suspended to a desired volume for a specific concentration. Created with BioRender.com 13

Figure 5. Immunomagnetic separation representation where the target pathogen attaches to the antibodies (the affinity biorecognition molecule) with the magnetic particle. The magnet then attracts the magnetic particles with the target pathogen attached. This step allows for the rest of the sample matrix to be removed and for the target to be resuspended into a desired volume. Thus, both the purification and concentration step can be completed. Created with BioRender.com. 14

Figure 6 Filtration example were membranes with different cut-off sizes remove particles of different sizes. Created with BioRender.com 15

Figure 7. Bead-end filtration configuration showing the flow moving perpendicular to the membrane. 18

Figure 8. Cross-flow filtration system with the flow running perpendicular to the membrane. 21

Figure 9. Amplification plot with a baseline-subtracted fluorescence. (Source - Bio-Rad [97]) 26

Figure 10. Flow cytometry overview with sheath fluid focusing the particle suspension for analysis. The light scattering and fluorescence detection is also shown. 28

Figure 11. Fluorescent microscope schematic showcasing the specimen specific wavelength (green line) reaching the plate to excite the sample. The specimen then emits two wavelengths of light (purple, red lines), the weaker one of which is sorted out, and the strongest (red) reaches the eye piece..... 29

Figure 12. An enzyme tagged organism comes in contact an added substrate. When combined, they produce a reaction that emits light for luminescence detection. 31

Figure 13. Mechanism for filtrate and retentate collection per filter. Step 1 consist of pushing the sample through the filter. In step 2, 4 mL of 1× PBS is pushed through the same filter and collected in the same filtrate tube. Then, in step 3, the filter direction is flipped in order for any retained particle on the membrane surface to be collected in the retentate. Created with BioRender.com 39

Figure 14. **A.** 5 µm pore size filter shows larger E. coli filtrate recovery at 40% with a smaller standard deviation as compared to the 33% results from the 10 µm pore size filter. **B.** The smaller pore sized filters show more optimal E. coli recovery in the retentate for both filter diameters with the 0.22 µm pore size filter resulting in higher recoveries, around 40%, for both filter diameters as compared to the 0.45 µm pore size filter recoveries. (n = 3 for all filters) 41

Figure 15. The 0.22 µm and 0.45 µm pore size filters appear to show no statistically significant difference in the retentate recovery as a function of filter diameter. The 0.22 µm pore size filter recoveries under both diameters is around 40% while for the 0.45 µm pore size filter, the recoveries range on average from 15-20%. 42

Figure 16. Of both 25 mm diameter filters, the 0.22 µm pore size filter has an average retentate recovery twice as great as that of the 0.45 µm pore size filter..... 42

Figure 17. A 5 µm por sized PVDF syringe filter recovers 40% of the 2 µm beads in the filtrate while a little over 20% are recovered in the retentate. These two recoveries were determined to be statistically significantly different ($p = 0.014$) using an unpaired t-test. 45

Figure 18. Representation of the individual beads, each at 10^6 beads/mL, mixed to form the interferents sample tested with a concentration of 3.3×10^5 beads/mL. Not shown, the 0.40 µm beads. Created with BioRender.com. 46

Figure 19. Double filter filtration system (DFFS). Outlined are the 4 steps involved in the purification and concentration of a sample using a 5 µm and a 0.45 µm pore size filter. Steps and schematic adapted from Isabel et. al. [85]. Created with BioRender.com 47

Figure 20. 23% of the 2 µm beads were recovered from a mix of interferent undergoing purification with a 5 µm pore size filter and recovery with a 0.45 µm pore size filter. (n = 2) 48

Figure 21. Image A showcases the interferents sample with the 2 µm and 10 µm beads mixed together each at a final concentration of 3.3×10^5 beads/mL for each bead size. Image B showcases the sample pos-filtration, where the 10 µm beads were removed an on average 23% of the 2 µm beads were recovered. Pseudo color magenta viosualization. (Fluorescent microscope-Zeiss AxioObserver Z1) 49

Figure 22. From left to right, the E. coli (at distinct starting concentration) average recovery from samples containing interferents: 25%, 33%, and 32%. Both axes are plotted in Log10. The gray line represents 100% recovery. 51

Figure 23. Five distinct volumes were used for retentate recovery of E. coli from the surface of a 25 mm diameter, 0.22 µm pore sized PVDF syringe filter. Triplicate runs for each volume were performed and technical triplicates for each run were analyzed and plotted. Comparing the E. coli DNA concentration as a function of the retentate recovery volume, there was a statistically significant difference between the following groups: 300 µL vs. 600 µL ($p = 0.023$), 300 µL vs. 900 µL ($p < 0.0001$), and 300 µL vs. 1.2 mL ($p = 0.0002$). The dotted black line represents the baseline or input bacteria concentration prior to the experiment. 54

Figure 24. E. coli recovery was above 80%, and at times over 100%, when 900 µL or more were used for a backflow step for retentate recovery. 55

Figure 25. The concentration factor for each retentate volume follows the same trend as the concentration data, as expected. Concentration factors between 4-6× can be achieved. 55

Figure 26. Double filter filtration system automation schematic. 57

Figure 27. Experimental set-up for the DFFS automation. 58

Figure 28. **A.** Position 1 of the schematic where the sample is pushed through the 5 µm filter for purification, followed by 1× PBS, and then through the 0.22 µm pore size filter where the target is captured on the surface while the rest of the volume goes to waste. The step takes 4.7 minutes. **B.** Position 2 of the system in which pump 3 pushes 1× PBS to execute a backflow step and reverse the flow direction through the 0.22 µm pore size filter for the recovery of the particles captured on the filter surface, i.e., retentate recovery. The step takes 50 seconds. 60

Figure 29. LabView program interphase for pump and valve control. 61

Figure 30. Around 5% of the 2 µm beads are recovered when tested individually while the samples containing only 10 µm sized beads show that essentially all the larger sized beads were removed. 63

Figure 31. From left to right, the E. coli (at distinct starting concentration) average recovery from samples containing interferents: 19%, 27%, and 29%. Both axes are plotted in Log10. The gray line represents 100% recovery, and each point is an average of two data points corresponding to the duplicate runs. 64

Figure 32. An average of approximate 4× concentration increase is achieved for the bacteria control experiment with the automated double filtration system. 66

Figure 33. **A.** The pre-automation and post-automation E. coli DNA concentration values were statistically different from each other ($p < 0.0001$). **B.** The data is represented in the form of retentate recovery were over 60% of the bacteria was recovered with the automation run. 66

Figure 34. **A.** The pre-automation and post-automation DNA concentration values were statistically different from each other ($p = 0.021$). **B.** A 2× concentration increase is achieved for the bacteria in the presence of interferents with the automated double filtration system. 68

Figure 35. **A.** The data is represented in the form of retentate recovery. On average, 40% of the bacteria was recovered with the automation run. **B.** Over 95% of interferents are removed from the sample using the automated double filtration system, per the 150 µL (16%) of the post-automation volume analyzed. 69

Figure 36. Analysis of luminescence signal (Log 10 scale) from the Influenza PA-NLuc virus stock in different concentrations (10-fold) with a negative control consisting of the viral media. Each concentration and sample were performed in triplicates. 87

Figure 37. Analysis of Luminescence signal (Linear scale) from the WNS/33 PA-NLuc virus stock in different concentrations (2-fold). Each concentration and sample were performed in duplicates..... 88

Figure 38. **A.** When mixed with interferents, the virus can pass through the filter without significant loss. Luminescence results of samples post-purification as compared to the pre-filtration, untreated sample. Technical triplicates for each of the three runs per filter are plotted. 900 µL tested samples consisted of 10^6 beads/mL for each bead (2 µm, 10 µm) and ~2×10^6 pfu/mL of virus in DMEM. **B.** Summary of recovery shown as recovery percentage, showing approximately all the viruses pass through the filter for syringe filters. There is a statistical difference between the two recovery groups ($p = 0.046$). 90

Figure 39. The graphs showcase the results of the fluorescent polystyrene bead recovery for both pore sized filters. Removal of both sized beads as beads were quantified with a flow cytometer (Cytek-Aurora) with 200 µL of each sample (~60% of the post-purification volume). **A.** Both sized beads removed. **B.** 10 µm bead removed and 40% of 2 µm bead recovered..... 92

Figure 40. Bead images captured using a fluorescent microscope (Zeiss AxioObserver Z1) for the prefiltration sample (**A**) and the post-5 µm filter filtration (**B**). The 2 µm beads are labeled red by the software for recognition, and the 10 µm beads are labeled in green. Not shown: image taken when using the 0.45 µm pore size filter – no beads observed. 93

Figure 41. Fluorescent polystyrene beads captured on filter membrane. 94

Figure 42. The TFF device in its varying positions. Position A shows the sample being loaded into the device. Position B and C showcase the sample being moved between syringes 1 and 2 with the waste being collected through the bottom nozzle. (TFF source-HansaBioMed Life Sciences; Icons source – BioRender.com)..... 95

Figure 43. **A.** Luminescence readings of the pre- and post-TFF samples for all three tests and their triplicates, along with a negative control (media). Paired t-tests yielded statistically significant differences between the pre- and post-TFF luminescence readings for all three runs: Run1 ($p = 0.0002$), Run2 ($p = 0.002$), and Run 3 ($p = 0.0003$). All

technical triplicates per test were plotted. **B.** Concentration factor of all three runs conducted in this experiment was a around 1.6×. 98

Figure 44. The addition of a syringe filter to the loading nozzle. 99

Figure 45. **A.** Statistically significant higher luminescence readings are achieved when comparing the pre-filtered sample readings with that of the integrated system with the 0.45 µm pore size filter ($p < 0.0001$) or the 5µm pore size filter ($p < 0.0001$). Between integrated system values, there was also a statistical difference ($p = 0.0005$). All technical triplicates for the three runs per filter pore size were plotted. **B.** Even with beads included as interferents (in concentration approximately equivalent to the analyte), we retain our ability to concentrate the target virus by ~1.6x with both pore size filters. ... 100

Figure 46. Post-filtration luminescence assay results as a function of varying air volumes applied in last step of the integrated system. **A.** The varying final air volumes showed no statistical difference in the luminescence readings for the use of the integrated system with the 0.45 µm filter. **B.** The varying air volumes produced statically different luminescence readings between the 5 mL and 15 mL ($p < 0.0001$), 5 mL and 25 mL ($p = 0.001$), and 15 mL and 25 mL ($p = 0.004$) volumes. All technical triplicates for each volume of air are plotted. 102

Figure 47. Recovery of beads post-filtration with the use of the 0.45 µm pore size filter (**A**) and the 5 µm pore size filter (**B**). 103

Figure 48. Recovery of the virus post-filtration under two pore-size filter conditions. Both yielded an average recovery of 30-40% with no statistically significant difference between the recovery obtained when using the two distinct pore size filters in the integrated system. 103

Figure 49. The automated TFF device schematic consisting of a peristaltic pump, valves, and the TFF device..... 106

Figure 50. Positions A-C showcase the sample being loaded, the sample being recirculated for concentration, and the final concentrated sample being collected, respectively. 107

Figure 51. Recombinant human SARS-CoV-2 Spike protein standard curve. If concentration was plated in triplicates. 120

Figure 52. Inactivated SARS-CoV-2 standard curve at varying concentrations. Each sample was plated in triplicates. 120

Figure 53. Inactivated SARS-CoV-2 calibration curve. Only concentrations from 10^7 to 10^8 pfu/mL yielded a detectable response on the SPR machine. The experimental samples' concentrations were below the limit of detection. 122

Figure 54. Calibration curve developed for the BPL inactivated SARS-CoV-2 virus. The point for the $5x105pfu/mL$ concentration and the $1x106pfu/mL$ concentration was an average of 2 and 3 data points, respectively with standard deviations of 0.68 and 3.65, respectively as well. All other points consist of one point, ad this is because there was a limitation in sample volume and accuracy of the sensor for those specific samples..... 123

Figure 55. A standard curve was generated for HRP by performing two-fold dilutions from the stock solution. The absorbance baseline is the value for the well under no reaction. Absorbance readings obtained using a plate reader. 126

Figure 56. Per bead size, flow cytometer and fluorescent microscope concentration calculations for triplicate runs are shown, i.e., each run was analyzed for bead concentration using both methods. The dotted line represents the starting concentration beads had been approximately diluted to. Data comes from the viral purification experiments (section 3.2). Log10 y-axis. 128

Summary

The COVID-19 global pandemic has led to the exploration and implementation of rapid tests for viral load identification and thus, control of the spread. For this, there are varying approaches with the gold standard being quantitative Polymerase Chain Reaction [1]and a potential more rapid alternate approach being the use of an antibody coated biosensor such as a field effect transistor (FET). Analogously, bacterial pathogens such as anthrax need sensing and quantification as well. Therefore, methods for pathogen collection and detection for both viruses and bacteria are needed.

Regardless of the analysis technique, it is ideal for samples to contain little to zero non-target particles or contaminants that might interfere with the detection approach. As such, traditional ways of purifying and concentrating samples prior to any type of analysis involve both chemical, physical, physiochemical, or biological approaches such as filtration, centrifugation, affinity chromatography, immunomagnetic separation, etc. Of these, we will focus on the physical approach, filtration, due to its simplicity, low cost, varying options, and ability to process large and small sample volumes. In this work, we investigate how well the method works for virus or bacteria in the presence of high interferent concentrations that could potentially be present in saliva samples or other hydrosol samples taken from an environment to be tested. The research presented here characterizes the applicability of syringe filters and a tangential flow filtration device for the purification and concentration of bacteria and virus samples, respectively. Furthermore, automation of such systems was explored.

Varying syringe filter pore sizes yielded different recoveries of bacteria for purifying and concentrating the sample. Furthermore, varying volumes were analyzed for

optimal recovery and concentration of the target. We also developed a fully automated method for double filter filtration to enable hands-free purification and concentration in 5.5 minutes for 5 mL of input volume with a 42 ± 13-fold enrichment improvement (n = 3). Furthermore, the purification and concentration of virus using a manually operated tangential flow filtration device was also explored and yielded modest concentration increases of around 2× with an enrichment improvement of up to 1,916 ± 1,839-fold (n = 3) under one configuration. By characterizing and automating these readily available items, we can enhance the detection of samples by decreasing labor time and processing complexity required for the purification and concentration of the target pathogens.

Chapter 1 Introduction

1.1 Motivation

1.1.1 Use cases

The current COVID-19 global pandemic has resulted in the disruption of our daily lives and caused the death of over 4.5 million people worldwide [2]. In order to limit viral transmission, protect individuals, and thus, help control the pandemic, rapid work was done to explore and implement viral tests [3]–[5].

At Georgia Tech, researchers developed a surveillance testing program to reduce the transmission of COVID-19 among the community. The test involves the analysis of a saliva sample, instead of the usual nasal or throat swab used for diagnostics tests [6]. The program then relies on a pooling approach whereby multiple individual samples are combined and tested as a group [7]. Like swab samples, the saliva samples are analyzed using the gold standard, nucleic acid amplification technique, Quantitative Polymerase Chain Reaction (PCR). PCR analysis helps detect the genetic material of the virus [1] and determine if there were high viral loads present in the samples. Though very sensitive, these tests have a turnaround time of anywhere from 24 hours to a few days [1], [8]. There are also antigen tests available that look for molecules on the surface of the virus but are less sensitive [8]. For both types of tests, interferents in the sample could lead to a specimen being rejected and the reading being inconclusive or leading to a false negative [7], [8].

Just as saliva samples could contain particles of interest to analyze and thereby be diagnosed, hydrosolized particles are another potential sample that could be analyzed for pathogen detection. It is well known that viruses and bacteria can be spread in the air

through coughing and speaking. These particles are traditionally described as either droplets, suspended particles above 5 μm in diameter, or aerosols which are below 5 μm in diameter. However, regardless of the size, simulation has shown that the particles can remain airborne for an extended period. [9] There has been great interest in exploring the capturing of aerosols for detection of SARS-CoV-2 [10], [11], as well as other viruses [12] and bacteria [13]. These samples are acquired as aerosols and turned into hydrosols through various means such as a wetted wall cyclone [14].

The Department of Homeland Security has sought to Develop instrumentation for detecting pathogens in aerosols through the development of its BioWatch Program, which looks to detect biological weapons through the analysis of a filter that captures air for a determined period of time [15]. However, this method becomes labor intensive and time-consuming due to the transport of the sample for analysis. Other stand-alone instruments, such as the Autonomous Pathogen Detection System (APDS), have also been developed to address the issues of time and labor-intensive analysis. With APDS, the capture, concentration, and detection of the particles using multiplexed PCR are all done within one system. [16] The system can perform sample analysis every hour over a span of 7 days, uninterrupted [17]. Yet, the equipment is bulky and requires regular maintenance to replenish reagents for the PCR analysis. Another approach taken by industry involves portable bioaerosol detectors [18] that are also bulky, heavy, and undeployable. However, because many of these approaches rely on labor intensive, time-consuming, and slower detection methods such as PCR, there is a delay from the time of the event to the time of the detection, which does not allow for rapid identification of possible infected individuals, and therefore, causes a delay in treatment. Thus, there has been an ongoing call for a next-

generation biosensor that lowers the system cost and has an integrated sampling and detection system. [15]

Common bacterial detection methods include nucleic acid-based sensing, cell culture immunoassays and biosensors. Some of these methods have drawbacks in terms of required time to obtain results. For example, qPCR can take anywhere from 6-48 hours while cell culture can take days. [19] One of the more promising biosensors under development is a field effect transistor (FET). FETs can be designed to contain antibodies on their surface for specific targets which could decrease labor time, increase the response time, decrease the cost of reagents, and can be mass produced using CMOS.

FETs could be integrated with a collection and filtration system which opens the door for the design of a deployable system that is of the proper size, weight, and power characteristics. This system would permit real time detection in a quick and effective manner without requiring the need for individuals to risk their lives for sample capturing and analysis, all the while saving time. Unfortunately, FETs are less sensitive than gold standard techniques like qPCR and interferents could significantly hamper the reliability of readings.

As a driving motivation for this thesis, there is a need for compact, automated methods for purification and concentration of target analytes (viral or bacterial), due to the non-specific and non-sensitive detection methods of FETs. This research seeks to address this need by concentrating by 1-2 orders of magnitude and enriching by 42-fold. Thus, we have a chance to use FETs in a way that replies PCR, thus avoiding the time, reagent, and labor cost associated with the procedure.

1.1.2 Field Effect Transistor

Field effect transistors (FET) are a promising detection technology that could be used for the detection of organisms for medical diagnostics, environmental monitoring, and bioresearch [20]. FETs typically have a self-assembled monolayer (SAM) coated in a specific substrate such as gold [21] or graphene [22], [23] and are functionalized with immobilized molecular receptors such as extracellular matrix protein [21] or antibodies [22], [23]. The surface of the FET is connected with a source and drain to generated electric current along the thin layer [24]. FETs control current flow via the application of voltage to the gate which can alter the conductivity between the drain and source [25]. When binding of a target to the surface occurs, a change in threshold voltage [21] or conductance [12], [23] can be recorded and analyzed to determine if the target was present in the sample. Figure 1 below is a general schematic of the cross-section of the FET showcasing the layers in the device as well as the molecular bioreceptor with the flowing target analytes becoming attached to them.

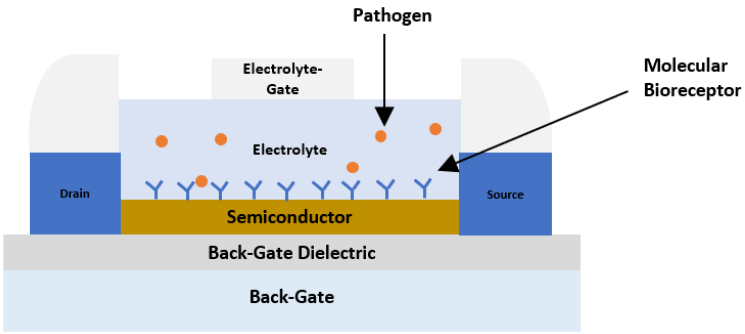

Figure 1. Cross-section of a FET with a look into the molecular bioreceptor layer on the surface of the chip.

Distinct types of FETs have been studied for the detection of different organisms such as the bacteria *Staphylococcus epidermis*. In that study, researchers used an extended-gate-field effect transistor with a SAM coated gold substrate and immobilized extracellular

matrix protein to detect *S. epidermis* at concentrations ranging from 3.8×10^6 to 3.8×10^8 CFU/mL, with a limit of detection (LOD) of 9×10^5 CFU/mL achieved. [21] Other bacterial detection work using a metal-oxide-semiconductor field-effect transistor (MOSFET) had a limit of quantitation of 1.9×10^5 CFU/mL. [26] Graphene based field-effect transistors have been used for *Escherichia coli* (*E. coli*) detection as well. These gFETs contained *E. coli* specific antibodies fixed on gold nanoparticles that helped selectively capture the bacteria [22], [23]. One device had good selectivity and rapid detection for concentrations of bacteria ranging from 10^3 to 10^5 CFU/mL [22] and the other was able to reach detect a lower bacterial concentration of 10 CFU/mL [23]. Graphene FETs have also been used for viral detection with one work detecting BHV-1, the major viral pathogen of Bovine Respiratory Disease (BRD) which is often found in cattle, using a target specific protein coated on the sensor. [27] In addition, work has been done using silicon nanowire FET for the detection of influenza, allowing for the detection of viruses at a concentration of 10^7 to 10^9 viruses/mL [12].

Though, as noted above, there appears to be a variation in the limit of detection for FETs, this could be due to differences in FET design (materials, geometry, surface chemistry). Overall, field effect transistors are easily fabricable [21], simple, rapid, and a suitable real-time, low-cost solution for detection [22], [23], [26]. Furthermore, they can be applied for pathogen detection in the areas of infection [21], [26], food [23], [27], water [22], [23], and aerosol pathogen detection [12], [23] making FETs attractive for further research and integration with other systems for capturing and real-time detection of samples [12], [27].

However, it has been noted by studies that a filtration step prior to the sample reaching the sensor would be beneficial [12], [22], [28], given we know that just as in saliva samples, interferents such as environmental pollutants found in air samples [12], [16] could be present in the collected sample which could interfere with the selectivity of the FET and therefore, its accurate sensing ability.

1.1.3 Interferents

In saliva, we expect to find a mix of water with electrolytes, mucus, proteins, squamous epithelial cells and leukocytes (white blood cells) as well as enzymes, immunoglobins, and lysozymes [29]–[32]. The components can vary in size with the larger components consisting of varying types of white blood cells ranging from 6 to 17 μm in diameter [33] and buccal epithelial cells with sizes as large as 60 μm [34]. Furthermore, if the test is taken throughout the day, food debris could be present in the saliva sample [4], [32]. Though it is asked of participants to not consume food within 30 minutes before sample collection [31], larger particles such as these [35] could still appear in the sample and would need to be removed to avoid a false negative or inclusive result from the test.

For pathogens found in aerosol samples, samples that later get turned to hydrosols, there are other particles of varying sizes that might be found along with them. Particulate matter or particle pollution are classified in two ways, PM_{10}, which includes inhalable particle with diameters 10 μm or smaller, and PM2.5, which includes fine inhalable particles with diameters 2.5 μm or smaller. Figure 3 illustrates how these diameters compare to a single human hair with is around 70 μm in diameter, around 30 times larger than the fine particles. [36]

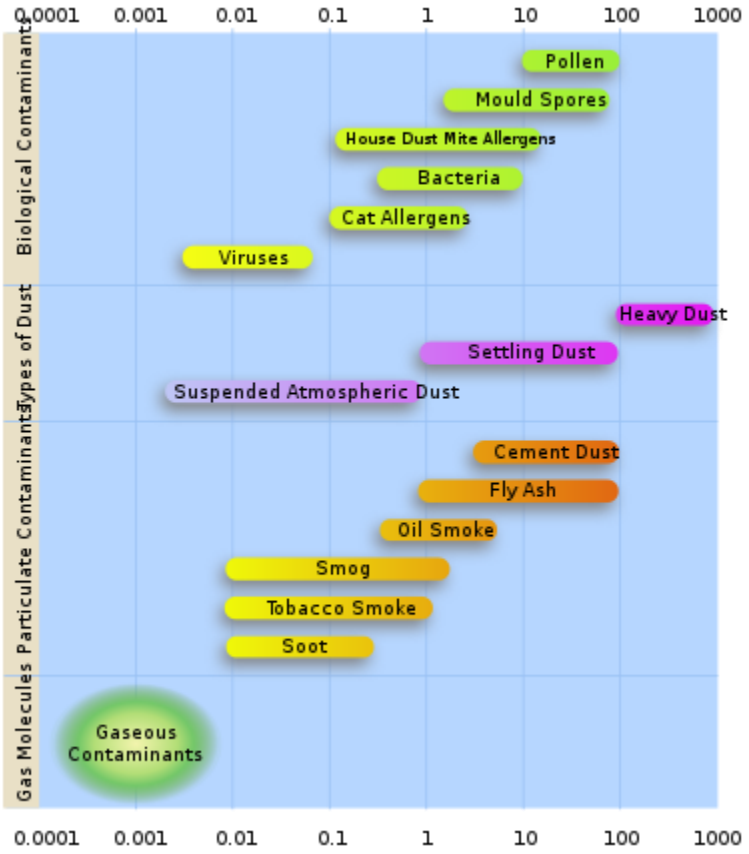

Figure 2. The diagram shows the atmospheric particulate matter types and distribution in micrometers. (Source: Jisaac9) [38]

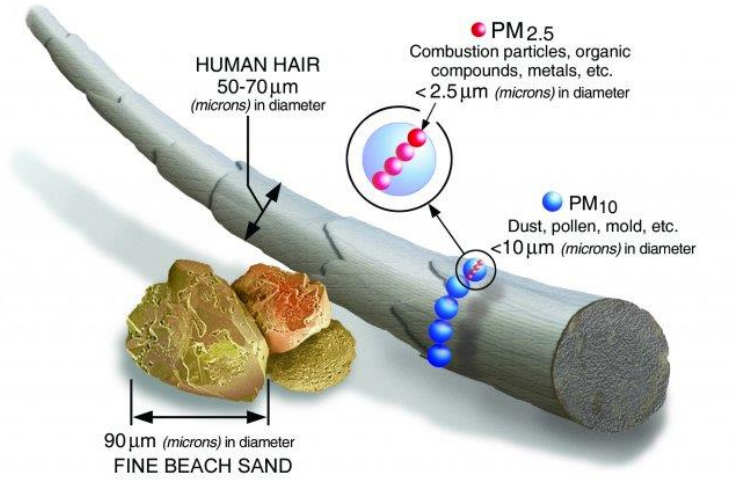

Figure 3. **S**ize comparisons of particulate matter particles (Source: EPA). [36]

Furthermore, Figure 2 shows particles that can be found in the air include dust, dirt, smoke, pollen, all often visible to the naked eye, as well as soot, allergens, pet dander, and spores [36], [37]. The particles can be emitted from unpaved roads, construction sites, fields, or fires, among many others [36].

Past studies have characterized the aerosol particle size distributions in urban atmospheres in Germany, for example [39] or in a coalmining area [40]. The work in Germany looked at particles in sizes ranging from 0.003 μm to 10 μm and they found the concentration of the particles varied by season as well. Another study conducted in both indoor and outdoor areas in China found that the distribution of particle size is different between indoor and outdoor areas, with indoor areas containing higher concentration of fine particles than outdoor levels. Furthermore, they also noticed variability in particle concentration indoor throughout the day, which suggests that human activity plays a significant role in indoor pollutions. [39]

As observed from the cited studies, the aerosol distribution in your area, in terms of size and shape, varies depending on where you are in the world and the environment's conditions, such as the time of year. For a more in-depth review into how aerosol particles are measured, analyzed, and modeled, refer to *Atmospheric Chemistry and Physics: From Air Pollution to Climate Change* by J.H. Seinfield and S.N. Pandis (2016) [41]. However, whether in urban or rural areas, significant concentrations of particles, with diameters ranging from nanometers to around 10 μm, as high as 10^6-10^7 per mL can sometimes be found [41]. In a scenario such as in a war zone or a highly urbanized area, we could expect to find concentrations as high as these which would need to be removed to ensure a higher success rate for our detection mechanism of our target pathogens.

1.1.4 Filtration

The above discussion on contaminants present in hydrosols (from aerosol) and saliva samples clearly highlights a need for a filtration step prior to the sensor. This filtration step should both purify and concentrate a sample to help enhance pathogen detection in a timely manner [19], [42], [43]. The method of filtration should consist of a design that's easy to modify and build from readily available parts, and that can be easily automatable. Furthermore, the system must be able to take in large volumes of a sample (mL) and output smaller volumes (µL) for the FET sensors [42] or any other adequate sample size reduction [19], [43]. These parameters will serve as basis for a system that can adapt to sample types quickly with both design, implementation, material purchase, and manufacturing time.

1.1.5 Organisms studied

Both bacteria and virus filtration were explored. For bacteria, certain types can be used as a biological weapon such as, for example, *Bacillus anthracis. B. anthracis* is a rod-shaped bacterium [44], around 1 µm in diameter [45], that causes Anthrax and is classified as a Category A (Highest priority) biological weapon by the CDC [46]. In this work, we chose to model bacterial pathogens with *Escherichia coli (E. coli)* (ATCC 25922) which is also a rod-shaped bacterium with an approximate 1 µm diameter [47]. *E. coli* is a bacterium that can be found in various places such as the environment, food, water, and intestines of people and animals [48] and has been used in many studies as an airborne pathogen [13] or as a the pathogen for water-borne and food-borne illnesses [49]. As for viruses, they can also be used as biological weapons [44] or can be infectious such as SARS-CoV-2. We chose to model viruses using H1N1 influenza strain A/WSN/33 which produces virions of around 80-120 nm in diameter [50]. For bacteria quantitation,

quantitative PCR was used, and for viral quantitation, the Nano-Glo Luciferase Assay (Promega) that targeted the enzyme (PA-NLuc) tagged virus.

1.2 Thesis Goals

From water purification to biological weapon detection, the samples we analyze include much more than our target sample. To accurately detect our targets of choice, the use of various labor intensive, and at times costly techniques, have been used. In this paper, we evaluate quick and easily implementable techniques for viral and bacterial purification and concentration. These methods are more cost effective and amenable toward automation, allowing for a decrease in not just cost, but also labor time.

In the past, techniques have been explored for filtration of samples, specifically the use of syringe filters and tangential flow filtration devices. However, no robust characterization of these filters for pathogen purification and concentration under a high interferents matrix, made using beads, has been tested, to the best of my knowledge. In this work, we explore a physical based filtration approach that meets the following criteria: modular design, use of readily available items, and automatability. The following chapters outline the chosen methods and the efficiency of each approach by characterizing its recovery and concentration factor increase. Furthermore, we explore the automation of such systems to allow for a less labor intensive, faster, and integrable filtration system that could be combined with a filed-effect transistor for quick, real-time downstream detection.

1.3 Overview of methods

1.3.1 Handling methods

To enhance a liquid sample prior to detection, both purification and concentration of the target pathogen (alternately referred to as a particle) is important, as previously

mentioned [43]. Before proceeding to discuss common techniques for both, it is important to accurately define what each term refers to. **Purification** in the sciences is defined as the removal of interferents from a sample [51]–[54]. It defers from the term 'separation' in that the latter is the splitting of a mixture of substances into two or more products or a mixture of products. Thus, purification is a type of separation process that separates and isolates a desired target from a mixture by removing the contaminants or interferents present in the sample. [51]

Concentration refers to the number of a target divided by the total volume of a mixture [55]. To increase concentration, the total volume of a mixture is decreased while the number of the target pathogen remains constant [42] or the number of the target increases while the volume remains constant.

Purification and concentration of bacteria and viruses are done based on chemical, physical, physiochemical, or biological approaches, with some of the technique applying a combination of these principles. Techniques include affinity purification, filtration, centrifugation, evaporation, extraction, chromatography, crystallization, refining, immunomagnetic separation (IMS), among others. [43], [56]–[59] For the purposes of this study, we are mainly focusing on the discussion of the most practical techniques, those based on physical properties since they allow for more accessible and modular methods of purification.

The techniques we will discuss below can serve as both the purification and/or concentration step for the bacteria or virus treatment prior to detection.

1.3.1.1 Centrifugation

A common technique used for both viruses [58], [60] and bacteria [56] is centrifugation. In this technique based on mass or density, the sample is placed in a centrifuge and spun at a high angular velocity. This action causes the constituents of the sample varying in density or mass to separate. The centrifugal force experienced by the sample pulls the sample components apart with the particles experiencing the greatest centrifugal force having the fastest sedimentation rate and thereby reaching the bottom of the tube first. However, for particles with the same density, the separation is based on mass, and the heavier particles experience the greater sedimentation rate; for constituents of equal mass, it is then the one with the larger density that experiences the greatest sedimentation rate. There are two main centrifugation techniques for separating particles, with one of them being density gradient centrifugation where varying sucrose density concentrations are prepared and alternately layered in a centrifuge tube. The sample is then loaded to the top of the tube and placed in a centrifuge. During the process, components of the sample will move through the gradient and settle at a density level that matches the sucrose's. [43], [56]–[58] For biological research, there exist different types of centrifuges that differ based on the volume of the sample and the speed of the centrifuge [61]. However, as an example, centrifugation systems can pellet bacteria from 100-200 mL samples over 5-10 minutes [42].

Though effective, the process is time consuming, laborious, and relies on large and heavy benchtop equipment that's difficult to integrate and move [42], [60].

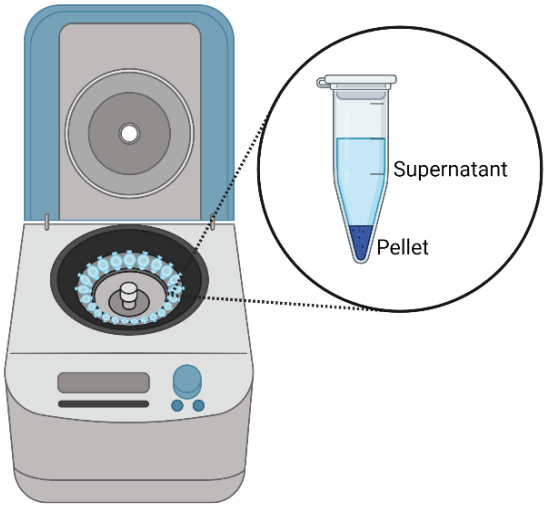

Figure 4. Microcentrifuge with 1.5 mL tubes in place. Zoomed in we observe the separation that occurs post-centrifugation where the separation based on mass or density causes a pellet with the target pathogen to form allowing for the supernatant to be removed and the pellet to be suspended to a desired volume for a specific concentration. Created with BioRender.com

1.3.1.2 Immunomagnetic separation (IMS)

Immunomagnetic separation (IMS) was first developed in the 1980s and consist of a magnetic particle with a specific affinity biorecognition molecule that selectively recognizes a target particle. [42], [43], [56] A short incubation time allows the target to be recognized and to attach to the magnetic particle. This attachment allows the sample to be manipulated using a simple magnet. This biological method is widely used to separate targets from other organisms or to purify targets from interferents in a sample, and has been used for both bacteria [43], [62] and viruses [43], [63]. Though a straightforward concept and efficient, it is limited to small volumes. Furthermore, it still yields low concentration efficiencies. [42]

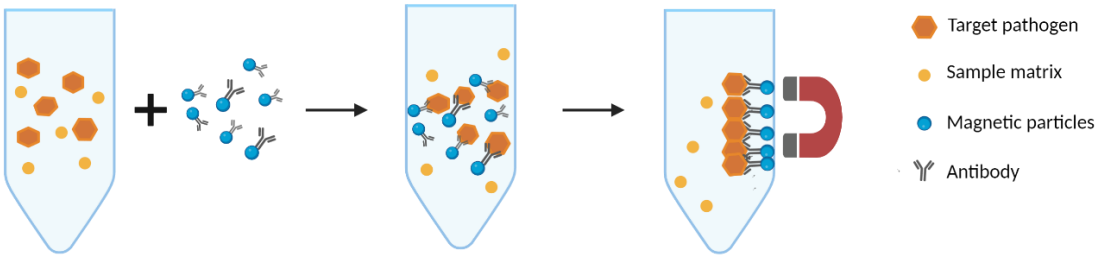

Figure 5. Immunomagnetic separation representation where the target pathogen attaches to the antibodies (the affinity biorecognition molecule) with the magnetic particle. The magnet then attracts the magnetic particles with the target pathogen attached. This step allows for the rest of the sample matrix to be removed and for the target to be resuspended into a desired volume. Thus, both the purification and concentration step can be completed. Created with BioRender.com.

1.3.1.3 Filtration

Using size as a parameter for sample purification, we can use filtration to remove contaminants or interferents from a sample by using a specific pore-sized filter to capture the interferent. The solution collected post-filter is referred to as the *filtrate* while the material retained on the surface is called the *retentate* [57]. There are various techniques used for filtration such as gravity filtration and suction filtration, which use filter papers. There are also membrane filters that come in different materials and pore sizes. Out of the types of membrane filters, they include a centrifugal filter with a membrane of a particular molecular weight cut-off. There also exist a syringe filter in which the filter is in a casing that can be attached to a syringe. The sample is then easily pushed through the filter. As a third example, membrane filters can be placed in a disposable filter system and a vacuum is used to draw the filtrate through the membrane. [57]

Filtration techniques allow for adjustment in its filtration velocity of the sample depending on the volume, composition, porous size of the membrane, the sample interferent matrix, and the flow rate of the system. However, one of its main limitation is its poor selectivity since it's only based on a sample separation process. [42] Yet, filtration can be inexpensive and straightforward to implement [56] and is used in various industries such as for water sampling [64] and quality monitoring [60], [65], food borne pathogen detection [43], [56], [66], and processing in the dairy industry [56], [67]. We will later explore some specific types of filtration configurations.

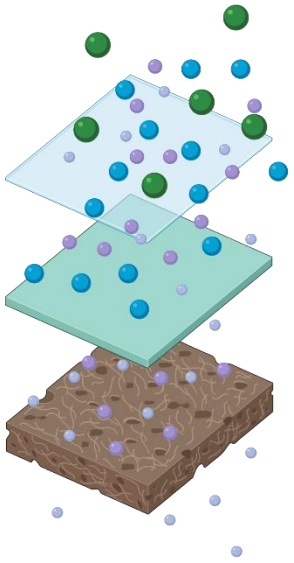

Figure 6 Filtration example were membranes with different cut-off sizes remove particles of different sizes. Created with BioRender.com

1.3.1.3.1 Microfluidics

Purification approaches have also been investigated on the microfluidics space for sub-micrometer [68] and micrometer particles [69], [70]. These systems allow for portability, compactness, and automation, among other areas [42]. Most of these techniques are label-free, which helps minimize organism damage, and exploits different physical properties of

the organism to separate constituents of the sample. These properties include size, shape, density, deformability, among many others, and the techniques can be classified into passive and active methods. Passive methods rely on the sample properties and include deterministic lateral displacement (DLD), inertial focusing, viscoelastic focusing, etc. The active method requires external fields and include dielectrophoresis, thermophoresis, acoustophoresis and optical focusing. [68]–[70]

Drawbacks for this system include the inability to scale up to industrial processes and loss of integrity over time. Furthermore, bubble formation or cell entrapment in the device leads to a short lifetime of the system and reduces purity levels after a few cycles [70]. Additionally, devices can often only take small volumes of input fluid and have flow rates lower than 1 mL/min [68], [70].

1.3.1.3.2 Microfiltration overview

Moving forward, we chose filtration as our purification and concentration method given its simplicity, low cost, varying options, and ability to process both large and smaller sample volumes [42], [56]. Focusing on the purification and concentration of a liquid under laminar flow, within filtration, there are various processes that can be chosen based on the size or molecular weights of the target particles. Such processes include microfiltration, ultrafiltration, nanofiltration, among a few other. [71] We will focus on microfiltration, a pressure-driven process where 1-3 bar (100-300 kPa) is typically applied for the retention of particles in a size range of 0.1 µm to 10 µm [72]–[74]. This wide range of sizes makes microfiltration suitable for a wide variety of fields and allows for the separation of virus, bacteria, aerosols, and other macromolecules from fluids [73]. This type of filtration process involves the use of a pore-sized membrane that come in different materials and can

operate in two configurations, dead-end filtration and crossflow or tangential flow filtration. [71]–[73], [75]

There are a variety of membrane materials, depending on the application, that are readily available. Some of these materials include cellulose nitrate, cellulose acetate, polypropylene, Poly(vinylidene fluoride) (PVDF), among a few others [72]. Cellulose nitrate and cellulose acetate were some of the original materials, and now polypropylene and PVDF, each with high porosity levels of 60-80% [76], have become more widely used.

Polypropylene, produced via hot and cold stretching and heat setting, is hydrophobic and thus has high solvent resistant. It is also chemically resistant and low protein binding for aqueous and organic solvent samples, but binds proteins, DNA, and RNA [77], [78]. Overall, it is a good material for biological sample filtration [77]–[79]. For this material, work has been done to modify the surface chemistry to change the hydrophobicity for hydrophilicity in order to broaden its applications and reduce membrane fouling [72], [80]. One study suggested wetting the polypropylene membrane with isopropanol can temporarily increase hydrophilicity [72]. Other work has used graft polymerization and plasma treatment [80].

PVDF is available in both hydrophobic and hydrophilic form but hydrophilic PVDF is often the optimal choice for protein-based sample because of its high non-specific binding. Furthermore, this type of material has random yet high defined pore structures, is compatible with organic and aqueous solvents, and can have a high flow rate applied. [72], [76]–[78], [81] The thickness for these membranes ranges from 100 to 130 μm [78].

Other commonly used hydrophilic membranes include polyethersulfone (PES), regenerated cellulose (RC), and polysulfone (PS). PES is low protein binding, has excellent

flow rates, can handle high temperature liquids, and is a mechanically strong membrane [76], [81], [82]. Likewise, RC is low protein binding, can handle high flow rates, and can process aqueous samples but only with a pH range of three to twelve [76], [79], [82]. Finally, PS is a hydrophilic membrane with low protein binding and high resistance to acids, bases, and surfactants. It typically comes in varying molecular weights and a pore size of 0.05 µm. [83]

Dead-end filtration

When the flow is perpendicular to the membrane surface, as can be observed in Figure 7, this type of relationship is referred to as dead-end filtration [71], [75].

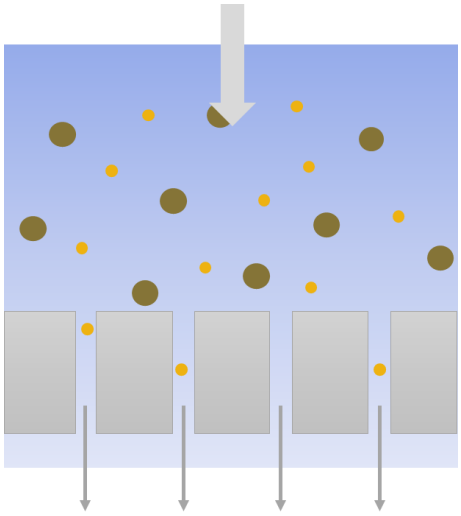

Figure 7. Bead-end filtration configuration showing the flow moving perpendicular to the membrane.

In this configuration, one of the major problems tends to be membrane fouling. Particles, at increased concentrations, block pores and then form a cake layer which acts as a barrier reducing the flux through the system [71], [72], [84]. Furthermore, this not only causes a reduction in flux, but could also decrease the recovery of a target pathogen if it was to be collected in the filtrate [84].

Caking or fouling is usually reversible when the cake formation is at the surface on the membrane, not within the membrane [75]. Work has been done to address this using different methods involving vibration of the membrane, backflushing, back pulsing, done by reversing the direction of the flow, and the use of secondary membranes [19], [72], [84]. Periodic backflushing has been explored for dead-end filtration configurations by controlling the flow using pulse width modulation (PMW) of the fluid velocity. This application led to significantly higher recovery of the targets and an increased enrichment [84].

Dead-end filtration models can be found in cartridges, such as syringe filters, and flat sheet [75]. Using syringe filters, past work has used them to purify bacteria from urine samples [85] and purify bacteria from a powdery matrix [86] to make the samples amenable for downstream detection. Here, we will focus on exploring the readily available syringe filters that come in different diameters, pore sizes, and materials.

Syringe filters are relatively affordable, can be easily found, can be used for small volumes, and can be compatible for automated filtration systems [76], [87]. Furthermore, they are typically cased in polypropylene, disposable, and come with varying pore sizes for a specific particle cut off and can be but with a female luer lock inlet and a male luer slip fitting outlet allowing it to be used with any syringe of choice.

When choosing filters, the type, pore shape, and pore dimensions can contribute to its ability to work effectively [43]. Furthermore, as noted previously, the material has a substantial effect on the performance of the system. A *first step* to selecting the best filter for your application, and the *second step* is to choose the pore size of the membrane; common sizes included 0.1 µm, 0.2 µm, 0.22 µm, 0.45 µm, 5 µm, and 10 µm [87]. These

parameters are chosen based on the type of sample being process and the objective of the experiment. For collecting your target in the filtrate, you would choose a pore size greater than it. To capture or retain your target on the membrane, you would choose a pore size smaller than your target's diameter. An additional element to consider when choosing a pore size is flow rate since larger pore sizes allow for faster flow rates [88]. After choosing a pore size, the *next step* is to choose the filter size based on the diameter.

The diameter of the filter affects the effective filtration area and dead volume inside the casing [87]. Common diameters include 4 mm, 13 mm, 15 mm, 25 mm, and 28 mm [87], with one of the influencing factors for choosing a diameter being the volume of the sample that will be filtered. It is recommended that for sample volumes less than 10 mL, a 13 mm diameter is suitable; for less than 100 mL or for most applications, a 25 mm diameter works best; for less than 250 mL or larger volumes overall, a 33 mm diameter. [79], [81], [82] With flowing a sample through the filter, particles will begin to block pores thereby reducing the usable portion of the filter and eventually causing fouling, as was discussed earlier. A smaller diameter may be prone to that happening quicker while a larger diameter filter can process dirtier samples [87]. Furthermore, larger diameters will have larger dead volume with 25 mm diameter filters having less than 200 µL and 13 mm ones having less than 100 µL [87], [89]. Yet, these larger diameters will allow for higher flow rates, though with caution since too high of pressure can block the membrane or damage it [87], [88].

It is of note that there are a variety of manufacturers that sell syringe filters, and each makes and tests membranes differently. Thus, there can be variations in filter performances between the same pore size and membrane material filter of two different vendors [76].

Cross-flow filtration

In a cross-flow filtration system, the flow is parallel to the membrane, such as can be observed in Figure 8 [71], [74], [75]. This set-up gives two outputs, a particle free permeate and a concentrated retentate containing the particles [74]. Though more complex and more expensive, the membrane lifetime cross-flow filtration is longer than for dead-end filtration and has been increasingly applied for solutions with high particle concentrations [74].

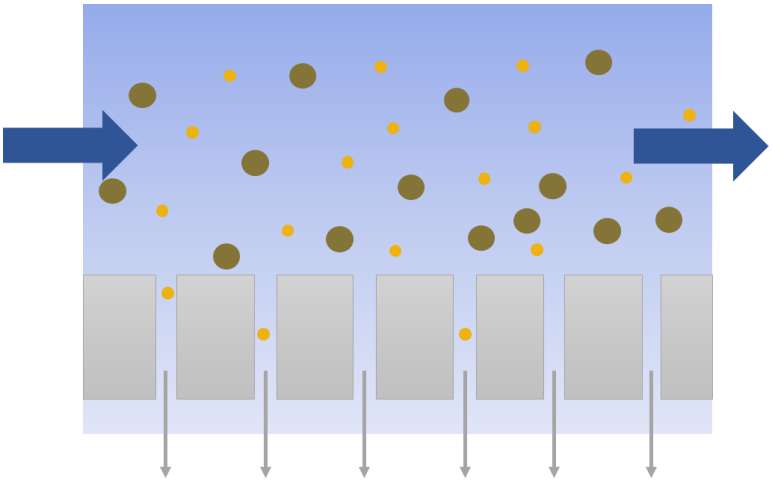

Figure 8. Cross-flow filtration system with the flow running perpendicular to the membrane.

In cross-flow filtration, the configuration helps prevent caking or the accumulation of components on the membrane that causes clogging of the pores [72], [75]. Thus, it tends to have a steadier flux. However, caking can still occur, and to combat this, studies have implemented oscillatory flow superimposed over the steady flow with a pulsatile flow, for example. Currently, there is a consensus that reversals in transmembrane pressure (TMP), the force that drives fluid through the membrane, over short periods of time disrupt the caking. In addition, cross-flow filtration often requires recirculation of processed samples in order to get higher recovery percentages. [84] Another problem found in cross-flow

filtration is that is difficult to eliminate sorption in the membrane which can lead to lower recoveries. There are various factors that can contribute to this including sample characteristics, process conditions, and membrane properties such as charge, morphology, and hydrophilicity. [90] However, though it has these drawbacks, the system is suitable for nanoparticle suspension purification. [72], [74]

Just as was mentioned for the dead-end filtration configurations, for cross-flow filtration there are a variety of membrane materials available. These membranes come in a wide range of molecular cut-offs or pore sizes, from 0.1 µm to 10 µm (microfiltration) and 0.0001 µm to 0.1 µm (ultrafiltration) and can be applied for both bacterial and viral samples [90], [91]. The performance of cross-flow filtration or tangential flow filtration (TFF) devices have shown to be variable with bacterial recoveries ranging from 32-68% for one study and viral recovery ranging from 11-98% for another study [90].

Some studies suggest specific materials work best for specific organisms. As an example, a study by Cai et al. found that PVDF membranes showed higher bacterial recovery while PES was a better choice for collecting viruses and RC was best for concentrating viruses. [90] Thus, it is important to know the composition of your sample to be processed, as well as the purpose of the process, prior to choosing a membrane material. After these steps, you then choose a pore size and required membrane area based on the sample volume and required final sample volume. [91]

Membranes in a cross-flow filtration configuration are commercially found in various formats such as cassettes, hollow fibers, tubes, among others [75], [91], and can be easily automated [66]. These can be purchased through various manufacturers such as Pall Corporation, Millipore Sigma, and HansaBioMed Life Sciences. For hollow fibers, the

membrane fibers or tubes are placed inside a polysulfone housing and enclosed with end caps [75], [83]. These membranes have been mainly designed for biomedical and food processing [66] and water purification purposes, but have been studied with other samples such as marine samples [90] and bacteria concentration [19].

1.4 Interferent surrogate

As was discussed in section 1.1.3, our samples, regardless of their origin, will contain other differently sized non-target particles that could interfere with the sensor thus highlighting the need for a purification and concentration step prior to detection. To model these non-target particles, fluorescent polystyrene beads can be used.

The beads are made of polystyrene, a polymer with a 1.05 g/cm^3 density, come in a 1% solids concentration, and are internally dyed with high-contrast colors. [92], [93] The beads, assumed to be spherical, are available in varying sizes from nanometers to over 10 μm in diameter, and come in various colors.

Because of the fluorescence, these particles can be detected with instruments including epifluorescence microscope, confocal microscope, fluorometer, fluorescence spectrophotometer, and flow cytometry [92], [93]. Thus, they are used in various industries and fields. Some of their applications include filter testing, flow racing, and biological research [92]–[94]. Looking deeper at filter testing, it is widely known that polystyrene beads are used for filter challenge studies as surrogates to biologic or environmental particulates [93], [95].

In our work, we used fluorescent polystyrene beads (Fluoro-Max Dyed Aqueous Fluorescent, Thermo Fisher Scientific, Waltham, MA) of the sizes 2 μm (#09-080-510)

and 10 µm (#09-980-450) with excitation/emission peaks of 412/473 nm and 468/508 nm, respectively.

1.4.1 Quantification methods

1.4.1.1 Quantitative Polymerase Chain Reaction (qPCR)

Polymerase chain reaction (PCR) is the gold standard technique for nucleic acid quantification, such as for DNA and RNA, due to its rapid, sensitive, and simple technique. Developed in 1983 by Kary B. Mullis and co-workers, the technique amplifies DNA using oligonucleotide primers, dNTPs, and a heat stable Taq polymerase. [96], [97]

The PCR mechanism can be broken down into three parts: denaturing, annealing, and extension. In denaturing, the dsDNA comes apart due to the high temperature in the reaction, 94-95˚C for 1-30 seconds. Step 2, annealing, lowers the temperature to 50-65˚C for 1-40 seconds, and the sequence specific primers anneal to the ssDNA template. The final step, extension, raises the temperature to around 72˚C and allows the DNA polymerase enzyme to extend each primer in the 5’ to 3’ direction. [96]

There are two main types of PCR. The first is conventional PCR where the detection of the amplified product is done by running the DNA sample on an agarose gel post reaction for end-point analysis. This approach takes extra labor time and resources. The second type is real-time PCR, of which we will focus on quantitative real-time PCR, also called quantitative PCR (qPCR). In this approach, a fluorescent molecule is included in the reaction and correlates the increase in fluorescent signal to an increase in the amount of DNA. This approach is less-time intensive and provides data for analysis immediately after the completion of the reactions. [98] For these reasons, we will focus on exploring further this type of PCR.

The fluorescent molecule used for qPCR include DNA binding dyes, such as SYBR Green, that non-specifically bind, i.e., they attach to any double stranded DNA, and sequence specific probes. Probes only bind to a targeted sequence within a double stranded piece of DNA, providing an additional level of specificity. Regardless of the molecules, the key is that the measured fluorescence correlates to the amount of the amplified product in each cycle. [96], [98]

When observing results from a qPCR run, we observe an amplification plot with Cycle number in the x-axis and fluorescence values in the y-axis. There are two clearly visible phases, one is an exponential phase, where the DNA doubles in each cycle, and the other a nonexponential phase, where a plateau is reached after the components become limited and the reaction is slowed. Both phases can be observed in Figure 9. The exponential phase increments over time and cycles until it reaches a detectable level. At this point, the cycle number at which it occurs is identified as the threshold cycle, C_T, and can be used to calculate the initial amount of template in the reaction. Overall, the threshold cycle number of a reaction is based on the amount of template available at the start of the reaction. A larger amount of template results in quicker amplification and therefore less cycles to reach a detectable fluorescence level, resulting in a high C_T value. [98]

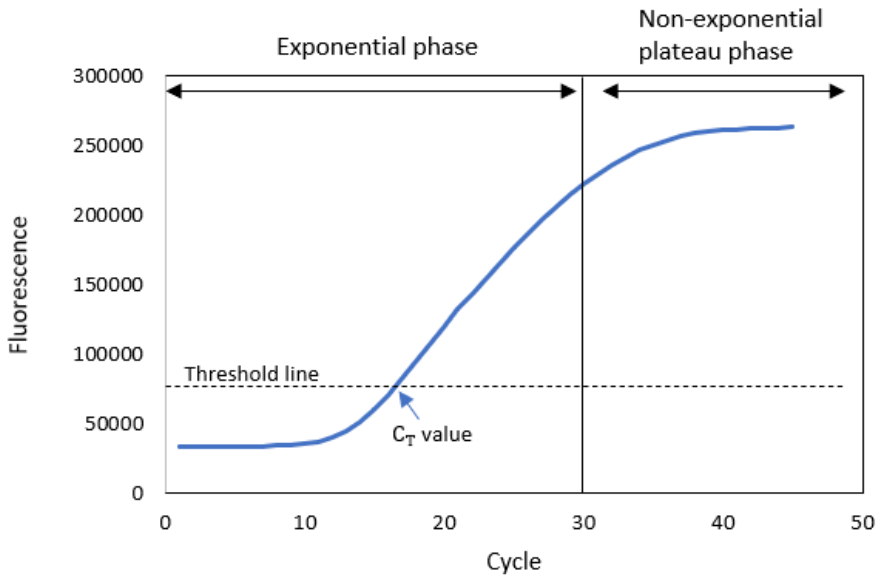

Figure 9. Amplification plot with a baseline-subtracted fluorescence.

To ensure qPCR results are reliable, serial dilutions of a known concentration template should be run in the plate along with the other reactions in order to generate a standard curve. This standard curve determines the equation for calculating the number of starting copies or concentrations of the other unknown samples. To determine the equation, the logarithm of the starting quantity or concentration of the templates is plotted against the C_T value of each sample. Using a linear fit, the equation for linear regression [y = mx + b] is calculated. Given the x-axis values are plotted in a logarithmic form, the equation is better represented as

$$C_T = m \times \log \text{quantity} + b$$

Based on the above equation, we calculated the quantity of an unknown sample, N, by rearranging to solve for that value as shown below.

$$N = 10^{\frac{C_T - b}{m}}$$

With the newly generated equation, the coefficient of determination (R^2) is generated as well and used to evaluate the assay standard curve, with an optimized qPCR having an

R^2 greater than 0.980. Another marker for an optimized assay is consistency across replicate reactions and even space between cycles. The ideal spacing between cycles, assuming perfect doubling occurs, is determined by the equation $2^n = 10$ with n being the number of cycles between curves at fluorescence threshold. Finally, the amplification efficiency, ideally between 90-105%, can also be evaluated using the slope of the standard curve and the following equations, $E = 10^{-1/slope}$ and % Efficiency = (E-1) × 100%. [98]

In all, qPCR is a powerful technique that has been used to quantify viruses [99], such as SARS-CoV-2, bacteria [100], and other organisms in samples for many applications.

1.4.1.2 Flow cytometry

Flow cytometry is a powerful technology that provides rapid analysis of single cells or particles in solution. Flow cytometers can analyze and/or purify cell population based on their fluorescent or light scattering characteristics using light sources and fluorescent light signals. The solution containing the particles is funneled, using sheath fluid, for single particles to flow past single or multiple lasers, as can be observed in Figure 10. When this happens, these light sources and signals are scattered, and detectors, such as photodiodes, read it and convert it into electrical signals. The information acquired is used to help indicate the size of the particle, count the number of particles, and in some cases, provide the concentration of particles in the sample analyzed. There are various types of flow cytometers available, yet all with the same underlying idea. Overall, flow cytometry is applied in a great number of areas including immunology, molecular biology, bacteriology, and infectious disease monitoring, among others, and can be used to analyze cells and other particles such as polystyrene beads [101]. [102]

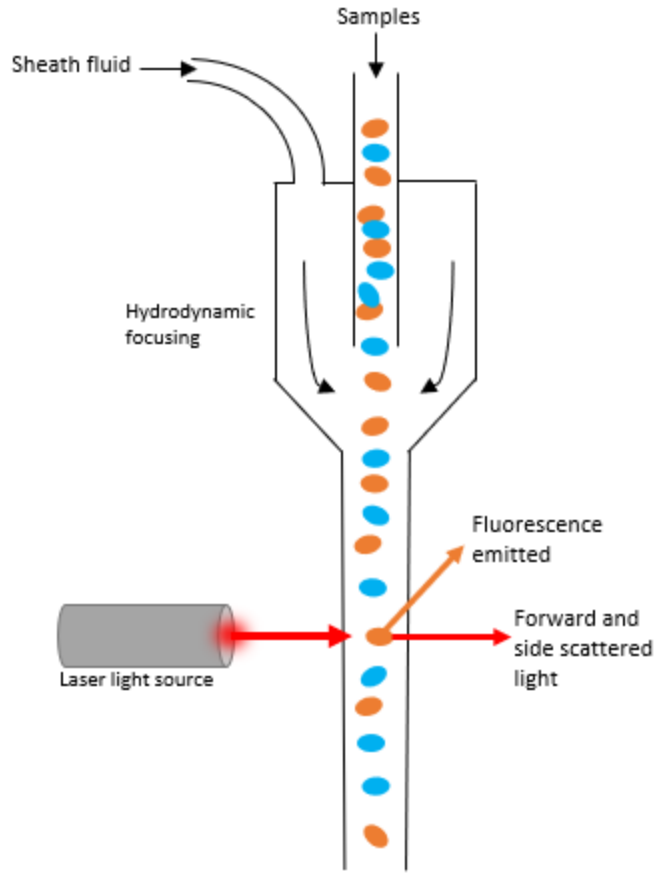

Figure 10. Flow cytometry overview with sheath fluid focusing the particle suspension for analysis. The light scattering and fluorescence detection is also shown.

1.4.1.3 Fluorescent microscopy

Fluorescent microscopes feature the same parameters as a conventional optical microscope but have the key addition of having a higher intensity light source, such as LEDS or a Xenon or Mercury arc-discharge lamp, that excites a fluorescent species in a sample being analyzed [103]. The microscope contains a selective excitation filter that only allows a specified wavelength of radiation that matches your specimen to go through, reflect on the surface of a dichromatic beam splitter, and pass through the microscope objective to excite the sample [104]. Once the specimen is being excited and electrons relax from a higher state to a lower one and emit a longer wavelength of light, the microscope

sorts out the weaker emitted light for a specific wavelength with the use of a barrier filter. The filter separates the fluorescent light from surrounding radiation, allowing you to see only what is fluorescing [103].

It is known that the majority of fluorescent microscope both excite and observe the fluorescence of a sample from above. These microscopes are known as epi-fluorescence microscopes, and they have helped paved the way for more advance microscopes like conofocal laser scanning microscopes, which can produce high resolution 3D images of specimens' subsurface [103]. Furthermore, all these microscopes are widely used in biology and the biomedical sciences for cell imaging as well as has been used for bead imaging [103], [105].

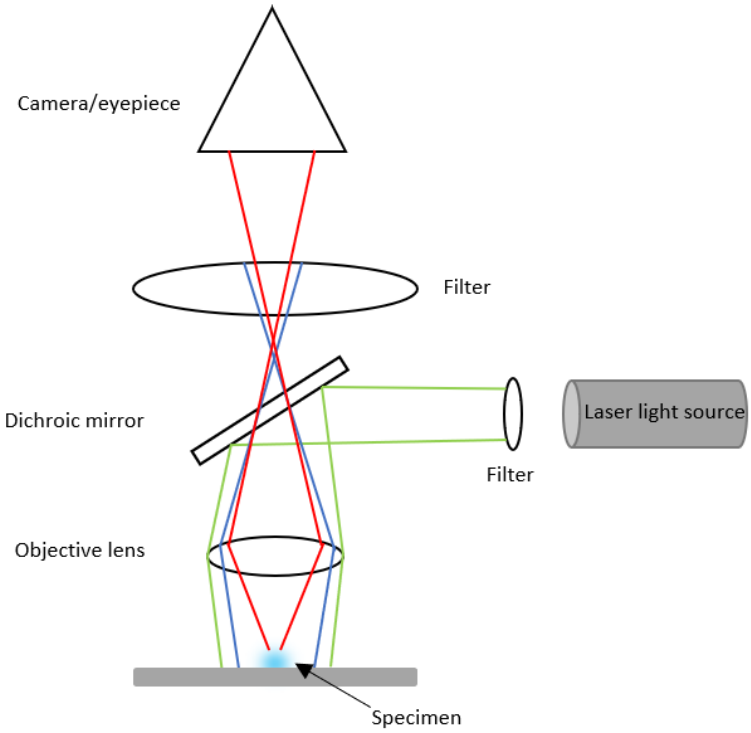

Figure 11. Fluorescent microscope schematic showcasing the specimen specific wavelength (green line) reaching the plate to excite the sample. The specimen then emits two wavelengths of light (purple, red lines), the weaker one of which is sorted out, and the strongest (red) reaches the eye piece.

1.4.1.4 Luminescence assay

Luminescence assays are a simple, less complex method for sensitive and high throughput measuring of biological processes [106]. The emitted light from luminescence assays comes from a biochemical or chemical enzyme mediated reaction. For the biochemical reaction to occur and the luminescence to be emitted, there's an addition of a consumable substrate luciferin [107] or a chemiluminescent assay to the sample containing a specific target enzyme. To detect the luminescence, the equipment used for analysis only requires a sensor, much simpler than the light source and sensor needed for absorbance or fluorescence. Commonly, a spectrophotometer or plate reader capable of luminescence signal detection is used to measure a luciferase-based reporter assay. For the reading, a photomultiplier in the plate reader converts the emitted light into an electrical signal that is easily readable and processible for analysis. [106]

Based on what was previously described, luminescence assays are easy to set-up and suitable for rapid, sensitive detection of target pathogens. Many of these assays are commercially available through companies, such as Promega, and are used for different purposes that include diagnostic immunoassays as well as food borne pathogen detection [108].

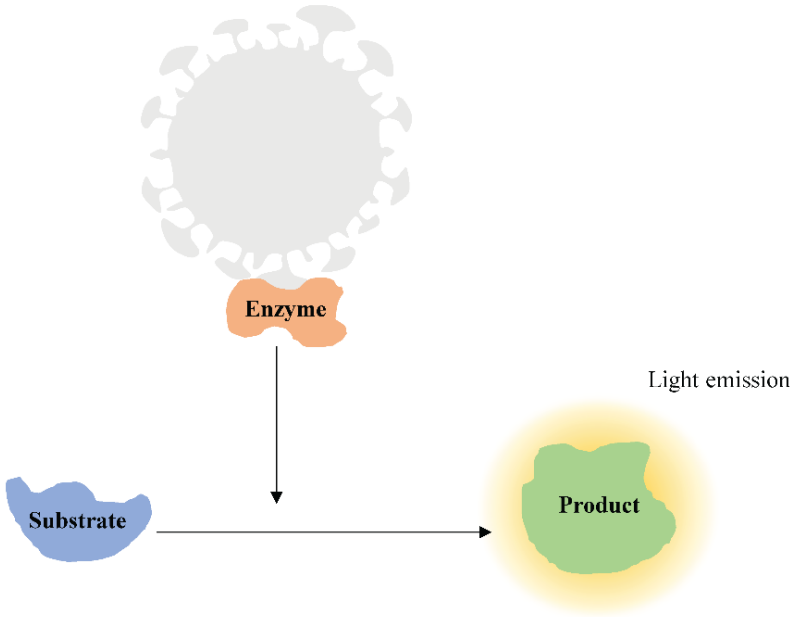

Figure 12. An enzyme tagged organism comes in contact an added substrate. When combined, they produce a reaction that emits light for luminescence detection.

1.4.1.5 Alternate quantification methods

For both organisms and beads, there are a wider variety of techniques for quantification than just the ones previously mentioned. In this section, we will briefly discuss three additional approaches that were tested in this work (see Appendix A) and that are used in research for various applications.

Another method, originally described in 1971, commonly used for detecting and quantifying soluble substances like antibodies and hormones, is ELISA (enzyme-linked immunosorbent assay). ELISA is a plate-based assay technique that works by having an antigen immobilized on a solid surface that's then linked with an antibody with a reporter gene attached. After an incubation period with an appropriate substrate, the activity of the reporter enzyme, reported as absorbance, is measured using a plate reader. [109]

An alternate, label-free, yet high-cost method for the areas of biology, biochemistry, and medical sciences is surface plasmon resonance (SPR). This optical biosensing technology, first used in the 1990s, consist of a biosensor with a ligand (capturing element), such as an antibody, immobilized on a sensor surface. The sample containing the target particle is then added and the targets are captured by the ligands on the surface. As more targets are captured and accumulate, there's a change in the refractive index in the evanescent field detected by SPR. The changes in refractive index can be used to determine the concentration of a target in a sample. [110]

In addition to SPR, waveguide interferometers also measure refractive index change on their surface. In this configuration, a waveguide structure guides the light propagation and confines the light in the low-refractive-index material filling the slot. [111]

Antibodies, proteins, and even beads can be tagged with different things, including biotin, a vitamin. A method for quantifying a biotinylated particle is a Biotin quantification kit, many of which are commercially available. These kits have a similar, yet simpler, mechanism to ELISA. For a quick estimation of the mole-to-mole ratio of biotin to target in a solution, the sample is added to a mixture of HABA and avidin, an acid that acts as a dye and a glycoprotein, respectively. Due to a strong affinity between biotin and avidin, when the mixture occurs, if there is biotin present, it will displace the HABA to bind to the avidin. This displacement causes a proportional decrease in the absorbance at 500 nm of the reaction, which can be measured using a plate reader. This change in absorbance is then related to the amount of biotin in the sample which can be used to roughly estimate the number of biotinylated particles in the tested sample. [112]

1.5 Nomenclature

This section defines important equations and terms used throughout the document for analysis.

$$\text{Recovery} = \frac{\text{Number of target particles in output}}{\text{Number of target particles in input}} = \frac{(\text{Target concentration} \times \text{Target volume})_{\text{output}}}{(\text{Target concentration} \times \text{Target volume})_{\text{input}}} \quad (1)$$

$$\text{Enrichment} = \frac{\left(\frac{\text{target concentration}}{\text{nontarget concentration}}\right)_{\text{output}}}{\left(\frac{\text{target concentration}}{\text{nontarget concentration}}\right)_{\text{input}}} \quad (2)$$

$$\text{Concentration factor} = \frac{\text{Concentration}_{\text{output}}}{\text{Concentration}_{\text{input}}} \quad (3)$$

Chapter 2 Bacteria purification and concentration

2.1 Bacterial methods

2.1.1 E. coli quantification

Bacteria preparation

For this work, we used the bacterial pathogen *Escherichia coli (E. coli)* (ATCC 25922) prepared by our collaborators, Dr. Jie Xu and her team at Food and Processing (Georgia Tech). The bacteria were propagated per vendor's instructions and was grown to concentrations of around 10^9 CFU/mL. A cell washing procedure was then implemented to resuspend the cells in 1× phosphate buffer saline (PBS) and the cells were stored in a refrigerator (3-4˚C) for later use.

DNA extraction

Bacteria DNA for samples or standards alike was extracted and isolated using the E.Z.N.A Bacterial DNA kit (Omega Bio-Tek, Norcross, GA) according to the kit's instructions; Tris-EDTA buffer was purchased independently (#97062-626, VWR, Radnor, PA). Typically, 1 mL per sample underwent extraction and the DNA was concentrated to a final volume of 150 µL in elution buffer from the kit.

Standards preparation

To prepare the DNA samples for the standard curve of the qPCR runs, DNA from an unknown concentration of bacteria was extracted and the Denovix dsDNA High Sensitivity Assay (Wilmington, DE) was used, per the manufacturer's instructions. The results yield a ng/µL concentration we later convert to copies/µL using the molecular weight of the 5, 226-kbp genome of this specific strand of *E. coli*. Taking dilutions into account, the concentration of the DNA stock is calculated in copies/µL and diluted down to a factor of

2×10^{x}, with nuclease free water or deionized, distilled water. 'X' is the power used to represent the length of the DNA stock. This sample is further diluted down in 10-fold to create 7-8 samples for the standard curve.

qPCR

PCR analysis was carried out in the StepOnePlus real-time system (Applied Biosystems) using specific primers and probe for targeting the 16S_ gene in *E. coli*, as has been done previous [113], [114]. The forward primer [5'-CAT GCC GCG TGT ATG AAG AA-3'], reverse primer [5' -CGG GTA ACG TCA ATG AGC AAA- 3'] , and probe [5'-/56-FAM - TA TTA ACT T/ZEN/T ACT CCC TTC CTC CCC GCT GAA /3IABkFQ/ - 3'], were manufactured by Integrated DNA Technologies, Inc. (Coralville, IA).

The PCR mix consisted of 5 µL of 5× PerfeCta MultiPlex qPCR ToughMix (95147-250, QuantaBio, Beverly, MA), 0.5 µL of each primer (each having been previously diluted down to 25 µM using nuclease free water), 0.5 µL of the probe (having been previously diluted down to 10 µM using nuclease free water), 5 µL of the DNA template, and 13.5 µL of nuclease free water to make up a 25 µL total volume per well.

The samples were placed in an Applied Biosystem Fast Optical 96-well, 0.1 mL rection plate (4346907, Fisher Scientific, Waltham, MA). All runs contained a negative control of nuclease free water and a positive control consisting of the *E. coli* standard DNA templates. The samples then underwent the following thermal conditions: 10 min at 95˚C, followed by 45 cycles, with one cycle consisting of 10 sec at 95˚C and 30 sec at 60˚C. The PCR analysis was performed in triplicates (technical triplicates) per sample, unless stated otherwise. The fluorescence data from the FAM channel was plotted against the cycle numbers, and the same threshold value in the linear range of the amplification was chosen

for the standards samples and unknown concentration samples. Interpolation was then used to calculate the exact cycle numbers where the amplification intersected with the threshold.

Bacteria enumeration

Prior to starting experiments, the PBS washed *E.coli* cells were vortexed to mix and break-up any pellet that might have accumulated in the bottom of the 50 mL tube. They were then diluted in 10-fold dilutions using 1× PBS (#21-040-CV, Corning, Glendale, AZ), plated on BHI agar plates (Hardy Diagnostics, Santa Maria, CA), and incubated at 37˚C for 24 hours. Quantification from plating informed the starting concentration of the bacteria prior to the experiment which allowed us to accurately dilute the bacteria down to a desired starting concentration and volume using 1× PBS.

2.1.2 Bead quantification

Fluorescent polystyrene beads were quantified using fluorescent microscopy (AxioObserver Z1, Zeiss; Oberkochen, Germany), and, occasionally, flow cytometry (Aurora, Cytek; Fremont, CA). Prior to analysis with these methods, we ensured bead solutions contained 0.5% of Triton X-100. This step was critical in ensuring the beads were monodispersed in the solution.

For the flow cytometer, a 96-well, clear, round bottom plate (Corning; Corning, NY) was used. We added 100-200 µL of sample volume per well. In fluorescent microscopy, we used disposable hemocytometers (#22-600-106, Fisher Scientific; Norcross, GA) and added 10 µL of a sample to the hemocytometer. To count the beads, images were taken of the grid under DIC light and the fluorescent channels DAPI (465 nm) for 2 µm beads and EGFP (509 nm) for 10 µm beads, with the following parameters: 5× resolution, NA: 0.25, Gain: 100. These images were then overlayed using Image J or Power point and the beads

counted per grid. Images were taken of the middle grid and the four corners of the hemocytometer. Once, counted, the equation below was used to determine the concentration of the beads in the sample tested.

$$\text{Concentration}\left(\frac{\text{beads}}{\text{mL}}\right)=\frac{\text{Total beads counted}}{\text{Number of squares}}\times 10^4 \text{ beads/mL}$$

2.1.3 Statistical analysis

Analyzed groups were tested for a normal distribution using the Shapiro-Wilk test, and Levene's test was used to verify for the homogeneity of variance assumptions. Based on the results of the assumptions test and the groups that were going to be compared, appropriate statistical methods were chosen and are described in each section. An alpha value of 0.05 was used for all methods.

2.2 Purification Results

2.2.1 Filter matrix

A series of differently pore sized and diameter sized syringe filters (see Table 1) were evaluated to assess their efficiency at recovering bacteria. All the filters, except for the 10 µm pore size filter, made of polypropylene, were made of hydrophilic Poly(vinylidene fluoride) (PVDF). The 10 µm pore size filter material was chosen to be different from the others due to lack of availability in the market for 10 µm pore size PVDF syringe filters. All filters were purchased sterile. ***Of note, moving forward, all tests for this chapter and the subsequent chapter were performed with the filters presented here.***

Table 1. Differently pore sized PVDF filters 13 mm and 25 mm in diameter tested for *E. coli* recovery.

Pore size (µm)	Filter diameter (mm)	Manufacturer
0.22	13	Millipore
0.22	25	Millipore
0.45	13	Millipore
0.45	25	Southern Labware
5	25	Millipore
10*	25	Tisch Environmental

*Material: Polypropylene

Method

The effectiveness of these filters was evaluated in two different ways, through the filtrate recovery and the retentate recovery. The *filtrate* is the output of the system once the sample is pushed through a syringe filter, and the *retentate* is the material retained or captured on the membrane surface once a sample is pushed through. The retentate is removed from the filter surface by reversing the liquid flow and pushing the liquid through the filter again, an action also referred to as backflow. Figure 13 shows the steps described here. Furthermore, for the recovery data, the *loss* is also included and was calculated by subtracting the filtrate and retentate recovery from 100%.

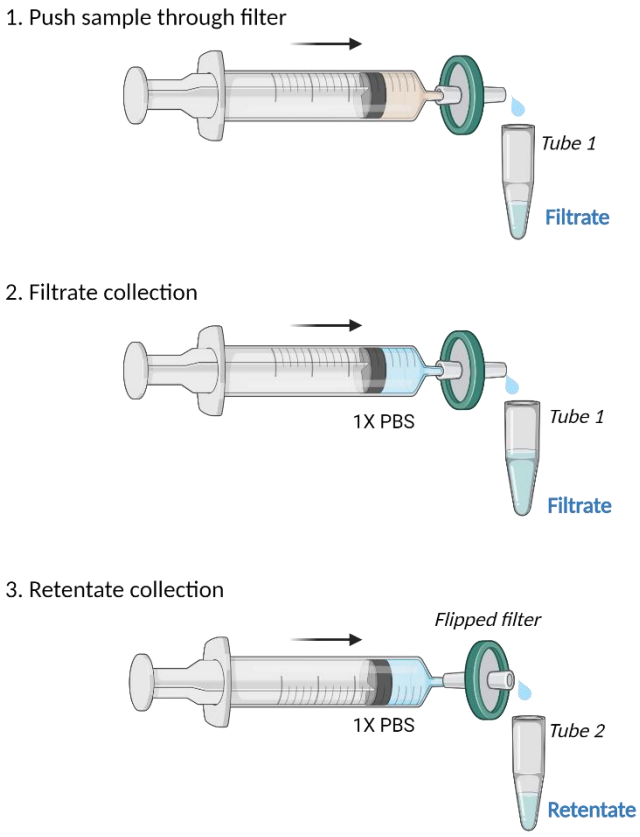

Figure 13. Mechanism for filtrate and retentate collection per filter. Step 1 consist of pushing the sample through the filter. In step 2, 4 mL of 1× PBS is pushed through the same filter and collected in the same filtrate tube. Then, in step 3, the filter direction is flipped in order for any retained particle on the membrane surface to be collected in the retentate. Created with BioRender.com

The tests consisted of the use of 1 mL syringes with a luer-lock fitting (plastic, BD, Franklin Lakes, NJ) to aspirate 1 mL of the diluted bacteria concentration onto the syringe. Then, the filter, previously primed with 1× PBS, was attached and the fluid pushed through with a constant flow rate of 2 mL/min using a syringe pump (Harvard Apparatus, Holliston, MA). This step was followed by attaching the filter to a new syringe containing 4 mL of 1× PBS to help ensure the sample was fully pushed through the filter; this 4 mL filtrate was collected in the same tubing as the previous 1 mL filtrate. The following step, and last step, was to reverse the fluid flow direction. We did this by flipping the filter direction and

attaching it to a syringe containing 1 mL of 1× PBS. The PBS was then pushed through to collect the retentate in new tubing. Finally, the final volumes for the collected filtrate and retentate were recorded since we expect variability in volumes between runs. These values were then used to calculate the recovery percentage after analysis. This procedure was performed three times per filter to create triplicates for each syringe filter. For each run, we used a new filter (always primed prior to use).

To create the samples for which the procedure would be performed with, the bacteria was diluted down to a concentration of 10^7 CFU/mL using 1× PBS. This concentration is comparable to studies found in literature [85]. The total volume the sample would be diluted to depended on volume that would allow the performance of triplicate runs per filter type.

For analysis, six 1 mL input volumes taken from the diluted stock (one sample per filter tested), 1 mL of the 5 mL filtrate output, and the full 1 mL of the retentate, per run, underwent DNA extraction and qPCR analysis as stated in section 2.1.1. The difference for the qPCR in this section is that the filtrate and retentate biological triplicates were analyzed once (not in technical triplicates). Volume differences between samples outputs were accounted for in the analysis. Of note, the 10 µm filter runs and analysis were performed on a different day but under the same conditions.

Results

Figure 14 shows the filtrate recovery, retentate recovery, and loss for each filter tested. The graphs are split into the filters of 25 mm diameter (A) and the filters with a 13 mm diameter (B). Observing the results, for optimal filtrate recovery, we see that a 5 µm pore size filter recovers 40% of *E. coli* in the filtrate, whereas the 10 µm pore size filter recovers

slightly less at around 33% with a larger standard deviation. For optimal *E. coli* retentate recovery, the 0.22 µm and 0.45 µm pore size filters, with both filter diameter had higher recoveries as compared to their filtrate recoveries. Comparing the results for these two smaller pore size filters, the 0.22 µm pore size filter results in higher retentate recovery across both filter diameters at ~40% recovery.

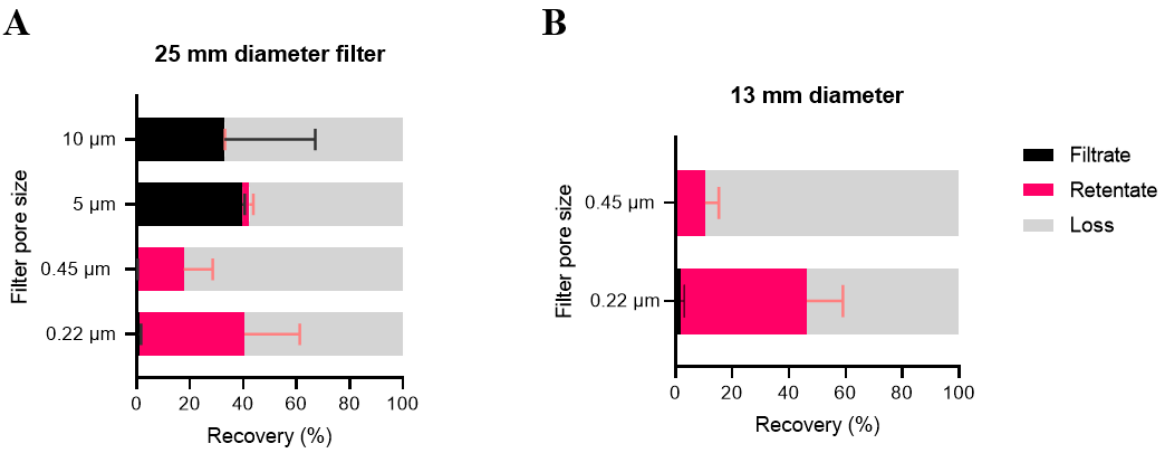

Figure 14. **A.** 5 µm pore size filter shows larger *E. coli* filtrate recovery at 40% with a smaller standard deviation as compared to the 33% results from the 10 µm pore size filter. **B.** The smaller pore sized filters show more optimal *E. coli* recovery in the retentate for both filter diameters with the 0.22 µm pore size filter resulting in higher recoveries, around 40%, for both filter diameters as compared to the 0.45 µm pore size filter recoveries. (n = 3 for all filters)

Figure 15 results focus on filter diameter as a potential influencing factor for retention recovery for both the 0.22 µm and the 0.45 µm pore size filters. The values from Figure 14 were replotted as a function of filter diameter for each of the two previously mentioned pore sizes. Per pore size filters, there appears to be no statistically significant difference in the retentate recovery between diameters. Furthermore, for the 0.22 µm pore size filter, the recoveries for both diameters are around 40%. For the 0.45 µm pore size filter, the difference appears to be a bit greater, but the recoveries range from 15-20%.

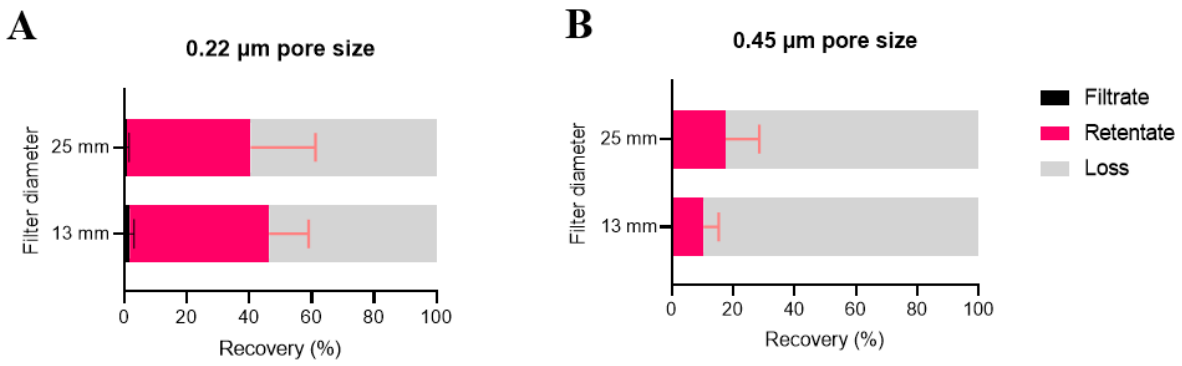

Figure 15. The 0.22 µm and 0.45 µm pore size filters appear to show no statistically significant difference in the retentate recovery as a function of filter diameter. The 0.22 µm pore size filter recoveries under both diameters is around 40% while for the 0.45 µm pore size filter, the recoveries range on average from 15-20%.

Final results for these experiments sought to evaluate whether there was any difference in retentate recovery between the 25 mm diameter filters for the 0.22 µm and 0.45 µm pore sizes. Again, we replotted the data from Figure 14 to make the comparison. Figure 16 shows the results, and via visual inspection, the 0.22 µm pore size filter appears to yield greater retentate recovery at around twice the average retentate recovery as compared to that of the 0.45 µm pore size filter.

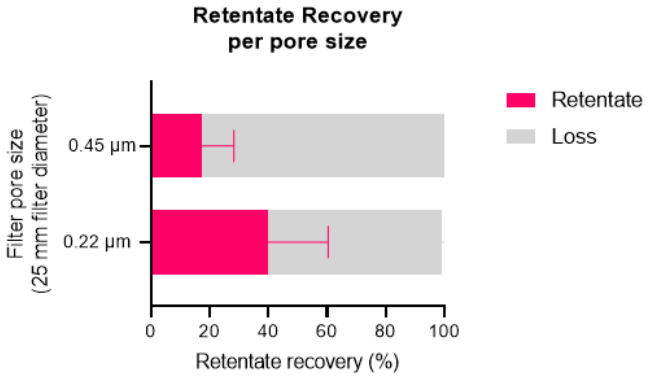

Figure 16. Of both 25 mm diameter filters, the 0.22 µm pore size filter has an average retentate recovery twice as great as that of the 0.45 µm pore size filter.

2.2.2 Individual beads experiment with filters separately

To evaluate the compatibility the PVDF syringe filters with the polystyrene fluorescent beads previously described in this work, we chose to perform some preliminary work to test beads individually with one smaller pore size filter, 0.45 µm, and with one larger pore size filter, 5 µm. The results would allow us to determine if the beads were a good interferent surrogate and would allow us to achieve a baseline recovery percentage for each bead.

Methods

Starting with the 0.45 µm filter, the 2 µm beads and the 10 µm beads were diluted each with deionized (DI) water to a concentration of 10^6 beads/mL, representative of a high interferent concentration [41], with 1× PBS and a final suspension that was 0.5% Triton X-100. 1 mL of the sample was aspirated into a 5 mL syringe (plastic, BD, Franklin, NJ), to which the filter was then attached, the sample pushed thorugh, and the filtrate collected. The procedure was performed in triplicates, per bead size. Pre-purification samples and each post-purification or filtrate sample (n = 3 per bead) was later quantified using fluorescent microscopy as described in section 2.1.2.

The 5 µm pore size filter was tested twice for filtrate recovery and retentate recovery of 2 µm beads. The filter was assumed to be able to remove the 10 µm beads given the beads are 2× as large as the pore size, therefore, the tests were conducted with only the 2 µm beads. The beads were prepared to the same concentration as previously described, with 1 mL of the sample loaded onto a 5 mL syringe. Then, the 5 µm pore size filter was attached, and the sample pushed through. An additional 4 mL of 1× PBS was pushed through the sample filter with the filtrate collected in the same tubing as the 1 mL filtrate.

Similar to what was described for the filter tests in section 2.2.1, the flow of the fluid was reversed by flipping the syringe filter, the 5 mL of 1× PBS was pushed, and the retentate was collected. Triplicates were performed for each of the two separate runs done. Furthermore, the tests for both pore size filters were done manually.

Results

As can be observed in Table 2, both the 2 µm and 10 µm beads were effectively removed from the output with the use of the 0.45 µm pore size syringe filter which confirms this method is reliable and effective with removing particles larger than 1 µm in size.

Table 2. Pre-purification and post-purification bead count used to assess the purification performance of 0.45 µm filter. The 2 µm and 10 µm were successfully removed (as observed in the 10 µL sample).

	Pre-Purification	**Post-Purification**
	Number of input beads (nominal) [$n = 3$ replicates]	Number of output beads (measured) [$n = 3$ replicates]
2 µm beads	1×10^6 beads	0 beads
10 µm beads	1×10^6 beads	0 beads

Focusing on the 5 µm pore size filter results, Figure 17 shows that around 40% of the beads were recovered in the filtrate. The filtrate recovery was statistically significantly different than the over 20% recovered in the retentate ($p = 0.014$).

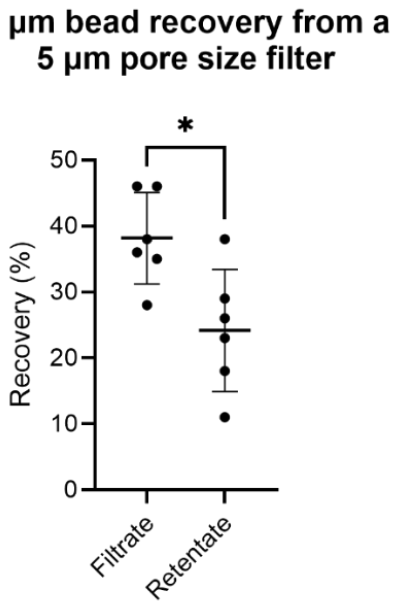

Figure 17. A 5 µm por sized PVDF syringe filter recovers 40% of the 2 µm beads in the filtrate while a little over 20% are recovered in the retentate. These two recoveries were determined to be statistically significantly different ($p = 0.014$) using an unpaired t-test.

2.2.3 Interferents with dual filter filtration

After testing the performance of the filters individually, the next step was to use two filters to create a filtration system for purification and possible concentration of a target particle, similarly to what has been done in previous work [86]. This double filter filtration system (DFFS) consists of a four-step process where the larger pore size is the first step to remove larger contaminants and the smaller pore size is later used to capture the target particle. Then, the retentate can be recovered to a desired concentration by controlling the backflow volume. We performed preliminary tests with a sample containing interferents, i.e., the differently sized beads mixed together.

Method

The sample used for these tests consisted of mixing three differently sized fluorescent beads, each diluted with deionized (DI) water and Triton X-100 to a 10^6 beads/mL

concentration in 0.5% Triton X-100. When the 0.40 µm, 2 µm, and 10 µm beads were mixed, the concentration for each bead became 3.33×10^5 beads/mL.

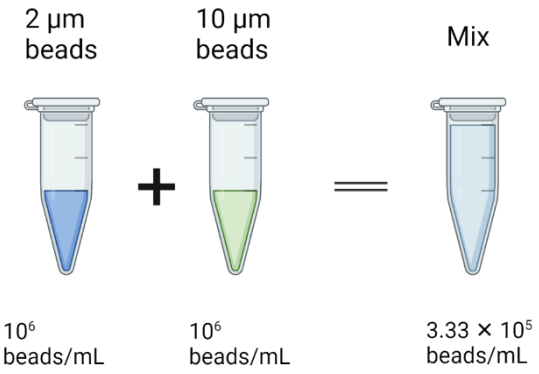

Figure 18. Representation of the individual beads, each at 10^6 beads/mL, mixed to form the interferents sample tested with a concentration of 3.3×10^5 beads/mL. Not shown, the 0.40 µm beads. Created with BioRender.com.

The procedure for this experiment consisted of aspirating 1 mL of the sample to a 5 mL syringe, same as used in previous tests. A 5 µm pore size filter was attached to the syringe containing the sample, and the sample was pushed thorugh with the filtrate being collected in a 15 mL tube. The following step involved attaching the filter to another 5 mL syringe containing 4 mL of 1× PBS. This extra volume was pushed through and the filtrate collected in the same 15 mL tube as before. The 5 µm pore size filter was discarded and a new 0.45 µm pore size filter was attached to a new 5 mL syringe. This set-up was then used to aspirate the 5 mL sample present in the 15 mL tube. After this, the 0.45 µm filter was attached to a 5 mL syringe containing 1 mL of 1× PBS that was pushed through and the final system output or retentate was collected in a 1.5 mL tube. For these double filter filtration system (DFFS) studies, we *primarily care about the analysis of the retentate as*

this is the sample that should contain our target particle. The steps, performed manually, are shown in Figure 19.

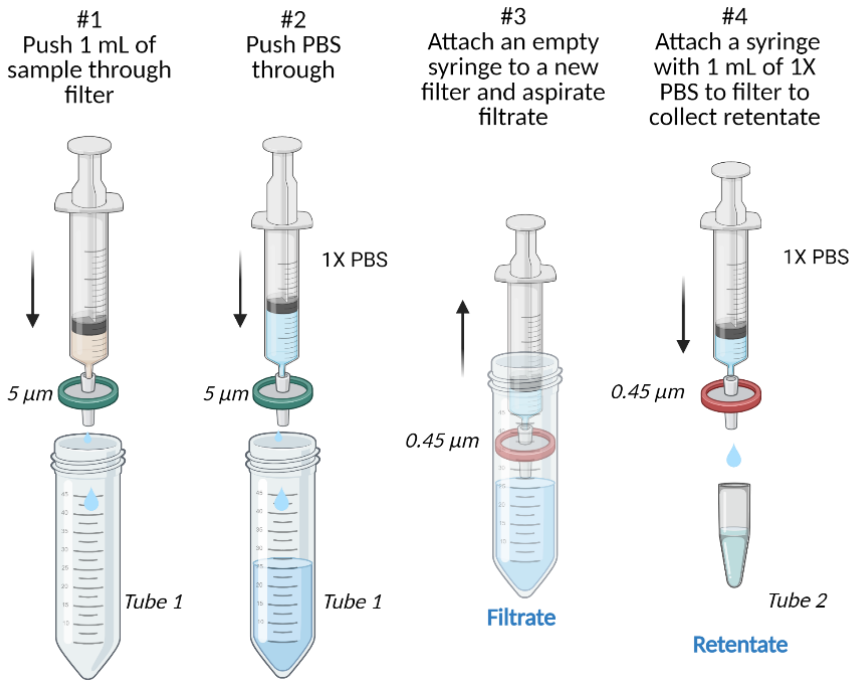

Figure 19. Double filter filtration system (DFFS). Outlined are the 4 steps involved in the purification and concentration of a sample using a 5 µm and a 0.45 µm pore size filter. Steps and schematic adapted from Isabel et. al. [85]. Created with BioRender.com

The test was performed in duplicates (n = 2), and the pre-purification (input), preserved prior to the runs, and post-purification (retentate) samples were quantified using fluorescent microscopy as previously discussed in the beginning of the chapter. Of note, the 0.40 µm beads were not quantified given their size did not allow for the microscope approach to accurately quantify them. Additionally, the interest in this study is of how larger sized interferents will interact with our filtration approach, thus, only the 2 µm and 10 µm beads were quantified.

Results

The limited data set yielded the removal of close to 100% of the 10 µm beads in the samples, close to 100% purity for the 2 µm beads and an average recovery of 23% for the 2 µm beads, as evaluated with 1% (10 µL) of the total output volume. Figure 20 shows the recovery values while Figure 21 shows an image of the bead population pre-filtration and post-filtration with the removal of the 10 µm beads after going through the system.

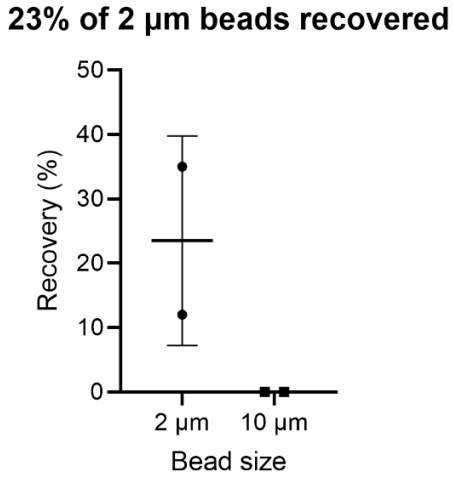

Figure 20. 23% of the 2 µm beads were recovered from a mix of interferent undergoing purification with a 5 µm pore size filter and recovery with a 0.45 µm pore size filter. (n = 2)

A

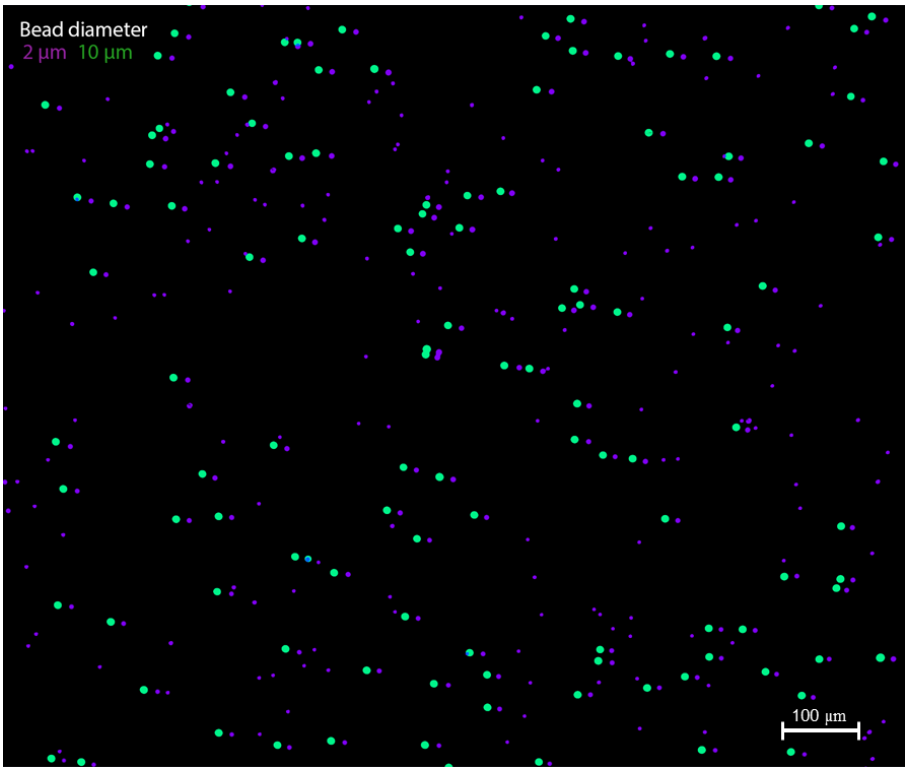

B

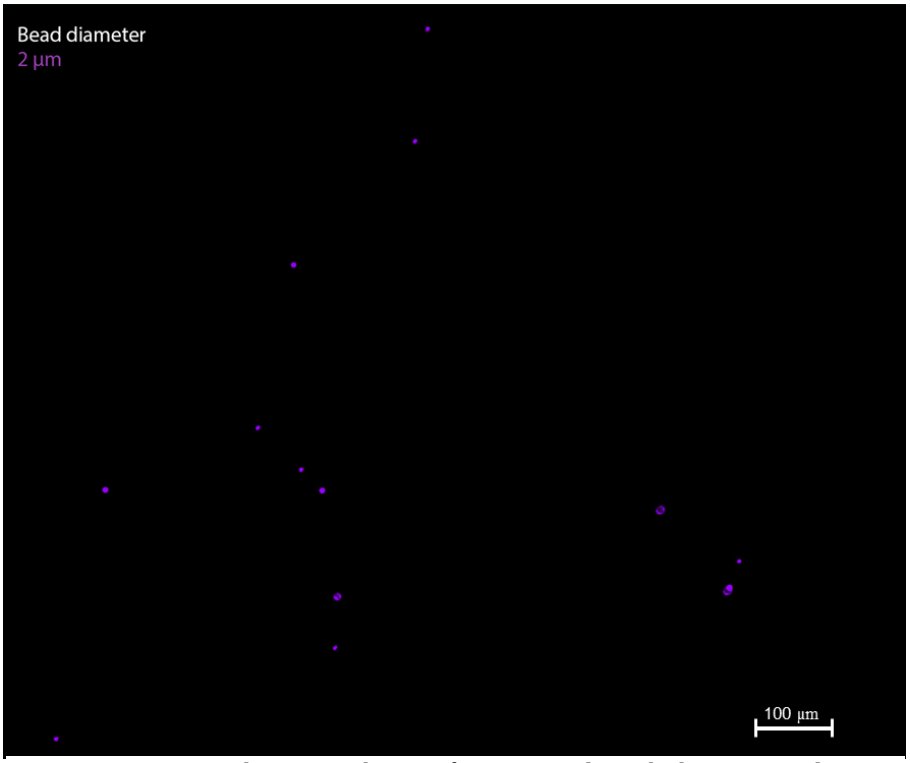

Figure 21. Image A showcases the interferents sample with the 2 µm and 10 µm beads mixed together each at a final concentration of 3.3×10^5 beads/mL for each bead size. Image B showcases the sample pos-filtration, where the 10 µm beads were removed an on average 23% of the 2 µm beads were recovered. Pseudo color magenta viosualization. (Fluorescent microscope-Zeiss AxioObserver Z1)

2.2.4 Bacteria with interferents with dual filter filtration

Methods

A similar test to that in subsection 2.2.3 was performed except this time, the target pathogen, *E. coli*, was included in the sample in substitution for the 2 µm beads. The 0.40 µm and 10 µm beads were diluted down to desired concentrations in the same way as before, while the bacteria were diluted down to three different starting concentrations of 10^8, 10^7, and 10^6 CFU/mL using 1× PBS. Three distinct samples were created by combining the interferents with one of the three *E. coli* starting concentrations. Once combined, the bead concentration for the 0.40 µm bead became 10^6 beads/mL and for the 10 µm bead, 6×10^5 beads/mL; for the bacteria, the concentrations were diluted down to final concentration of 3.33×10^8 CFU/mL, 3.33×10^7 CFU/mL, and 3.33×10^6 CFU/mL, in their respective mixes.

The procedure followed for the samples is the manual DFFS, the same as in the previous subsection where just the interferents were tested, and triplicate runs were performed for each of the three samples (biological triplicates). For the analysis, the focus was on the retentate recovery calculation for just *E. coli* since we had previously studied the bead recovery. As previously outlined, using qPCR following DNA extraction of each sample, each of the three pre-filtration (input) samples were analyzed in technical triplicates (each DNA sample was added to three distinct wells, 5 µL of the DNA sample per well). The post-filtration biological triplicate samples for each of the three different bacteria and bead concentration samples were analyzed once (no technical triplicates in the assay). Furthermore, for the recovery calculations, the post-filtration volumes were assumed to be the same as the pre-filtration volumes (1 mL).

Results

In Figure 22, the results for the tests can be observed where the x-axis looks at the pre-filtration bacteria DNA concentration, the y-axis looks at the post-filtration DNA concentration, and the gray line represents 100% recovery. Each point is an average of three data points and represents the three different bacteria concentrations tested. For the samples containing the bacteria concentration of 3.33×10^8 CFU/mL, the recovery average was 32%, for the samples with bacteria concentration of 3.33×10^7 CFU/mL, the average recovery was 33%, and for the final samples with 3.33×10^6 CFU/mL of bacteria, the average recovery was 25%.

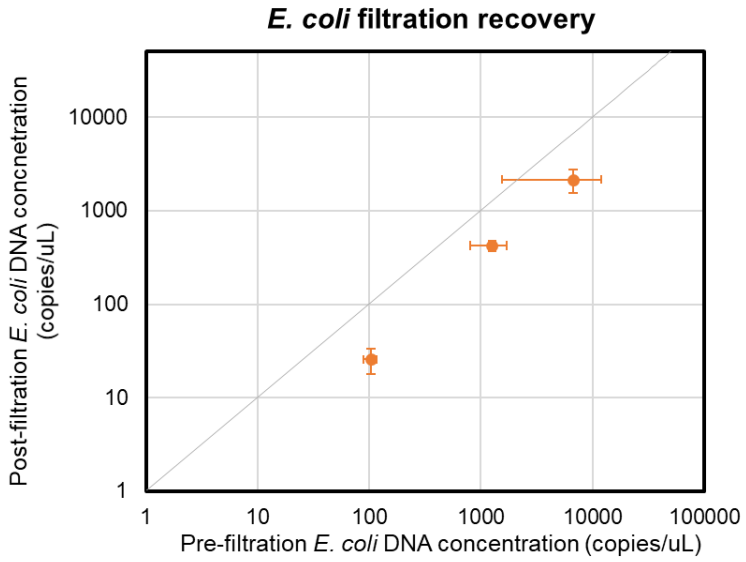

Figure 22. From left to right, the *E. coli* (at distinct starting concentration) average recovery from samples containing interferents: 25%, 33%, and 32%. Both axes are plotted in Log10. The gray line represents 100% recovery.

2.3 Concentration Results

2.3.1 Bacteria experiment with 0.22 µm pore size filter

Another important aspect in addition to purifying a sample is increasing the concentration of the target particle. We do this by capturing our target on a membrane surface and then reversing the flow direction of the liquid to resuspend the captured or retained bacteria. The efficiency of the procedure is assessed through the retentate recovery. Furthermore, one way to increase the concentration of the recovered bacteria is to decrease the volume bacteria are resuspended in. Thus, here, we investigate an optimal retentate recovery volume/backflow volume for our application with the use of the 25 mm diameter 0.22 µm pore size filter for our bacteria capturing and retention step. As shown in the previous subsection and in subsection 2.2.1, this smaller pore size filter will allow us to achieve a higher retentate recovery for the *E. coli* than the 25 mm diameter, 0.45 µm pore size filter.

Methods

The tests performed required the same procedure as that for the filter tests described in subsection 2.2.1 and outlined in Figure 13. A syringe pump running at 2 mL/min was used in each step to eliminate variability in flow rate caused by manual execution. Furthermore, the 5 mL syringe contained an input volume of 5 mL of bacteria instead of a 1 mL. We switched to a larger input volume to mimic a more realistic volume that the filtration system would receive from an upstream sample collection system.

The bacteria concentration was 10^7 CFU/mL suspended in 1× PBS, and five distinct 1× PBS backflow volumes, in increments of 300 µL (300 µL, 600 µL, 900 µL, 1.2 mL, and 1.5 mL), were evaluated for retentate recovery and increased bacteria concentration. For each volume, triplicate runs were performed, and for each run, a new, primed syringe

filter was used. After the runs, the retentate volumes were recorded, and the respective volumes per run, for both filtrate and retentate, were used to perform recovery calculations.

Statistical analysis

Due to not all data sets meeting the normal distribution assumption, the nonparametric Kruskal-Wallis (KW) test was used. The technique helped assess any statistically significant difference in the concentration of *E. coli* in the retentate as a function of the backflow volume.

Results

Varying the backflow volume yielded statistically significantly differences in concentration for varying backflows. In Figure 23, for each retentate recovery volume, all biological and technical triplicates were plotted. Using the statistical analysis method described previously, it was found there was a significant difference between the 300 µL and 600 µL backflow volume results ($p = 0.023$), between the 300 µL and 900 µL results ($p < 0.001$), and between the 300 µL and 1.2 mL results ($p < 0.001$). All other comparisons yielded not statistical difference.

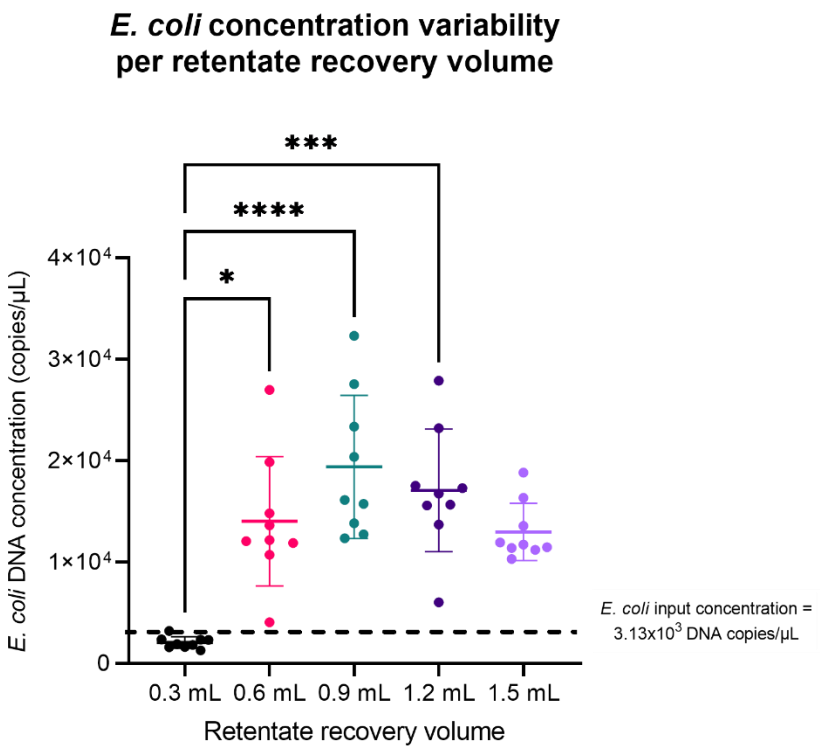

Figure 23. Five distinct volumes were used for retentate recovery of *E. coli* from the surface of a 25 mm diameter, 0.22 µm pore sized PVDF syringe filter. Triplicate runs for each volume were performed and technical triplicates for each run were analyzed and plotted. Comparing the *E. coli* DNA concentration as a function of the retentate recovery volume, there was a statistically significant difference between the following groups: 300 µL vs. 600 µL ($p = 0.023$), 300 µL vs. 900 µL ($p < 0.0001$), and 300 µL vs. 1.2 mL ($p = 0.0002$). The dotted black line represents the baseline or input bacteria concentration prior to the experiment.

The DNA concentration values of each technical triplicate per biological triplicate were averaged. Then, to obtain the concentration factor (equation (3) as described in the section 1.4 Nomenclature) each of the three retentate concentration (output concentration) values were divided by the bacteria DNA concentration of the input.

$$\text{Concentration factor} = \frac{\text{Concentration}_{\text{Retentate}}}{\text{Concentration}_{\text{Input}}}$$

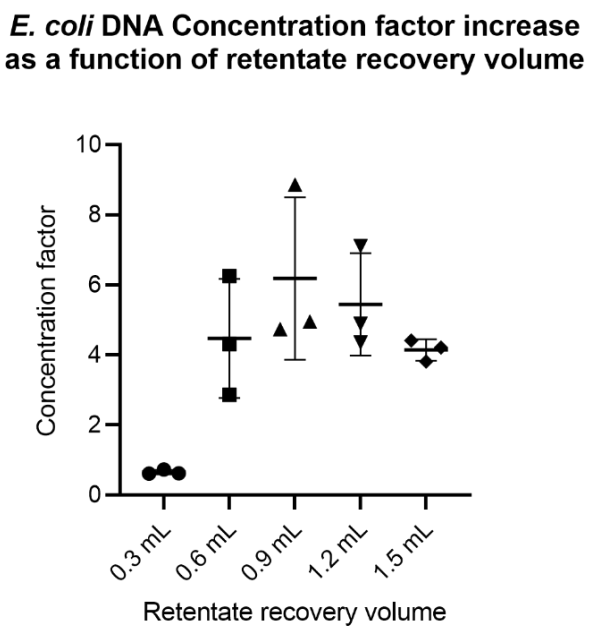

Figure 25. The concentration factor for each retentate volume follows the same trend as the concentration data, as expected. Concentration factors between 4-6× can be achieved.

The results in Figure 25 show that anywhere from a 4-6× concentration factor increase can be achieved. Furthermore, observing the recovery of the *E. coli* per retentate recovery volume in Figure 24, recovery was above 80% for the volumes 900 µL and above.

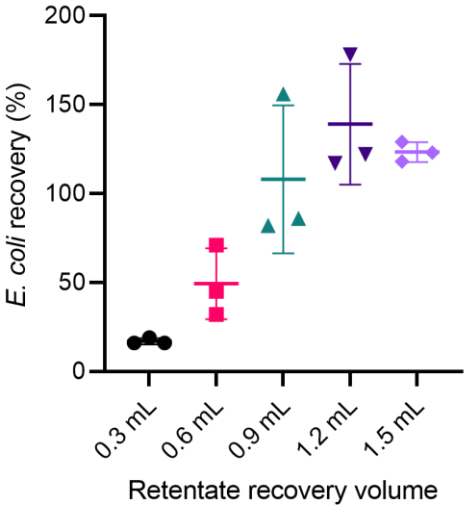

Figure 24. *E. coli* recovery was above 80%, and at times over 100%, when 900 µL or more were used for a backflow step for retentate recovery.

2.4 Automation

A key aspect of creating a system for quick, less labor-intensive pathogen identification is the automation of such systems. Automating helps decrease human labor required, save personnel time for the performance of other immediate tasks, and can help standardize a process, thereby eliminating any extra variability that comes from human handling. When the double filtration system was done manually, one run took 3-5 minutes, though literature reports 2 minutes [85]. Nevertheless, there were variabilities between runs with aspects such as the pressure applied and the flow rate under which each liquid was pushed through the filter. By automating the system, we ensure each sample undergoes the same process. Furthermore, we can optimize the design, such as by easily control the running time for the procedure.

2.4.1 Dual filter filtration system design (DFFS)

The DFFS automated system is composed of a variety of easily attainable materials in addition to the PVDF, 25 mm diameter smaller pore sized filters (0.22 µm, 0.45 µm) and the larger pore sized filter (5 µm) described previously. Two 3-way rocker valves (#BU-244696, Darwin Microfluidics, Paris, FR) help control the direction of the flow with three syringe pumps (Harvard Apparatus, Holliston, MA) controlling the flow rate of the liquids. EVA plastic tubing with an inner diameter of 0.02” and an outer diameter of 0.06” (#1883T1, McMaster-Carr, Elmhurst, IL) was used and connected to the filters through the use of gage 23 (ID: 0.017”, OD: 0.025”) syringe needles (#75165A684, McMaster-Carr, Elmhurst, IL), one polypropylene, male luer adapter T-junction (#EW-45508-75, Cole-Palmer, Vernon Hills, IL), and male-to-male luer lock adapters (#EW-30800-14, Cole-

Palmer, Vernon Hills, IL). Additionally, valve fittings for 1/16" OD tubing (# UX-02020-75, Cole-Palmer, Vernon Hills, IL) were used to connect the tubing to the valves.

Figure 26 shows as schematic of the overall layout of the automation while Figure 27 is a more detailed look at the experimental set-up. A main driving parameter for the system design was the decrease of dead volume to ensure the majority of the sample was processed and passed on to the biosensor. For this, we chose the smallest diameter tubing available made of a semi-flexible material, compatible with aqueous solutions, that is often used for delicate and precision applications. This tubing dictated the syringe needles needed and the valves' fitting size.

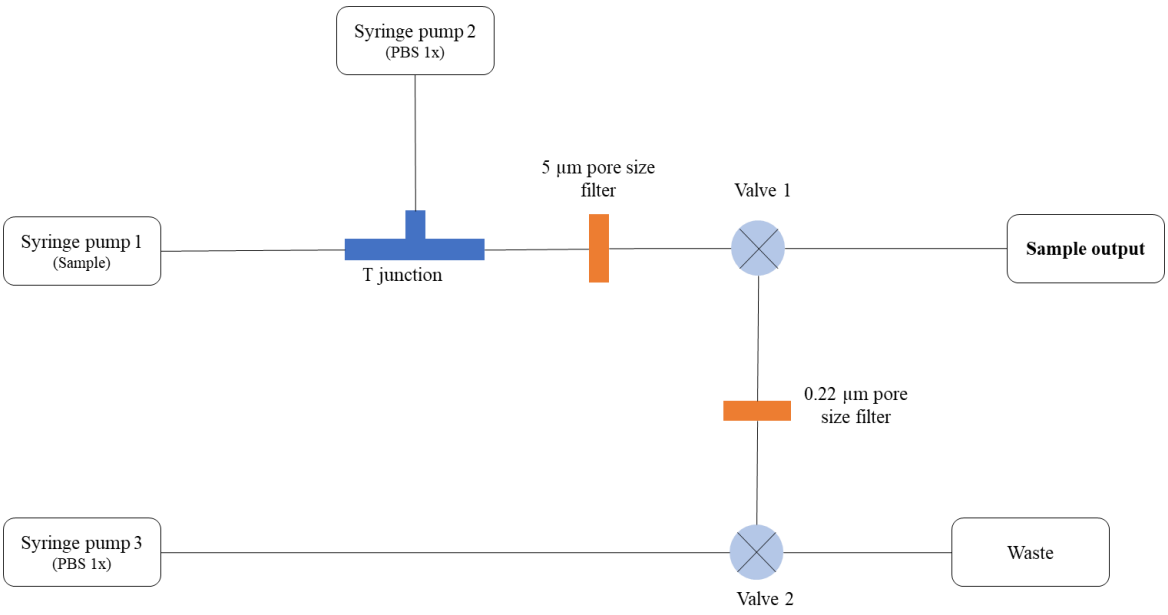

Figure 26. Double filter filtration system automation schematic.

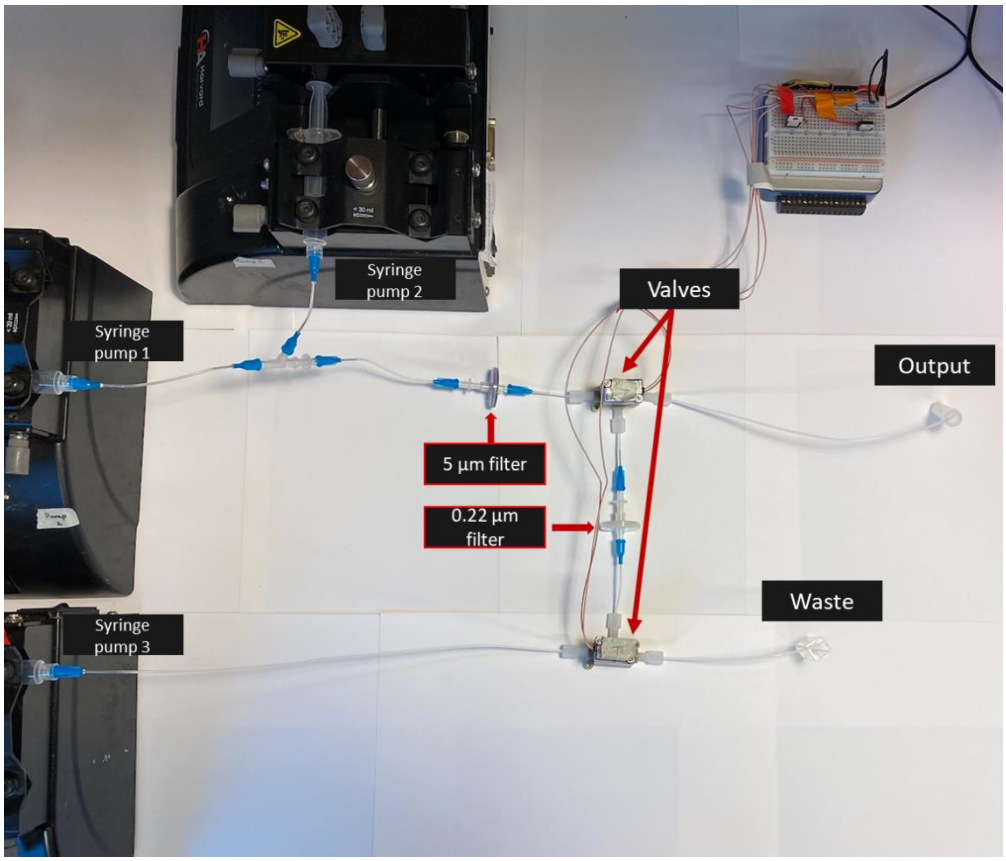

Figure 27. Experimental set-up for the DFFS automation.

For the automation, there are two configurations that it undergoes in one run. The first configuration (Figure 28A) is the purification and capturing step of the system. The sample passes the 5 µm filter, to eliminate larger sized contaminants, followed by the 0.22 µm filter where the bacteria is captured on the membrane surface. For the second configuration, shown in Figure 28B, the valve openings switch, and the third pump is activated to push the 1× PBS through the 0.22 µm pore size filter for retentate recovery.

When choosing the run time of the system, dead volume in the tubing was taken into consideration. To do so, the length of the tubing and the inner diameter of each piece of tubing was used to calculate the volume. For position A in the automation, we found that around 100-150 µL of the sample could be lost between the tubing and the T-junction before the PBS was added via pump 2 to ensure the bacterial sample was pushed through

the filters. If enough sample was available, we programmed the pump to push through 5.15 mL of sample to ensure a 5 mL sample volume made it through the filter. Similarly, for Position B of the automation, around 200 µL of dead volume was present in the tubing leading from the 0.22 µm pore size filter inlet to the system output. Because the output volume of the concentrated sample should be around 900 µL, the 200 µL dead volume would significantly impact the final sample concentration. As such, a semi-automated configuration was developed where, for position B, the pump was programmed to run for 15 sec to collect the 200 µL dead volume into one tube. After the 15 seconds, a pause was added to allow for a change in output collection tube. Then, pump 3 resumed for 27 seconds to push through 900 µL of 1× PBS for retentate collection. Overall, taking a 5 mL volume as the input volume, the entire system took around 5.5 minutes to run at a flow rate of 2 mL/min.

For cleaning, the optimal cleaning steps between wells involve washing with 70% ethanol, followed by DI water, and then with the last step of priming with 1× PBS, given that, prior to runs, all tubing is primed with PBS.

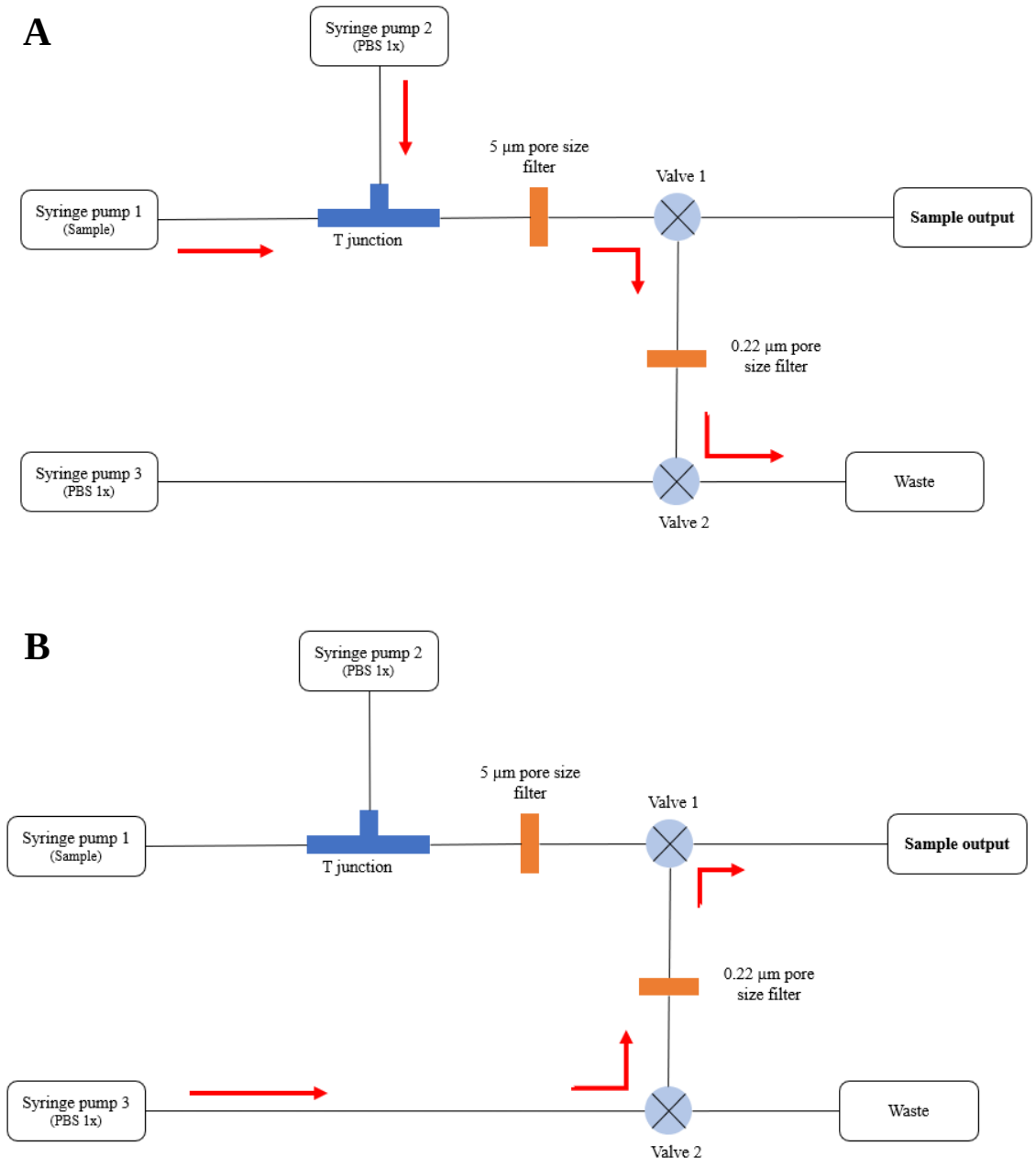

Figure 28. **A.** Position 1 of the schematic where the sample is pushed through the 5 µm filter for purification, followed by 1× PBS, and then through the 0.22 µm pore size filter where the target is captured on the surface while the rest of the volume goes to waste. The step takes 4.7 minutes. **B.** Position 2 of the system in which pump 3 pushes 1× PBS to execute a backflow step and reverse the flow direction through the 0.22 µm pore size filter for the recovery of the particles captured on the filter surface, i.e., retentate recovery. The step takes 50 seconds.

2.4.2 System control

To automate the system, all three syringe pumps were connected to a custom LabView program with the help of a 16-bit DAQ (USB 6002, National Instrument, Austin, TX). Harvard Apparatus provides an interface for syringe pump connections with LabView that we adapted. Furthermore, a valve control software was added to the program. Figure 29 shows the interphase of the LabView program where the pumps and valves can be individually controlled as well. For automation, an easy to set-up CSV file containing three columns is created an upload onto the LabView program. The three columns are Item, Value, and Units. The pump or valve being controlled is specified in the Item column while the time each item should be running for is specified in the Value column with the units being seconds.

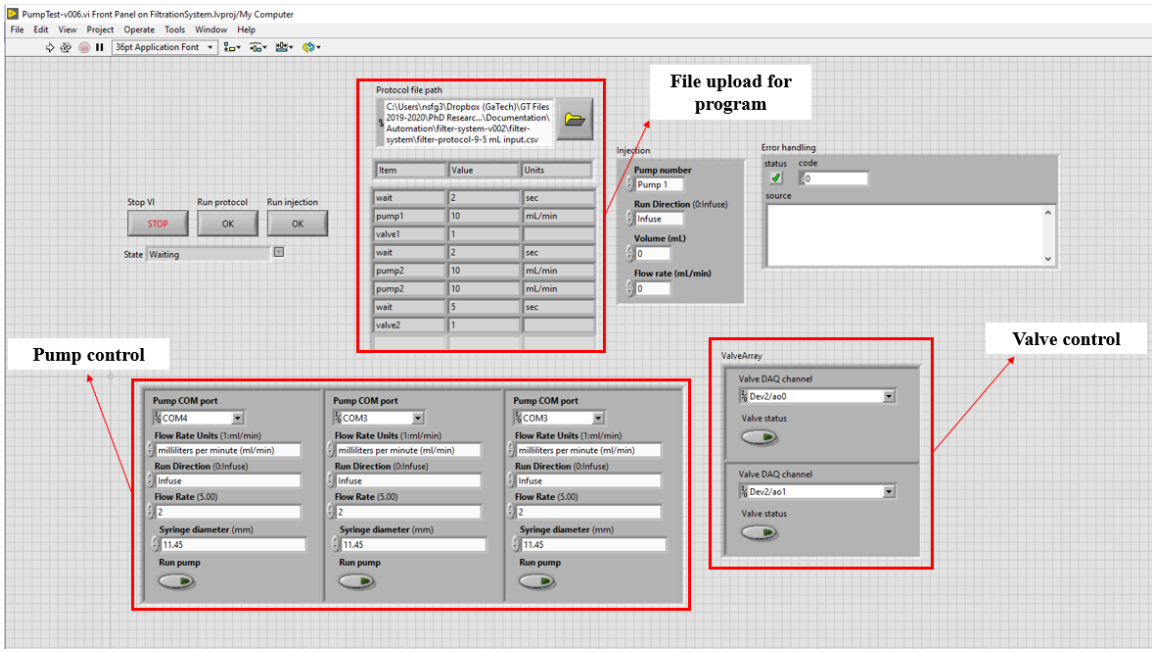

Figure 29. LabView program interphase for pump and valve control.

2.4.3 Individual interferents experiment

Prior to testing the automated system with our target pathogen, we tested the system with individual interferents, i.e., fluorescent beads sized 2 µm and 10 µm, to evaluate how the system works in the presence of these samples. The goal was to study how well the automated DFFS removed interferents.

Method

For these runs, a 0.45 µm pore size filter was used for the retention step since the tests were performed prior to optimizing the smaller pore size filter for our particle recovery. However, the system should work similar to that with a 0.22 µm filter given the smallest particle tested was a 2 µm bead. Once set-up, the automation for these runs took around 3 minutes given that the input volume was 1 mL, not 5 mL. Furthermore, the retentate recovery backflow volume was 1 mL as well since the goal of the study was to assess purification and recovery of the target, not to assess concentration factor increase.

The beads were diluted down to 10^6 beads/mL each, as previously described in other subsections, and the cleaning protocol consisted of DI water and later priming with 1× PBS in between runs. Triplicate runs per bead were performed with new filters for each run, and the results quantified using fluorescent microscopy as previously described.

Results

Figure 30 shows that the recovery for the 2 µm beads, when tested in the system, is on average around 5%

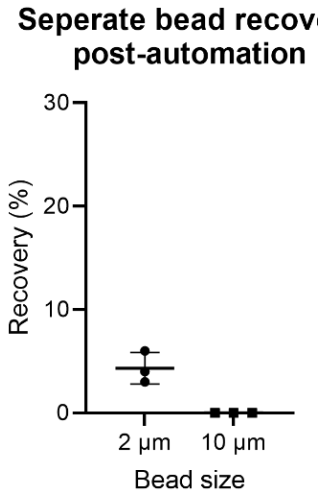

Figure 30. Around 5% of the 2 µm beads are recovered when tested individually while the samples containing only 10 µm sized beads show that essentially all the larger sized beads were removed.

2.4.4 Bacteria control experiment (0.45 µm filter and 5 µm filter)

Following the bead testing procedure, we performed the same test but just with our target pathogen, *E. coli*, to assess how well the system worked at recovering the target pathogen.

Method

Again, here, a 1 mL input volume of the sample was used along with a 1 mL volume for the retentate recovery step. The bacteria were diluted down to three starting concentrations using 1× PBS: 10^7 CFU/mL, 10^6 CFU/mL, and 10^5 CFU/mL. For each concentration, duplicate runs were performed (n = 2) with new syringe filters used for each run. For analysis, qPCR was used as described previously with the only difference being that each sample was analyzed once (one technical replicate) in the PCR assay. Thereby, these tests serve to give a general idea of what the system behaved like with the bacteria.

Results

Across all three data points, the bacteria recovery post-filtration from the system was anywhere from 19%-29%. Figure 31 showcases these values along with the standard deviation for the y and x-axis. The gray line in the graph represents 100% recovery.

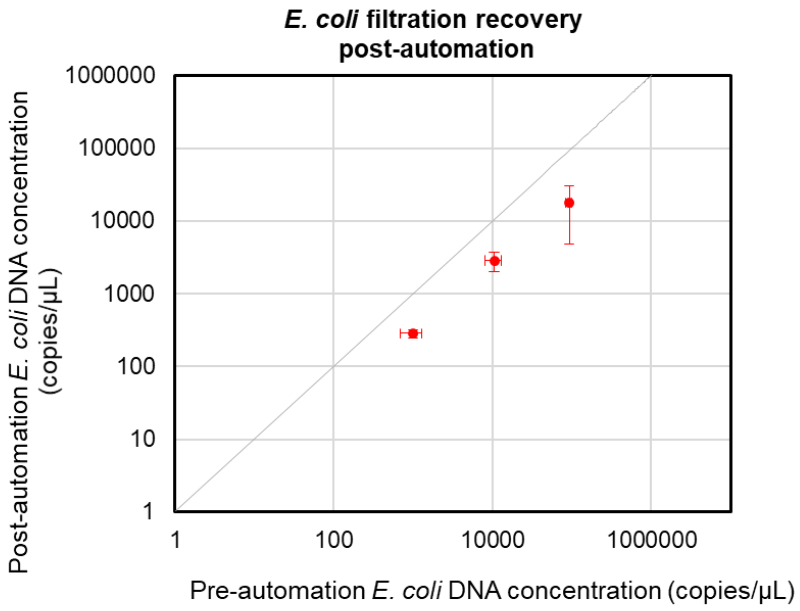

Figure 31. From left to right, the *E. coli* (at distinct starting concentration) average recovery from samples containing interferents: 19%, 27%, and 29%. Both axes are plotted in Log10. The gray line represents 100% recovery, and each point is an average of two data points corresponding to the duplicate runs.

2.4.5 Bacteria control experiment (0.22 µm filter and 5 µm filter)

With a new smaller pore size syringe filter in place for more optimal *E. coli* capturing, the control experiment for automation was repeated.

Method

The automated system here works as described in subsection 2.4.1., where the input sample volume was 5 mL, and the retentate recovery backflow volume was 900 µL. Furthermore, the dead volume present in the tubing was taken into consideration leading to the use of the semi-automated step, as previously described in subsection 2.4.1.

Triplicate runs for an *E. coli* concentration of 10^7 CFU/mL were performed, with new, primed filters being used for each run. Furthermore, for these samples, the qPCR was run as originally described, technical triplicates for the input or pre-automation samples and for the post-automation samples. To clean between runs, 1× PBS was used.

Results

Figure 33 shows the results of the bacteria DNA concentration pre and post automation (A) and how that translates to the recovery of the bacteria. In Figure 33A, all technical triplicates for all biological triplicates are plotted, Welch's t-test was performed to compare the two groups. Results showed a statistically significant difference between the pre-automation and post-automation *E. coli* DNA concentration ($p < 0.0001$), indicating an increase in concentration. Figure 33B then shows the recovery of the bacteria was on average around 60%. In addition, Figure 32 shows an average concentration factor increase of close to 4×.

The post-automation volumes (ideally 900 µL) were on average 913 ± 38.6 µL.

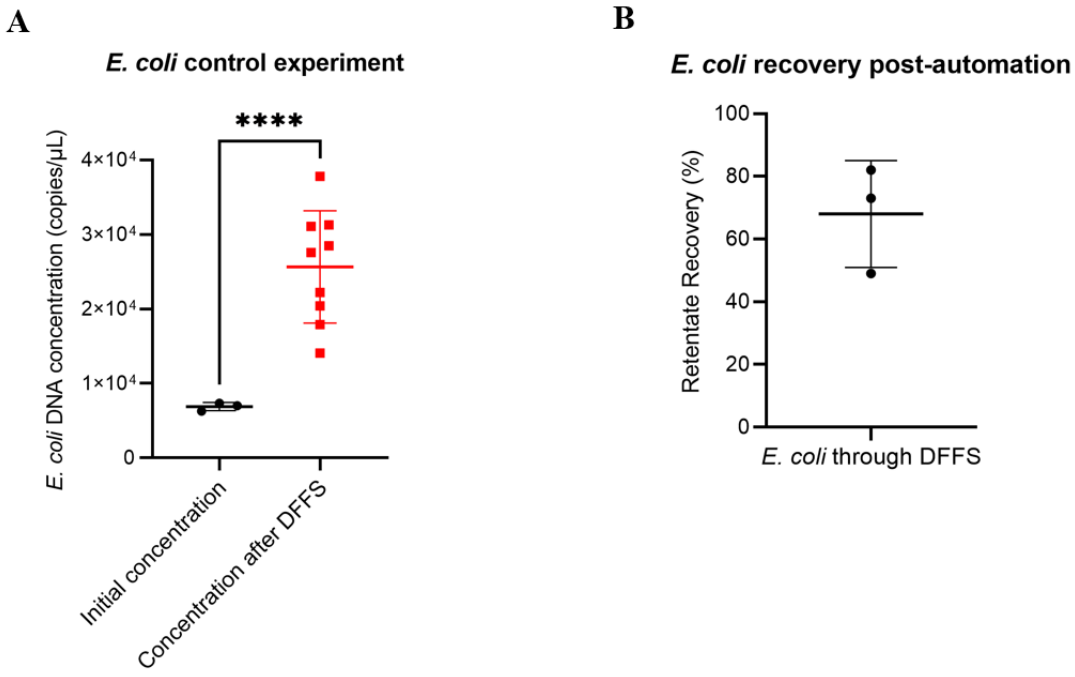

Figure 33. **A.** The pre-automation and post-automation *E. coli* DNA concentration values were statistically different from each other ($p < 0.0001$). **B.** The data is represented in the form of retentate recovery were over 60% of the bacteria was recovered with the automation run.

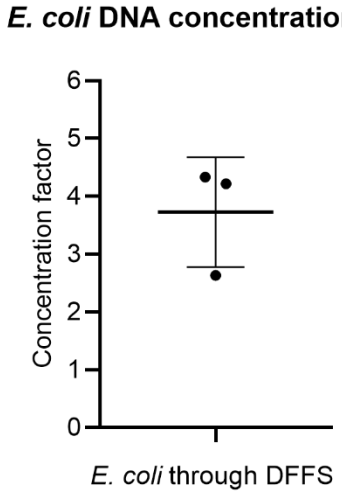

Figure 32. An average of approximate 4× concentration increase is achieved for the bacteria control experiment with the automated double filtration system.

2.4.6 Bacteria with interferents (0.22 µm filter and 5 µm filter)

Method

The automated system here works as described in subsection 2.4.1. and 2.4.5. This time, the sample consisted of bacteria mixed with interferents (2 µm and 10 µm beads). When mixed, the bacteria concentration became 10^7 CFU/mL while the bead concentration for each became 10^6 beads/mL. Of note, the beads for these runs were prepared slightly differently, they were prepared without the addition of Triton X-100. The removal of the surfactant would allow for little possibility of lysing the cell and would furthermore be more representative of a world sample were larger size particles might agglomerate and form clumps.

Triplicate runs were performed, with new, primed filters used per run. The cleaning step between runs consisted of 100% ethanol, followed by water, and then 1× PBS to prime the entire system. The qPCR mix for this experiment consisted of a similar mix as stated in the methods section with a difference of using 12.5 µL of 2× concentrated PerfeCta qPCR ToughMix (95112-012, QuantaBio, Beverly, MA) and 6 µL of nuclease free water to make up a 25 µL total volume per well. For these runs, beads were quantified using flow cytometry.

Results

E. coli concentration post-automation is shown to be statistically different than that from the pre-automation sample ($p = 0.021$), based on an unpaired t-test. This indicates an increase in concentration of the sample as can then be observed in Figure 34B, where there's an average concentration factor of 2×.

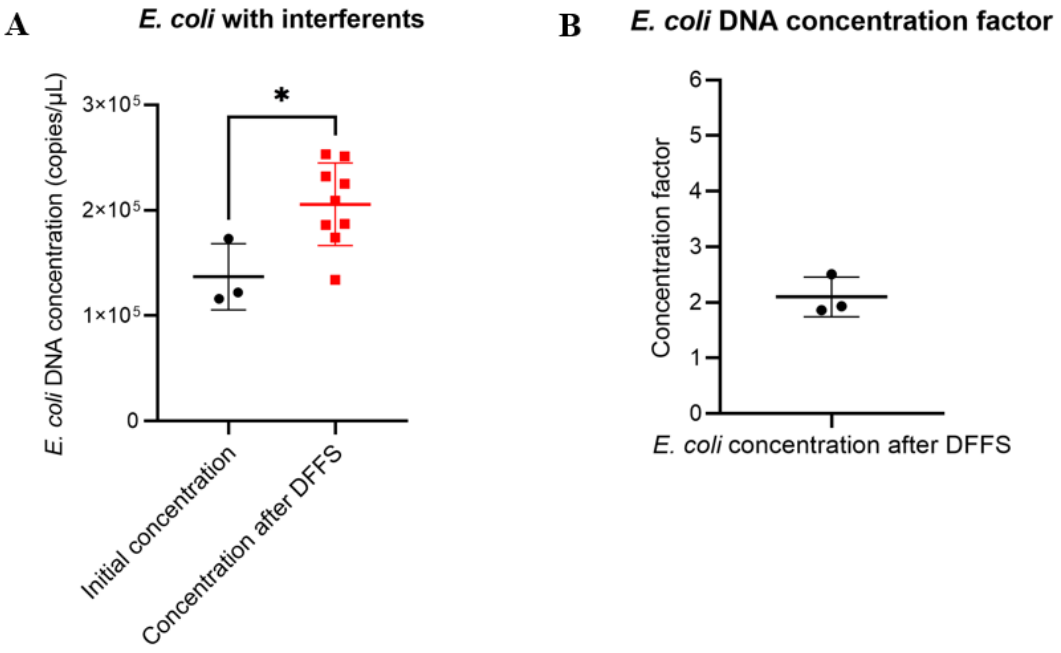

Figure 34. **A.** The pre-automation and post-automation DNA concentration values were statistically different from each other ($p = 0.021$). **B.** A 2× concentration increase is achieved for the bacteria in the presence of interferents with the automated double filtration system.

When observing the bacteria recovery in Figure 35A the bacteria of the recovery is on average around 40%. Furthermore, Figure 35B allows us to observe that over 95% of the interferents are moved from the sample after going through the automated system. Taking these factors into account, we get a 42 ± 13-fold enrichment improvement ($n = 3$).

The post-automation volumes (ideally 900 µL) were on average 958 ± 8.5 µL.

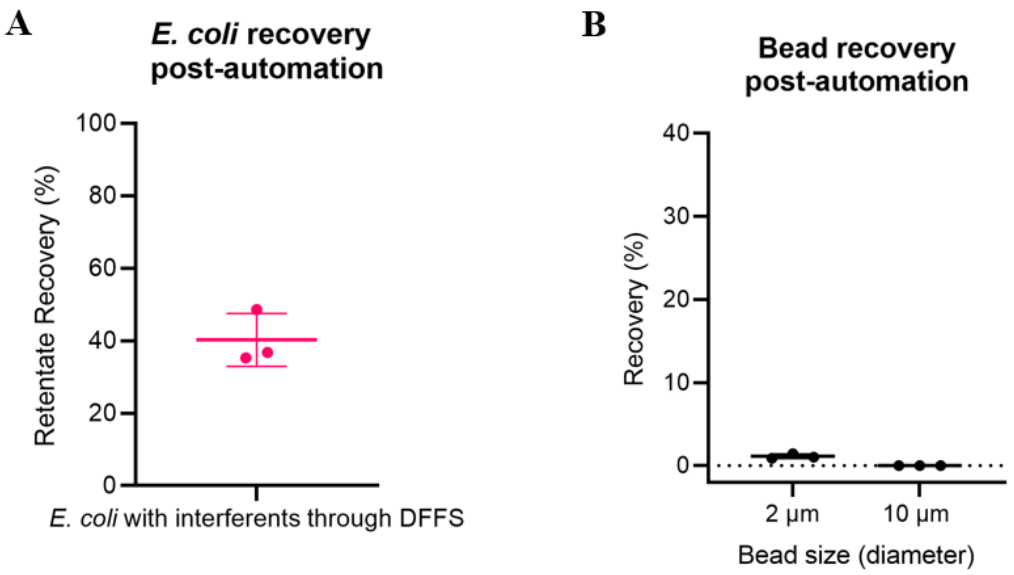

Figure 35. **A.** The data is represented in the form of retentate recovery. On average, 40% of the bacteria was recovered with the automation run. **B.** Over 95% of interferents are removed from the sample using the automated double filtration system, per the 150 µL (16%) of the post-automation volume analyzed.

2.5 Discussion

As expected, the smaller pore size filters yielded higher recovery values for the retentate than the filtrate while the opposite was true for the larger pore size filters. Results also serve to support the use of PVDF for the filter material because as outlined earlier in this work, it is an excellent choice due to its high non-specific binding, high flow rate compatibility, and compatibility with organic and aqueous solvents.

Observing the 10 µm pore size filter, a similar average filtrate recovery percentage as for the 5 µm filter was observed but with a larger standard deviation. Given that the pore size is twice as large, we would expect a larger recovery value. This suggest the membrane material could be influencing the results. Studies, such as Zhang et al.'s, [85] have found that there are materials that could be incompatible with a target pathogen. For example,

they found cellulose acetate recovered a low number of bacteria (*E. coli*) in the filtrate as compared to other same pore sized filters with different material pore size [84]. In the case of the evaluated 10 µm pore size filter, polypropylene might not be compatible with our sample given that this material is hydrophobic, and its hydrophobicity might be what is resulting in the lower and more varied recovery numbers. To improve its performance, isopropanol could be used to switch its hydrophobicity to hydrophilicity [72] or a different membrane material could be searched. Yet, the current results might not be enough to definitively conclude that the difference in material is what is causing the 10 µm pore size filter to have an on average lower retentate recovery of the bacteria as compared to the 5 µm pore size filter.

To reach an appropriate conclusion, we would need to perform a test where the same set-up is kept, but we additionally test the performance of a 10 µm pore size filter made of PVDF and a 5 µm pore size filter made of polypropylene, and then compare those results to the previous work. By performing this 2-by-2 comparison, we would be able to reach more definite conclusions with regards to the possible effect of membrane material on recovery. This test was not performed due to time and resource constrictions but moving forward would be appropriate to execute. However, based on the results we did obtain, we chose the 5 µm pore size filter for optimal bacteria retentate recovery. Furthermore, this filter would be the same material as the other small sized filters which eliminates any potential variability attributed to membrane material. In addition, the smaller pore size will allow for exclusion of larger interferents in comparison to the 10 µm pore size filter.

Of note, there are other larger pore size filters available in the market, such as 2 µm and 8 µm pore size. However, they were not chosen for a variety of reasons. The 5 µm pore

size filter was chosen over the 2 µm pore size filter for a factor of safety for the bacteria. Given *E. coli* has a diameter that can range from 0.5 to 1 µm, using a pore size too close to the upper limit of the bacteria diameter could interfere with the filtrate recovery of the bacteria. This is due to pore sizes not all being 2 µm in diameter and thus potentially being smaller and trapping the bacteria inside not allowing it to go fully through. As for the 8 µm pore size, they are harder to find in the market at a desired diameter and material, so, we instead went with a pore size representative of the 10 µm particulate matter group (PM_{10}).

Shifting our focus to the smaller sized filters, we observed no significant difference between the recovery when using a 13 mm diameter versus a 25 mm diameter. Thus, though potentially holding larger dead volume, the 25 mm diameter was chosen in order to allow for higher flow rates [88]. Then, comparing the 25 mm diameter performance of both the 0.22 µm and the 0.45 µm pore sized filters, we observe that the 0.22 µm filter would be a better choice for our application as it yielded a higher average filtrate recovery though we found no statistically significant difference between the results of the two differently pore sized filters. Thus, the 0.22 µm filter was determined to be the optimal choice for target capturing and retentate recovery. This was similarly to what was observed in previous studies [85].

After testing our filters with bacteria, we chose to evaluate a larger and smaller pore size filter with individual interferents, i.e., fluorescent polystyrene beads, and found that the 0.45 µm pore size eliminated the 2 µm and 10 µm beads while the 5 µm pore size filter recovered around 40% of the 2 µm beads in the filtrate, leading us to conclude the remaining percentage is lost inside the filter and filter casing. Reasons for this might be that the bead size is too close to the nominal pore size, and variabilities in the pore sizes

could be influencing the trapping or release of these size beads. However, treating the 2 µm as an interferent would mean the 5 µm pore size filter is an effective filter for removal of interferents. Furthermore, when the 0.45 µm and the 5 µm pore size filters were used together for the manual dual filter filtration system (DFFS) run, we observed, from a limited data set (n = 2), that around half of what was previously recovered for the 2 µm beads are recovered here (20%). This extra loss could mean that the beads are not only getting removed with the 5 µm pore size filter, but also with the 0.45 µm pore size filter during the retentate recovery step. However, given this test contained a sample composed of a mix of beads, it could also be that its interaction between the beads might have caused some clogging on the 5 µm pore size filter surface, leading to a lower 2 µm bead recovery.

The execution of these manual test highlighted the need for a more accurate aspiration step execution to ensure the full 5 mL sample went through the 0.45 µm pore size filter (Figure 19, step #3 of DFFS), as there was variability in the amount of volume aspirated for the 0.45 µm pore size filter aspiration step that could affect overall sample recovery.

Shifting our focus to the automation runs, the manual aspiration step problems are addressed because the set-up ensures the full sample goes through the inlet of the smaller pore sized filter, eliminating the variability present in this step when performed manually. Once the set-up was established, for the automation runs testing beads individually, only the 2 µm beads were recovered, ~5% of them. The system was then updated to use the smaller pore size filter, 0.22 µm, for retention, versus the 0.45 µm pore size filter used prior, and then challenged with a sample containing bacteria with beads. Results yielded the 2 µm bead recovery was even less than 5%. This lower recovery in the automation could be attributed to loss of beads inside the tubing and valves. It is of note that the sample

did not contain additional surfactant. This lack of additional surfactant tends to cause agglomeration of the beads which could cause then cause them to be bigger than the 5 µm thereby eliminating them and contributing to the lower bead recovery. Treating the 2 µm beads as interferents, then this is beneficial for our system, we want to eliminate as much of it as possible.

Now, focusing on bacterial recovery, manual DFFS with bacteria and interferents (section 2.2.4), where the 0.45 µm pore size was used for retention, yielded an approximate *E. coli* recovery of 30% when tested with different starting concentrations. This suggest the system performance was relatively constant regardless of the starting target pathogen concentration. However, the low recovery might suggest that the bacteria might be getting lost inside the filter through absorption, as we observed in the filter matrix test, since the 0.45 µm pore size might be too close in size to that of the target pathogen, *E. coli*. *E. coli* has a diameter that can vary between 0.5 µm and 1 µm, which could be causing some of the bacteria to penetrate the filter deeper than the membrane surface and therefore, not be collected in the retentate when the backflow step (Figure 19, step #4) is implemented.

In an automated set-up of the experiment, using the 0.45 µm pore size filter for retentate recovery, the bacteria control experiment yielded slightly lower recovery values to that of the manual runs with interferents. This is interesting given for this sample had no interferents, but it might suggest the automated system can work similarly to a manual run yet there is some loss of bacteria occurring. The extra loss could be coming from how the volumes were handled with the dead volume present in the system. Furthermore, the recovery for the bacteria is still low and from the filter matrix results, we know then that the adequate filter choice for retentate recovery is the 0.22 µm pore size, 25 mm diameter

syringe filter. Thus, switching the automated system set-up to have the 0.22 µm pore size filter, and performing another control experiment of just *E. coli*, results yielded an average recovery of a bit more than 60%. These results are around twice as much as with the 0.45 µm filter, thus confirming this pore size filter is the optimal choice for our target pathogen and system.

Adding to these automation experiments, we tested the system with the bacteria with interferents to showcase a sample with a contaminant matrix that is more representative of a real-world sample. Under this load, the automated DFFS's recovery for the bacteria went down to around 40% while over 95% of both size beads were removed from the system, yielding an enrichment factor increase of 42 ± 13-fold. In work by Isabel et al. [86], the original inspiration for pursuing the automation of a dual filter filtration approach, they tested their manual approach on *B. atrophaeus* subsp. *globigii* spores under different powdery conditions. They were able to recover 51 ± 17% of the bacterial spores while in comparison we recovered 40 ± 6%, about 10% less on average. Yet, it is important to recall differences between the two works which involved the use of different interferents, different target pathogens, different quantification methods, as well as the handling of the procedure manually (Isabel et al.) versus the automated run for us. The target pathogens used for both works had comparable diameters and shape, therefore, the factor that could be affecting results the most is the type and amount of interferent used as well as the handling process. Nevertheless, it shows that the physical purification and concentration approach using syringe filters can be successful at recovering pathogens from different contaminant matrices whether performed manually or in an automated fashion.

The decrease in recovery of the bacteria in our automated system could be due to its interaction with a highly agglomerated interferent matrix since the beads mix contained no surfactant to monodisperse them. The agglomeration could lead to increase caking or fouling in the membrane which could have influenced the decrease in bacteria recovered. Yet, there are other reasons to explore that would help explain, in general, why we may get varying bacteria recovery per experiment under similar conditions or why the standard deviations for the recoveries may vary.

The gram-negative property of the organism of choice, *E. coli*, could be affecting the recovery we are calculating. Studies have found that whether bacteria are gram-positive or gram-negative is the most important parameter in determining cell wall flexibility. The cell wall structure, specifically the cross-linked polymer layer, peptidoglycan, is different for these two types of classifications, with a gram-positive bacterium having a thicker layer (20-80 nm) and a gram-negative bacterium having a thinner layer (2-6 nm). The thinner layer makes the bacteria more elastic and therefore, more deformable, and likely to pass through pores of smaller sizes than its size. Thus, this could be another explanation for why, on average, the recovery for a 0.45 μm pore size filter isn't as high while, for the 0.22 μm pore size filter, recovery is higher. It should also be noted that these more deformable organisms can construct a more compact and higher resistance cake leading to a filtration flux decrease and potentially lower recovery. [72]

Our analysis technique is an additional aspect worth exploring that could help explain variations and standard deviations in some of the recoveries calculated in this work. The qPCR analysis process carries with it potential for variability through various means. The manual steps involved with DNA extraction and then sample preparation of the qPCR assay

require precision and consistency. Yet, things like pipetting errors will occur and contamination could happen if samples are not treated properly. Furthermore, reagents need to be properly diluted with a nuclease free water and they must be kept at a cold temperature when outside the freezer. All this variability can ultimately affect the final concentration calculated per sample and thus the results we analyze.

DNA quantification specifically, can be one of the biggest causes of error in organism nucleic acid recovery. Performing this step manually, with a larger number of samples at a time, can lead to inconsistencies in the process between samples and thus varying recoveries of DNA per sample. This is due to the varying steps that are carried for each sample to reach the final product of extracted DNA. For each step, there are pipetting errors that could also accumulate. The variabilities in this process are then reflected in the qPCR results, such as when we achieve above 100% recovery.

Studies have been conducted to see how uncertainty in qPCR can affect results with two of those main sources of uncertainty being the measurement of the threshold cycle (Ct) value, and the predicted DNA content of the unknown sample from the standard curve [115]. An alternate method like bacterial plating would help eliminate much of this variability but would take more time and resources to perform and could only give us information on viable cells. On the other hand, qPCR could allow for the detection of a target pathogen present at low concentrations in a sample, but the assay requires optimization to ensure this is the case. In all, controlling the environment where the qPCR is executed is important to ensure little chance of contamination. Furthermore, it is important to vortex and mix the bacteria sample prior to DNA extraction, and the extracted DNA prior to qPCR, in order to ensure the samples are dispersed and an equal amount of

the sample is added to the mix. Steps in the qPCR procedure should also be standardized, such as the creation of a batch of the assay without the addition of the DNA prior to adding it to the qPCR plate. This is best practice to eliminate variability coming from inconsistency in mixing that could arise if the assay was mixed into each well individually. Furthermore, it can also account for pipetting errors.

qPCR has been used in other studies for quantification [66], but it is important to remember that the standard deviations in the qPCR calculated concentration values can attribute to significant variations in the recovery values calculated. This might explain why, for the same filter and same organism, the recovery values varied across different experiments. However, this technique is still highly quantitative and beneficial for showing us the performance of our system.

In addition to controlling the cleanliness and steps when doing qPCR to ensure the most accurate results possible, there are other measures we could be taking during experimentation to optimize recovery, the first of which is the addition of surfactant to our bacteria samples.

The manual runs with bacteria and beads discussed earlier (section 2.2.4) that yielded recovery values between 25%-32%, were samples that contained around 0.002% of TritonX-100 (surfactant) to ensure the beads in the sample acting as interferents would be monodispersed. The other experiments conducted with beads, specifically those experiments that included the use of a 0.22 μm pore size filter, did not include surfactant in the sample. The surfactant was added to the output samples in order to analyze the beads with flow cytometry and/or fluorescent microscopy. With regards to surfactant, literature has stated that, for TritonX-100, even just around 0.1% would be enough to lyse up the cell

[116]. However, the results from the earlier work mentioned, suggest that less than 0.01% could be used in the sample and help with system performance. This could be hypothesized since the manual dual filtration system with the 0.45 µm pore size filter performed better than what was observed in Figure 15B results from the filter matrix experiments where surfactant was not present in the samples. Other authors have also used surfactant, specifically 0.002% Tween 20, with their *Salmonella enteric*a serovar Enteritidis samples [66]. They recommended the use of surfactant as it can help lower the interfacial tension between the membrane surface and the attached cells which can help improve retentate recovery. Thus, moving forward, the addition of this element could be implemented to see if enhance recovery is observed.

Another potential approach that could be implemented in the system is the addition of quick back pulses. These pulses would be introduced by quickly and alternately changing the direction of the flow to help generate vibrations, this would then help remove any fouling on membranes that might have been created. This could help increase pathogen recovery as studies conducted have shown [84].

Aside from target pathogen recovery, target pathogen concentration is important for preparing a sample for downstream biosensor detection. Figure 23 shows the *E. coli* concentrations as a function of varying backflow or retentate recovery volume of 1× PBS used to recover the bacteria captured on the 0.22 µm pore size filter from a 5 mL input volume. Results follow an almost parabolic shape; however, statistical analysis shows only a few pairs are significantly different from each other. More runs would need to be performed to further study if a significant, parabolic shape exists. Yet, the results do make it clear that a volume below 600 µL for this system should not be used as it will yield lower

concentration values. Furthermore, a volume of greater than 1.2 mL should not be chosen either as it yielded a non-significant concentration difference when compared to the 300 µL results. Observing the concentration values obtained with the 900 µL volume, it had the largest statistical difference with the 300 µL concentration values, hinting at this being a good choice for optimal concentration of the sample.

Comparing the results to similar work in the literature, Isabel et al. [85] did not find a statistically significant difference between the use of a water or 1× PBS volume of 300 µL, 500 µL, and 1 mL for their spore recovery. Though different volumes, our results agree in that the values ranging between 500 µL and 1 mL did not yield statistically different results from each other. However, for us, results for the 300 µL volume were statistically different as compared to results from volumes in the ranges of 500 µL to 1 mL. Differences arise in the experimental methods, such the use of different materials, and that could explain the difference in results. For example, their work used a different filter (0.45 µm pore size, 13 mm diameter), but of the same material as us (PVDF), and a different target pathogen (*B. atrophaeus* subsp. *globigii* spores) that, though have a similar size (0.92 to 2.27 µm by 0.53 to 1.11µm) [85], might differ in surface chemistry. Furthermore, procedure variability, such as the constant pressure and flow rates applied to the filters on each run, and analysis variabilities through qPCR or bacterial plating, could all contribute to slightly different results.

Another group that used the same *E. coli* strand as this work, performed a study on concentration using the same 0.22 µm pore size filter but with a smaller diameter. Testing three different starting *E. coli* concentrations, in a sample where the bacteria was mixed with urine, the authors verified that the 10-fold dilution in volume (from 2 mL to 200 µL)

was met with the bacteria concentration. They found that for all three different starting concentrations, they were close to achieving the 10-fold increase in concentration as expected. This approach is different than our concentration approach, but it serves as motivation to test our automated system with varying starting *E. coli* concentrations to see if the performance holds. [85]

Moving on to discuss the concentration factors achieved in this work, the concentration factors for the volumes from 600 µL to 1.2 mL were similar and ranged on average from around 4-6×. This is lower than what other work has achieved for recovery, where a 10-fold concentration increase occurred.

Furthermore, observing the *E. coli* recovery percentages, high recoveries, above 50%, for the bacteria are achieved. For both the 1.2 mL and 1.5 mL values, above 100% recovery is achieved. The variability in the DNA extraction and qPCR procedure could help explain the above 100% value, as previously discussed. Other works that have used qPCR as a quantitation technique have also encountered results like these and have attributed it to relative standard deviations [19].

Based on the results observed, the 600 µL, 900 µL and 1.2 mL volumes would be adequate choices for the bacteria concentration. Yet, the recovery data then showed that between the three volumes, the 900 µL and 1.2 mL volume yielded the highest bacteria recovery. But, when observing Figure 20, as mentioned earlier, the 900 µL volume had the largest statistical difference with the 300 µL concentration values. Based on these results, the 900 µL was chosen as the optimal volume for concentrating our sample from a 5 mL input. This volume would also help meet the microliter volume required for FET sensing. The 900 µL volume was then implemented into our automation experiments, as previously

discussed, and the output volumes were 958 ± 8.5 µL, so just a slight variability in performance as to be expected. We used the semi-automation approach (where we manually switched the output collection 1.5 mL tube) to ensure the dead-volume of the system was collected in a separate tube than our concentrated sample. Results (not shown) yielded that no bacteria were present in the dead-volume output samples collected, thus, indicating the run time for dead-volume collection was accurate at solely removing the PBS present in the tubing.

Moving forward, for repeatability of the target pathogen purification and concentration per run, one key aspect in ensuring constant performance of the system, especially the automated system, is cleaning. In this work, we found it important to properly clean tubing between runs using 70-100% ethanol followed by DI water and later primed with the 1× PBS [19]. Failure to do so will lead to decrease automation performance via decreasing bacteria recovered per subsequent run. This is especially true in samples where there are bacteria present with interferents, since, as we hypothesized from earlier results, some of the interferents that do not get removed by the 5 µm pore size filter, remain within the system's tubing. Another point to ensure each run is standardized is to ensure that the placement of filters in the automation are consistent. The filter should be placed in the direction from inlet to outlet to ensure the sample flows through the inlet first, as it would in a normal syringe-syringe filter configuration. This would mean that for retentate recovery, the backflow volume enters through the outlet of the syringe filter and goes out through the inlet. Furthermore, the filter position relative to gravity can have an impact on how the filter performs since the fluid displacement across the filter is affected. But the effect of such placement was not studied here.

2.6 Conclusion

Filter material and pore size are important parameters to ensure adequate and efficient pathogen filtration or retention, and our results allow us to reach various conclusions. The first is that PVDF material works well for our bacteria recovery. The second is that smaller pore size filters allowed for the capturing and retentate recovery of bacteria. In this case, the 0.22 µm pore sized filter was the better choice to ensure a lower possibility of the target pathogen penetrating the filter deeper than the membrane surface and thus allowing for higher retentate recovery. Thirdly, we also investigated whether filter diameter could impact results and observed from our data that the diameter yielded a none statistically significant difference in recovery of the bacteria. All these facts allowed us to conclude that the 25 mm diameter 5 µm pore size filter was the optimal choice for highest filtrate recovery while the 25 mm diameter 0.22 µm pore size filter was the best for retentate recovery. Both filters contain a PVDF membrane, and the 25 mm diameter permits higher flow rates [88], making this amenable for automation.

The dual filter filtration system (DFFS) can be run manually, but when automated, in 5.5 minutes, at a flow rate of 2 mL/min, it can concentrate a 5 mL input sample of bacteria by a factor of 2× and recover, on average, 40% of the bacteria while removing over 95% of the interferents and yielding a post-automation volume of 958 ± 8.5 µL. This then results in an enrichment factor of 42 ± 13-fold (n = 3).

For the automated system, the run time can be adjusted easily through the custom LabView program. Furthermore, the semi-automated step included to account for dead volume in the output is easily automatable by adding an extra valve right before the output

that would redirect the volumes after a certain run time or by automating a platform, separate from the DFFS automation, that can switch collection tubes when indicated.

There is room for improvement, but seeing the results for this automation run, we can conclude the system is effective, to a certain extent, at both purifying and concentrating our target pathogen when mixed in a high interferents matrix. Approaches that could be taken to improve the performance could focus on removing possible caking and fouling from the membrane surface via pulsing, adding a small percentage of surfactant to encourage *E. coli* detachment from the filter membrane, and further standardizing the qPCR quantification process as much as possible.

Overall, the results discussed confirm that a sized based, physical mechanism can be used for bacterial purification and concentration under cleaner samples or highly contaminated samples. Furthermore, the process was successfully automated and showed promising results for bacterial recovery, purification, and concentration.

Future work

To further progress this research, various optimization works can be done. The same material type but from different manufacturers could be tested and compared to those evaluated in this work to determine the best filter on the market for our application. Manufacturers each have a slightly different fabrication method, so their filter performance will vary. Furthermore, it can be studied how a higher or lower flow rate than 2 mL/min could affect retentate recovery and the time it would take the system to run. For investigating possible trends between the retentate recovery volume and input sample volume for concentration, the same retentate recovery volumes as before would be used

but with varying input volumes larger than 5 mL such as 10 mL, 15 mL, etc. to see if there is a relationship that holds throughout.

To enhance bacteria recovery, the addition of 0.002% of surfactant to the bacteria sample should be explored and similar tests to those discussed in this work would be re-conducted in order to compare the bacteria recovery across the two conditions and reach a conclusion. Additional work that could be done with *E. coli* is to test the automated system with different starting concentrations of the bacteria but with the same interferents concentration to see if the recovery percentage holds or to verify at what *E. coli* starting concentration point the performance of the system drops. Furthermore, the beads could be substituted with interferents more representative of the real-world contaminants such as dust and pollen that could be acquired from NIST.

An additional automation configuration to test that could help minimize caking and fouling in the filters is the use two larger pore size filters in series. This approach would allow for the gradual removal of larger interferents. It has been studied prior [86] but did not yield significant results. We performed one automation run with a 10 µm and a 5 µm pore size filter in series, and it also yielded nonsignificant results. However, as was observed in earlier data for the 10 µm filter, polypropylene appears to not an optimal membrane material for our sample. Thus, this approach could be further pursued by using a 10 µm pore size filter made of a different, more compatible hydrophilic, low protein binding material. Then, we could more accurately determine if this alternate configuration could yield greater bacterial recoveries and optimal bacterial concentration.

Chapter 3 Virus purification and concentration

3.1 Viral methods

3.1.1 Influenza H1N1 quantification

Experiments were conducted using the H1N1 influenza strain A/WSN/33 obtained from our collaborator, Dr. Phil Santangelo (Georgia Tech) and his lab, with the virus purchased through BEI Resources, NIAID, NIH: Influenza A Virus, A/WSN/33 (H1N1) PA-2A-NLuc (PASTN), NR-49383. The influenza virus (80-120 nm) comes with a luciferase enzyme (PA-NLuc) specific for our luminescence quantitation technique assay through the modification of its polymerase subunit A (PA) gene to accommodate the NLuc gene (PA-SWAP-2ANluc50 (PASTN)). The stock used for these experiments were viral particles collected from the supernatant of 1549 cells infected with MOI 0.01 H1N1 – WSN/33 PA-2A-NLuc and suspended in media consisting of Dulbecco's modified Eagle Medium (DMEM) and Bovine serum albumin (BSA). This way of developing the virus ensures there is no free-flowing enzyme in our sample and therefore no non-viral binding that is occurring in our experiments when reading luminescence using the assay.

As mentioned, we used the Nano-Glo Luciferase Assay (Promega) to obtain a qualitative analysis of our results. To prepare the sample for analysis, we used a 1:50 Nano Glo substrate to sample mix ratio with the substrate being added directly on to the wells of the plate to make a total volume of 100 µL. The 96-well, white, flat bottom plates (Corning, NY) were placed in a plate reader (Gen5, BioTek Instruments, Inc., Winooski, VT) for the luminescence reading with a gain of 100. Samples were plated in triplicates unless stated otherwise.

3.1.2 Bead quantification

Similar to what was done for the bacteria work, fluorescent polystyrene beads were quantified using two methods, flow cytometry and fluorescent microscopy. Prior to analysis with these methods, we added 10% Triton X-100 to the samples to make the final solution 0.5% Triton X-100. This step was critical in ensuring the beads were monodispersed in the solution for analysis.

For the flow cytometer, a 96-well, clear, round bottom plate was used. We added 100-200 µL of sample volume per well. In fluorescent microscopy, we used disposable hemocytometers and added 10 µL of a sample to the cytometer after mixing to ensuring the beads were monodispersed. To count the beads, images were taken of the grid under DIC light and the fluorescent channels (CasBI (419 nm) for 2 µm beads and FAM (518 nm) for 10 µm beads with the following parameters: 5× resolution, NA: 0.25, Gain: 100. These images were then overlayed using Image J or Power point and the beads counted per grid. Images were taken of the middle and corner grid of the hemocytometer. Once, counted, the same equation as shown in Chapter 2 was used to determine the concentration of the beads in the sample tested.

Previous work has looked at quantifying fluorescent beads both with microscopy and flow cytometry and found that the correlation of quantitation for both techniques was in high agreement [117]. Furthermore, they concluded there was less variation in flow cytometry readings since the method allows for a sample size several folds greater than the sample size for the microscopy count. Thus, we mainly used flow cytometry for these studies, but we verified initial results with fluorescent microscopy (see Appendix B).

3.1.3 Statistical analysis

Values were tested for a normal distribution using the Shapiro-Wilk test, and Levene's test was used to verify for the homogeneity of variance assumptions. Based on the results of the assumptions test and the groups that were going to be compared, appropriate statistical methods were chosen and are described in each section. An alpha value of 0.05 was used for all methods.

3.1.4 Virus calibration curve

Prior to performing any experiments, we ensured the influenza sample, tagged with a NanoLuc Luciferase enzyme, reacted with our Nano-Glo Luciferase Assay. To assess at what dilution ranges the influenza was detectable, we prepared a range of 10-fold dilutions of the concentrated influenza stock using DMEM.

Figure 36 shows the results of the previously mentioned test indicating the most optimal detection range being between the undiluted viral stock and a 10-fold dilution of that sample.

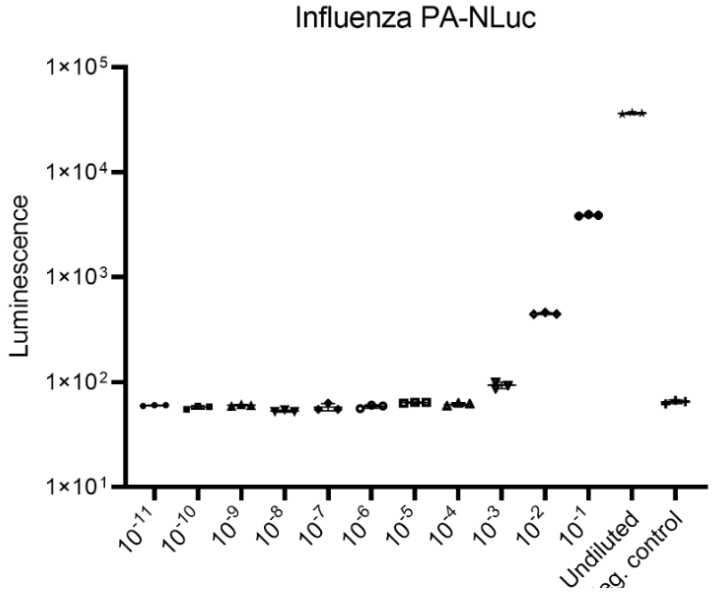

Figure 36. Analysis of luminescence signal (Log 10 scale) from the Influenza PA-NLuc virus stock in different concentrations (10-fold) with a negative control consisting of the viral media. Each concentration and sample were performed in triplicates.

We performed a second experiment, this time using 2-fold dilutions, to investigate if the region of concentration between the stock and the first 10-fold dilution was linear. Results in Figure 37 show that the luminescence readings do not visually follow a linear trend with the decrease in concentration or increase in dilution of the sample. However, for this case, the relationship between the luminescence and the concentration of the virus was assumed to be linear due to the small region of viral concentration we can operate in using the luminescence assay. Furthermore, an equation was generated, using the luminescence readings and an estimated concentration of the virus (~10^7 pfu/mL stock), with results confirming the linearity assumption was valid. Thus, the assumption was kept and the luminescence value readings from the wells were used as the concentration value for our calculations.

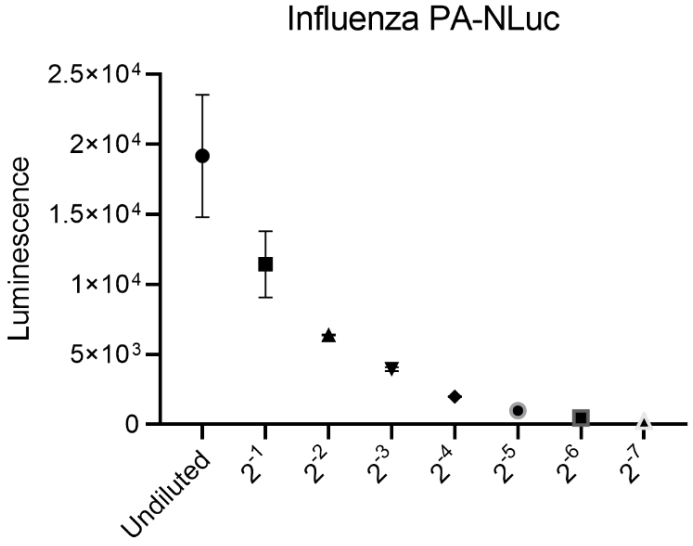

Figure 37. Analysis of Luminescence signal (Linear scale) from the WNS/33 PA-NLuc virus stock in different concentrations (2-fold). Each concentration and sample were performed in duplicates.

3.2 Virus purification

Methods

To determine the best viral purification method, we tested the efficiency of a 0.45 µm and a 5 µm pore size filter, both 25 mm diameter and made of a hydrophilic polyvinylidene fluoride (PVDF) syringe filter. For a virus sample from saliva or captured through an aerosol sample, it can be assumed that virions encapsulated and/or associated with larger inorganic or organic matter could disassociate into free virions upon suspension into a liquid phase. If this is the case, the smaller pore size (0.45 µm) would work best to purify. If the opposite is true and the virus does not disassociate, then a larger pore size (in this case 5 µm) would be best in order to capture as much of the virus as possible.

To test the 0.45 µm and 5 µm pore sized syringe filters, we created a sample containing virus and 2 µm and 10 µm fluorescent polystyrene beads. The beads were diluted with the viral media, DMEM, and once mixed, yielded a 10^6 beads/mL concentration per bead. *No surfactant was added to the beads to avoid disruption of viral particles.* This mix mimicked a high concentration of aerosol particles that might be found in an environment [41]. A 3-fold dilution of the virus stock was performed with DMEM as well, yielding an approximate 3.33×10^6 pfu/mL concentration of the virus (assuming the starting concentration to be ~10^7 pfu/mL). We then combined the virus with the beads at a 3 to 5 ratio to result in 0.9 mL input volumes for each run.

For each of the two syringe filter types, tests were performed in triplicates with a new syringe filter for each run. Each time, the membranes were primed using 1-1.5 mL of DMEM, and the 0.9 mL sample containing the virus and beads was infused via a 1 mL luer-lock syringe followed by the injection of 1 mL of air, at a manual flow rate of

approximately 1 mL/min. The output samples were collected and analyzed for the recovery of the virus using our Nano-Glo Luciferase Assay, and the removal of the beads was analyzed through flow cytometry and fluorescent microscopy.

Results

Figure 38A shows the luminescence assay the pre-filtration sample and those samples that went through the filters. The post-filter luminescence readings yielded lower numbers as compared to the pre-filtration values.

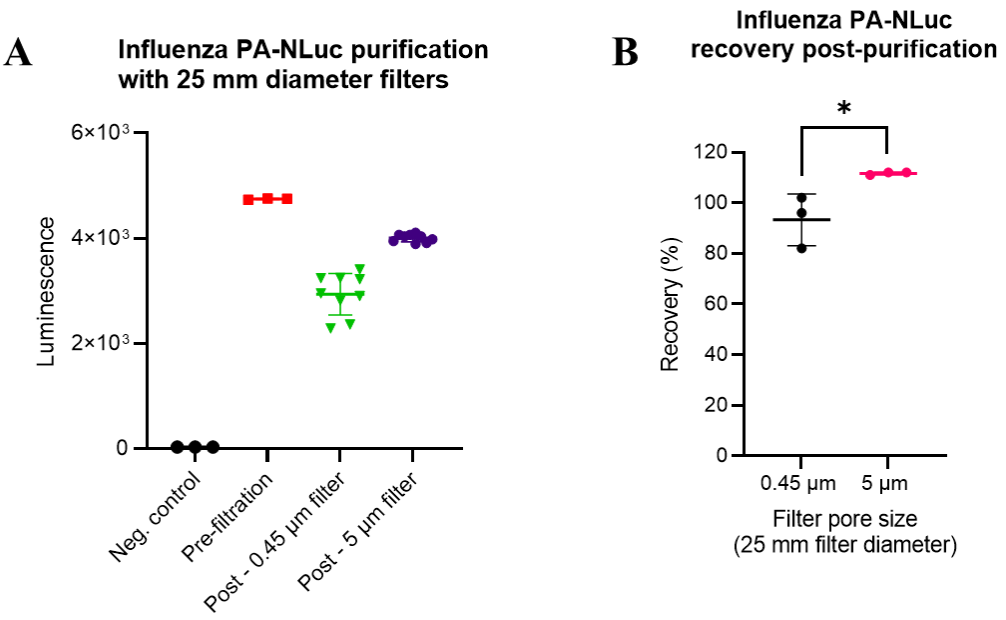

Figure 38. **A.** When mixed with interferents, the virus can pass through the filter without significant loss. Luminescence results of samples post-purification as compared to the pre-filtration, untreated sample. Technical triplicates for each of the three runs per filter are plotted. 900 µL tested samples consisted of 10^6 beads/mL for each bead (2 µm, 10 µm) and ~2×10^6 pfu/mL of virus in DMEM. **B.** Summary of recovery shown as recovery percentage, showing approximately all the viruses pass through the filter for syringe filters. There is a statistical difference between the two recovery groups ($p = 0.046$).

Furthermore, Figure 38B shows the recovery of the virus per filter pore size with the equation below showcasing how it was calculated. For this case, we assumed the relationship between the luminescence and the concentration of the virus to be linear, as previously discussed.

$$\text{Recovery} = \frac{\text{Luminescence}_{\text{Post-filtration}} \times \text{Volume}_{\text{Post-filtration}}}{\text{Luminescence}_{\text{Pre-filtration}} \times \text{Volume}_{\text{Pre-filtration}}}$$

*The luminescence is used as a surrogate for the concentration.

As can be observed, results for the 5 μm pore size filter yielded recoveries higher than 100% while the resulting recoveries when using a 0.45 μm pore size filter averaged to be around 90%. Using a Non-parametric, unpaired t-test (Mann-Whitney) to compare the recovery values, we obtained statistically significant results between them ($p = 0.046$).

For the next step in this experiment, we wanted to prove was the successful removal of interferents from the sample. Figure 39 shows the recovery results of both beads when using the 0.45 and 5 μm filter. As evaluated in ~60% of the output or post-purification volume using flow cytometry, the 0.45 μm pore size filter removed both sized beads and the 5 μm pore size filter recovered only around 40% of the 2 μm. For the filters, the removal of the 2 μm (red) and 10 μm (green) beads and retention of the 2 μm beads for the 5 μm filter were observed through fluorescent microscopy as well (Figure 40), and the capturing of the 10 μm beads can be observed on the filter surface (Figure 41).

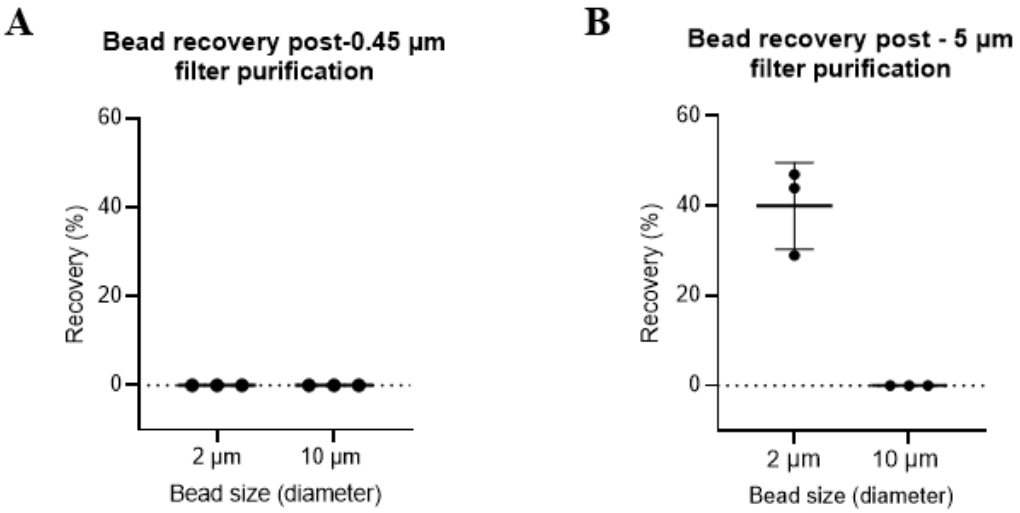

Figure 39. The graphs showcase the results of the fluorescent polystyrene bead recovery for both pore sized filters. Removal of both sized beads as beads were quantified with a flow cytometer (Cytek-Aurora) with 200 µL of each sample (~60% of the post-purification volume). **A.** Both sized beads removed. **B.** 10 µm bead removed and 40% of 2 µm bead recovered.

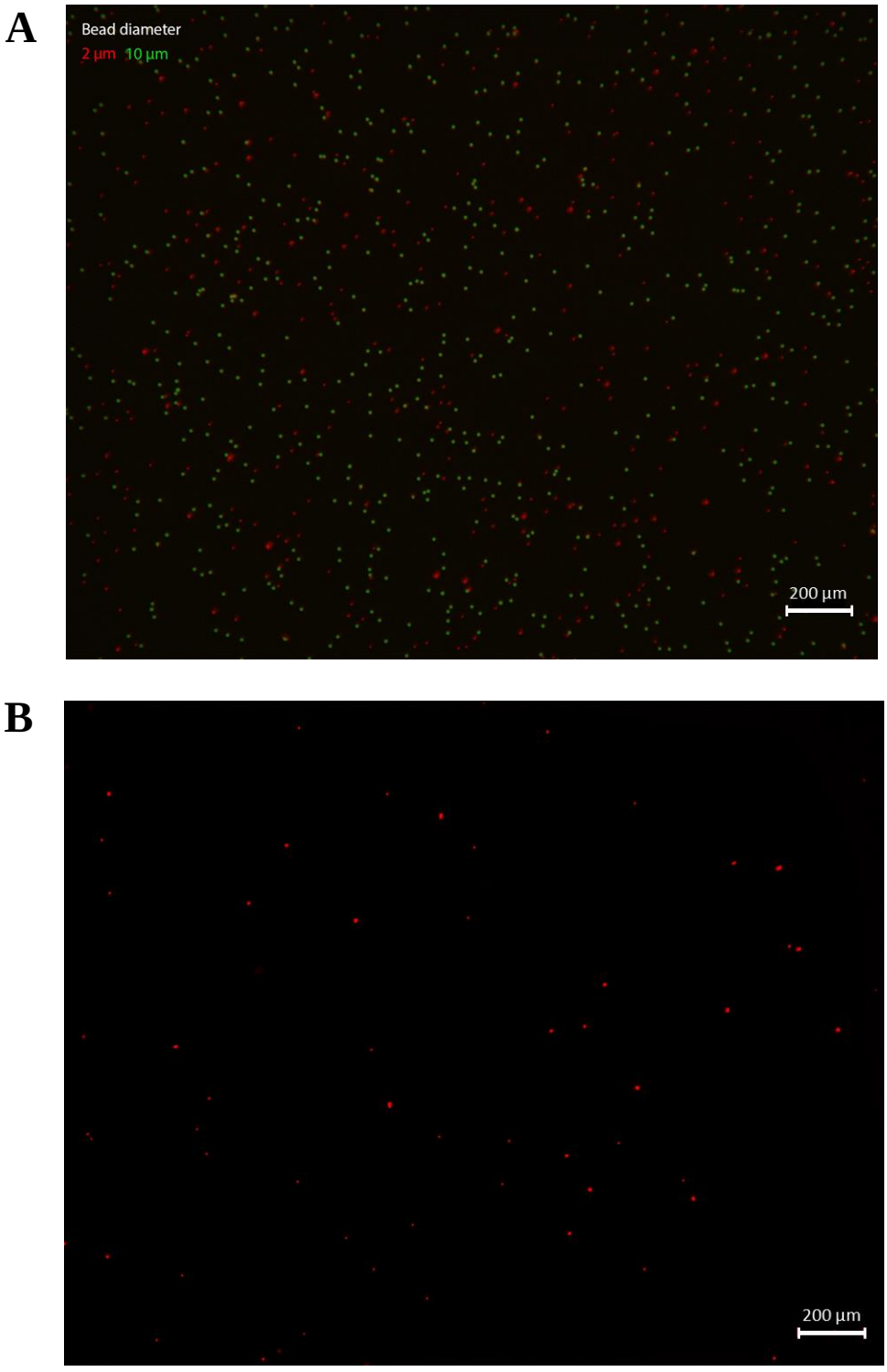

Figure 40. Bead images captured using a fluorescent microscope (Zeiss AxioObserver Z1) for the prefiltration sample (**A**) and the post-5 µm filter filtration (**B**). The 2 µm beads are labeled red by the software for recognition, and the 10 µm beads are labeled in green. Not shown: image taken when using the 0.45 µm pore size filter – no beads observed.

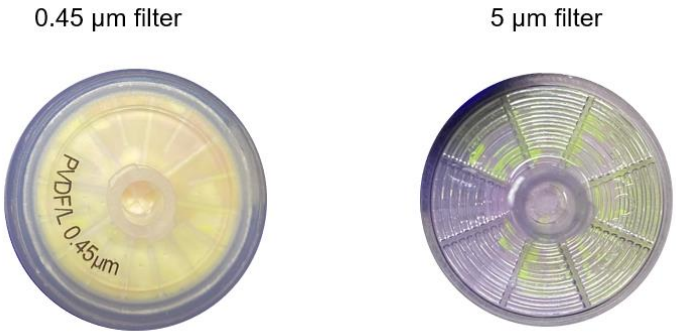

Figure 41. Fluorescent polystyrene beads captured on filter membrane.

The purification step using the 5 µm pore size filter yielded an enrichment factor of around 7 ± 2-fold for the virus as compared to the interferents in the sample, and when using the 0.45 µm pore size filter, the enrichment factor was 52,257 ± 30,207-fold.

3.3 Virus concentration

Tangential Flow Filtration device

We purchased a tangential flow filtration (TFF) device (TFF-Easy, HansaBioMed Life Sciences; Estonia) composed of hollow polysulfone fibers with a 5 nm pore size. This pore size retains any sample larger in size in a volume called the retentate and removes any sample smaller than the pore size which is collected in waste or permeate. The TFF device can take an input volume ranging from 5 to 15 mL, and when cleaned properly, can be reused up to 20 times (per vendor indication). To use the TFF device manually, two clean syringes are connected to the top two nozzles and a 5 mL syringe containing the desired sample is placed on to the outer most right nozzle (see Figure 42A). This sample is pushed into syringe 2, and the valve is then turned to connect 5 mL syringe 2 and. Syringes 1 and 2 are pushed alternatively to move the sample through the hollow fibers in between both syringes (see images B and C) with the smaller size particles collected in the waste. The

motion for this device continues until the desired final volume is achieved in one of the syringes. To collect the desired volume and ensure all sample is removed from the filter, switch the valve positioning, and open the side nozzle to load air into the empty syringe and switch the valve positioning once more to inject the air through the filter to collect the volume on the other syringe. The syringe with the volume is then removed from the TFF device and collected in a 1.5 mL tube for analysis.

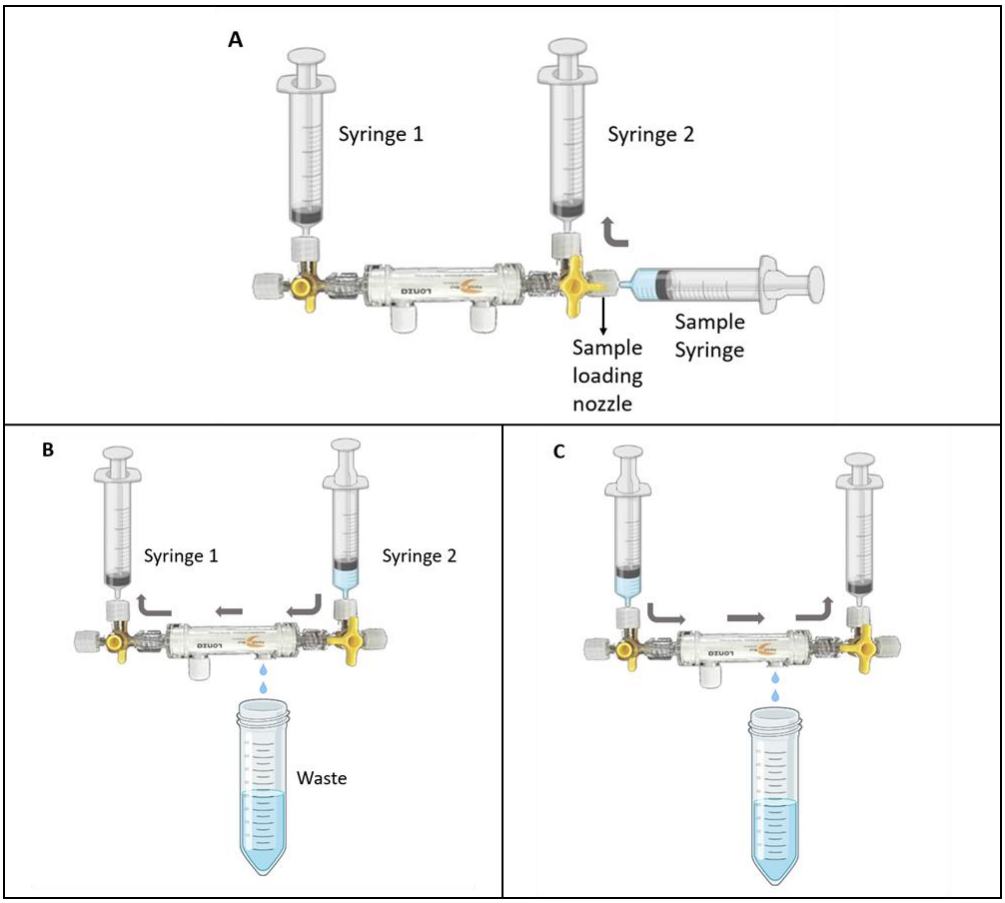

Figure 42. The TFF device in its varying positions. Position A shows the sample being loaded into the device. Position B and C showcase the sample being moved between syringes 1 and 2 with the waste being collected through the bottom nozzle. (TFF source-HansaBioMed Life Sciences; Icons source – BioRender.com)

Results

The TFF device test results are shown in Table 3 and showcase a volume concentration factor varying from 7- to 20-fold (based on the starting sample volume and final sample volume). For the experiment, we performed a 5-fold dilution of the influenza stock to achieve a volume of 6 mL. 5 mL of this sample was aspirated into a syringe and loaded into the TFF device as described previously. One pass through the hollow fibers was considered one "press", and the number of presses were counted until we obtained less than 1 mL of the sample in one of the syringes. This parameter was chosen to able to concentrate the sample as much as possible all the while having enough volume to meet the downstream detection volume requirements as well as volume storage requirements. We performed the experiment three times, with the cleaning protocol performed in between; each test yielded a varying number of presses required to achieve a less than 1 mL of the sample. Thus, each test resulted in different final volumes and therefore, a distinct volume concentration factor. It is apparent that the achievable volume concentration factor depends on the number of presses used in the system.

Of note, we observed that between test 1 and 2, test 2 used an extra press through the TFF device but resulted in a higher concentrated sample volume and thus lower volume concentration factor. A potential explanation for these results is that the cleaning process needs to be optimized in between samples. The cleaning protocol, validated by the vendor, consist of using NaOH 0.5N, followed by nuclease free water, 70% ethanol, and finished with nuclease free water. When doing the subsequent device tests after the first, bubbling was occurring, which could be partially due to the bovine serum albumin (BSA) protein

present in the influenza media, but also by a need for a more thorough final water cleaning step within the protocol.

Table 3. Results from the three TFF device runs. The number of presses required to push the sample through the TFF device to collect a volume of less than 1 mL is recorded, along with the final concentrated volume.

	Run 1	Run 2	Run 3
Input volume	5 mL	5 mL	5 mL
Number of presses through TFF device	4	5	3
Concentrated volume	250 µL	550 µL	700 µL

As shown the table, we were able to successfully reduce the volume of the solution containing the virus. However, we needed to assess the concentration within the volume in order to determine the concertation factor.

To perform the qualitative luminescence test, again as previously described, we used a 1:50 Nano Glo substrate to sample mix with the pre-TFF sample (input) and the post-TFF sample (output) for each test, with a 100 µL as the final volume per plate. Each sample was analyzed in triplicates using a white 96-well plate on a plate reader with a gain of 100. The results for the samples are shown in Figure 43A.

As can be observed, the standard deviation was small between the triplicates of each sample. Furthermore, a paired t-test yielded a statistical difference between pre- and post-TFF samples' luminescence values: Pre-TFF1 vs Post-TFF1 ($p = 0.0002$), Pre-TFF2 vs Post-TFF2 ($p = 0.002$), and Pre-TFF3 vs Post-TFF3 ($p = 0.0003$). Directly comparing the pre- and post-TFF luminescence values, we can calculate concentration factors as observed in Figure 43B, which show to be steady at ~1.6-fold throughout all three tests.

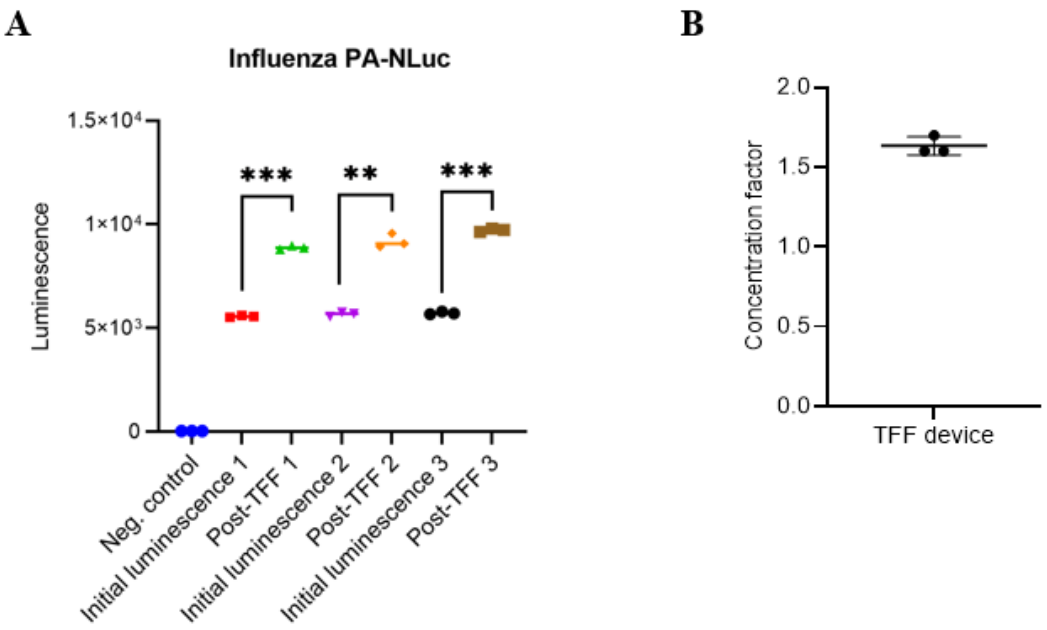

Figure 43. **A.** Luminescence readings of the pre- and post-TFF samples for all three tests and their triplicates, along with a negative control (media). Paired t-tests yielded statistically significant differences between the pre- and post-TFF luminescence readings for all three runs: Run1 ($p = 0.0002$), Run2 ($p = 0.002$), and Run 3 ($p = 0.0003$). All technical triplicates per test were plotted. **B.** Concentration factor of all three runs conducted in this experiment was a around 1.6×.

So as one can obverse, it is possible, using TFF, to obtain concentrations as high a 1.6-fold while achieving 7-20× reduction in volume (500 ± 187 µL).

3.4 Integration of purification and concentration

Design

Following successfully proving the recovery of virus and removal of interferents with our purification method, the next step involved combining the purification step with the concentration step using the Tangential Flow Filtration (TFF) device.

To incorporate the purification step in this system, the addition of a syringe filter must be included in the sample loading nozzle (see Figure 44). The syringe containing the sample connects to the filter and injects the sample through to collect any unwanted particles prior to having the rest of the sample enter the TFF device. This injection step

was followed by the injection of approximately 1 mL of air to ensure the recovery of most of the virus.

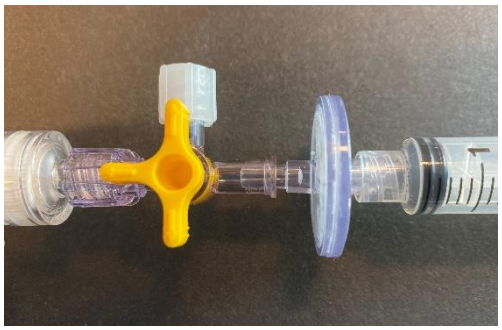

Figure 44. The addition of a syringe filter to the loading nozzle.

In these experiments, we tested the system with both differently pore sized syringe filters at a flow rate of about 1-2 mL/min performed manually so variability occurred. Triplicate experiments were done for each filter, and we used the same methods of viral and interferent quantification used previously, the luminescence assay and flow cytometry, respectively. Furthermore, the cleaning protocol in between samples was reduced to a 70% ethanol wash followed by DI water.

For these experiments, we used the same TFF device as for the concentration experiments and primed with nuclease free water prior to running samples. The same mixing ratio of beads and virus were performed to yield an input volume of 5 mL, and the viral stock was diluted 5-fold to allow for enough samples. *Again, no surfactant was added to the beads prior to runs to avoid disruption of viral particles.*

Results

The concentration results can be seen in Figure 45A, where the luminescence assay post-filtration (syringe filter and TFF) sample results, for both filter sizes, were analyzed in technical triplicates using the assay. A Nonparametric One-Way ANOVA- Brown-Forsythe test with Dunnett's T3 Post-hoc test was used to compare the luminescence results in Figure 45A. Results show that with the use of the TFF device plus either the 0.45 µm pore size filter or the 5 µm pore size filter, the luminescence readings statistically significant as compared to the pare-filtration sample ($p < 0.001$).

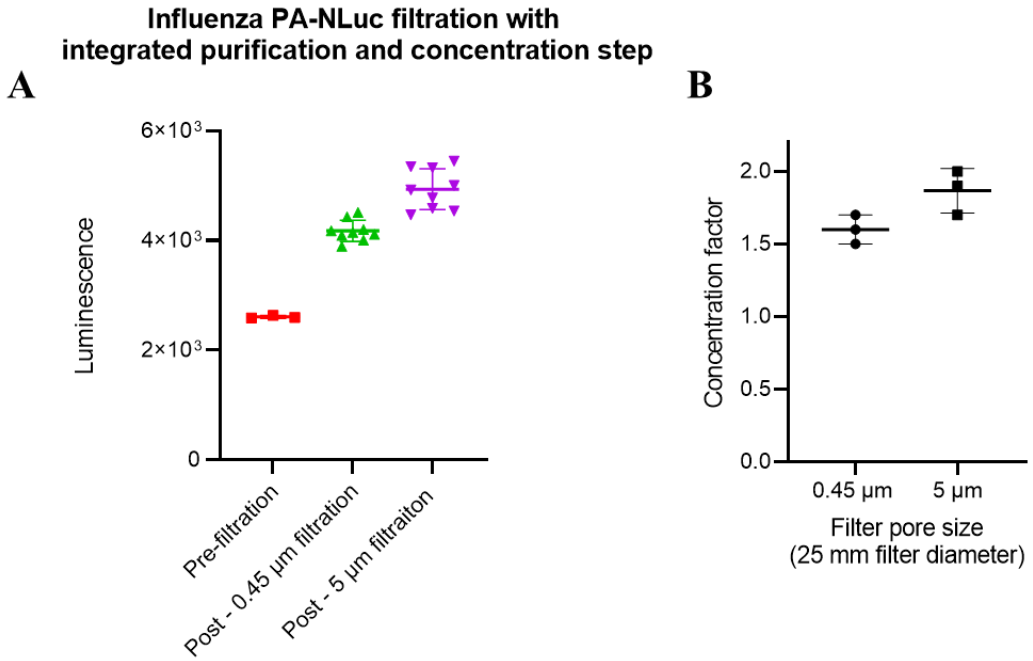

Figure 45. **A.** Statistically significant higher luminescence readings are achieved when comparing the pre-filtered sample readings with that of the integrated system with the 0.45 µm pore size filter ($p < 0.0001$) or the 5µm pore size filter ($p < 0.0001$). Between integrated system values, there was also a statistical difference ($p = 0.0005$). All technical triplicates for the three runs per filter pore size were plotted. **B.** Even with beads included as interferents (in concentration approximately equivalent to the analyte), we retain our ability to concentrate the target virus by ~1.6x with both pore size filters.

Comparing the luminescence readings, again assuming linearity between the luminescence values and the viral concentration, the concentration factors from these test results ranged from 1.6×-2× (Figure 45B).

The data in Figure 45A consisted of luminescence readings analyzed in technical triplicates for the three runs done using each syringe filter pore size. An additional factor that was considered in these experiments to determine what could help improve viral recovery was the variation of air pressed into the system in the final step of the procedure; this step is what helps collect remaining liquid in the TFF. Therefore, for each run per filter, a new final volume of air was used in the final step: 5 mL, 15 mL, and 25 mL.

Figure 46A shows that there was no statistically significant difference in the post-filtration luminescence results as a function of the varying final air volume applied to the system when using the 0.45 µm pore size filter (Nonparametric One-Way ANOVA-Brown-Forsythe test with Dunnett's T3 Post-hoc). On the other, when using the 5 µm pore size filter, statistical differences were observed (One-Way ANOVA, Tukey Post-hoc) between luminescence readings as a function of the following air volumes: 5 mL vs. 15 mL ($p < 0.0001$), 5 mL vs. 25 mL ($p = 0.001$), and 15 mL vs. 25 mL ($p = 0.004$).

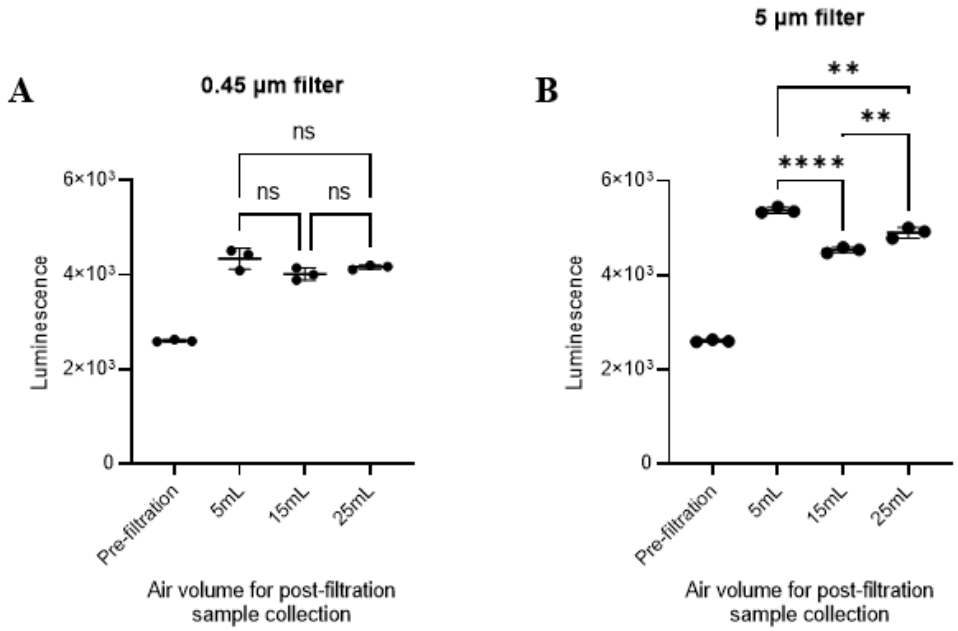

Figure 46. Post-filtration luminescence assay results as a function of varying air volumes applied in last step of the integrated system. **A.** The varying final air volumes showed no statistical difference in the luminescence readings for the use of the integrated system with the 0.45 µm filter. **B.** The varying air volumes produced statically different luminescence readings between the 5 mL and 15 mL ($p < 0.0001$), 5 mL and 25 mL ($p = 0.001$), and 15 mL and 25 mL ($p = 0.004$) volumes. All technical triplicates for each volume of air are plotted.

The results of the two distinct TFF and syringe filter integrated systems were evaluated through the recovery of the virus. As can be observed in Figure 48, both systems yielded about 30-40% recovery with the average being slightly higher when using the 5 µm pore size filter, a trend we observed in our purification experiments. However, using an unpaired t-test, we found there was no statistical difference between the two groups ($p = 0.213$).

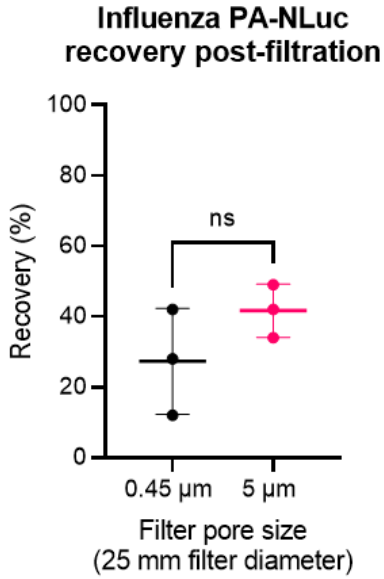

Figure 48. Recovery of the virus post-filtration under two pore-size filter conditions. Both yielded an average recovery of 30-40% with no statistically significant difference between the recovery obtained when using the two distinct pore size filters in the integrated system.

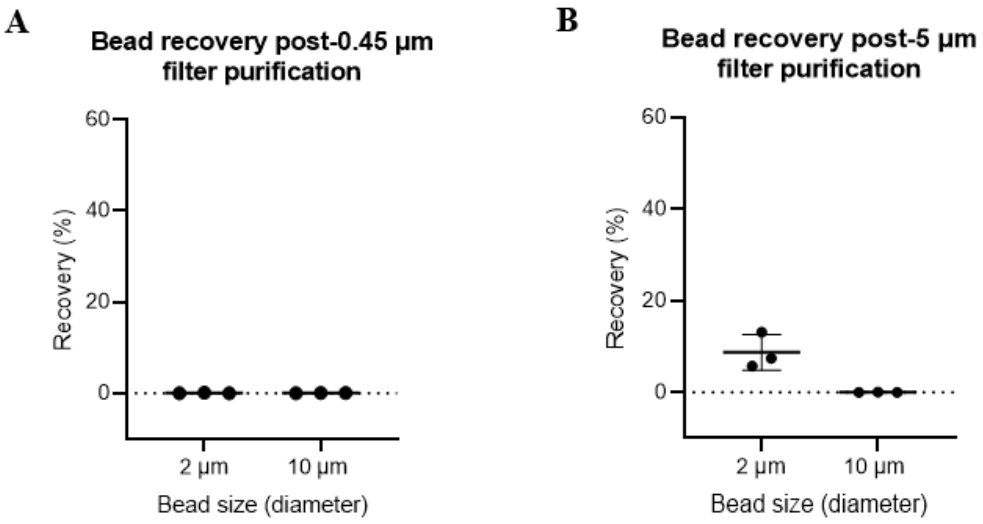

Figure 47. Recovery of beads post-filtration with the use of the 0.45 µm pore size filter (**A**) and the 5 µm pore size filter (**B**).

The second important aspect of this system to evaluate is the purification and removal of interferents. Using flow cytometry, the 2 µm and 10 µm beads were quantified with the results overserved in Figure 47 showing only around 10% recovery for the 2 µm beads using the 5 µm filter.

In all, this integrated purification and concentration system for viruses yields an enrichment factor of 10 ± 3-fold when using a 5 µm pore size filter for purification. When using a 0.45 µm pore size filter instead, the enrichment factor becomes 1,916 ± 1,839-fold. Overall, averaged across the two pore sizes, the 5 mL starting volume was reduced to 940 ± 313 µL. Additional details of the results for these experiments, such as final volumes per run, can be found in Appendix C.

3.5 Automation

3.5.1 Design

A key factor in rapid detection and response is the automation of the filtration system. This allows for a decrease in response time, labor time, and therefore, cost. Thus, we have explored the design of an automated system for viral purification and concentration with the methods previously studied and discussed in this chapter. Due to time constraints, only the conception of the design was possible, not its manufacturing.

In Figure 49, you can observe the schematic for the automation of the tangential flow filtration (TFF) device. The automated system consists of a two-channel peristaltic pump (#EW-78018-12; Cole-Palmer, Vernon Hills, IL) that controls the flow of fluid and air in the system.

In Figure 50, we observe in position A the sample being loaded by going through the purification step using the chosen previously tested syringe filter, in this case, 25 mm

diameter, 5 µm pore size filter. Position B then involves the recirculation of the sample in order to concentrate it down to the desired volume. Air can be added to the system as well as the volume decreases to ensure the sample continues flowing through the system and any potential change in pressure does not cause the tubing to collapse. Finally, position C demonstrates the switching of valves once more, this time to collect the concentrated sample. In this step, air can be added to the system as well to ensure all the liquid in the TFF is removed and collected.

In the schematic, washing and cleaning reservoirs can be observed. Controlled via the valves and peristaltic pump, the cleaning procedure will consist of deionized water, followed by 0.5 N sodium hydroxide (as recommended by the TFF vendor, HansaBioMed Life Sciences), water, 70% (vol/vol) ethanol, and finally water again [66]. Past studies have performed the cleaning step in between sample runs enabling the use of the TFF membrane to be 15 times before replacement [66]. To investigate ways to reduce procedure time and material usage, we will conduct studies to determine if an ethanol and water flush would be enough between runs to adequately clean the system as well as to guarantee the maximum usage of the TFF membrane. Our results for the concentration experiments lead us to believe this could be the case. However, the full cleaning method described above would still be employed at the end of a day's worth of experiments.

This automated system includes the addition of a flow sensor (Liquid Flow Sensor LPP10; Sensirion, Switzerland) to monitor flow rate and of pressure flow meter (#EW-32908-43; Cole-Palmer, Vernon Hills, IL) to ensure the flow rate readings are accurate and that the pressure is remaining constant prior to the flow entering the TFF and after exiting the TFF. This measurement is important because it helps to produce more consistent results

and can assist in troubleshooting system problems [91]. The system will include Teflon FEP tubing (McMaster-Carr, Douglas, GA), two 3-way valves (Darwin Microfluidics, Paris, FR), one 4-way valve (Upchurch Scientific, Oak Harbor, WA), and one 6-way valve (Upchurch Scientific, Oak Harbor, WA). The tubing diameter of the system can be modified accordingly to our peristaltic pump, dead-end filtration considerations, and TFF dimension of choice. TFFs composed of hollow fibers, come in varying lengths, materials, and surface areas, with many of them being available through various manufacturers such as Repligen (Waltham, MA). In all, the design is a modular, flexible automation system that can be used for our viral purification and concentration.

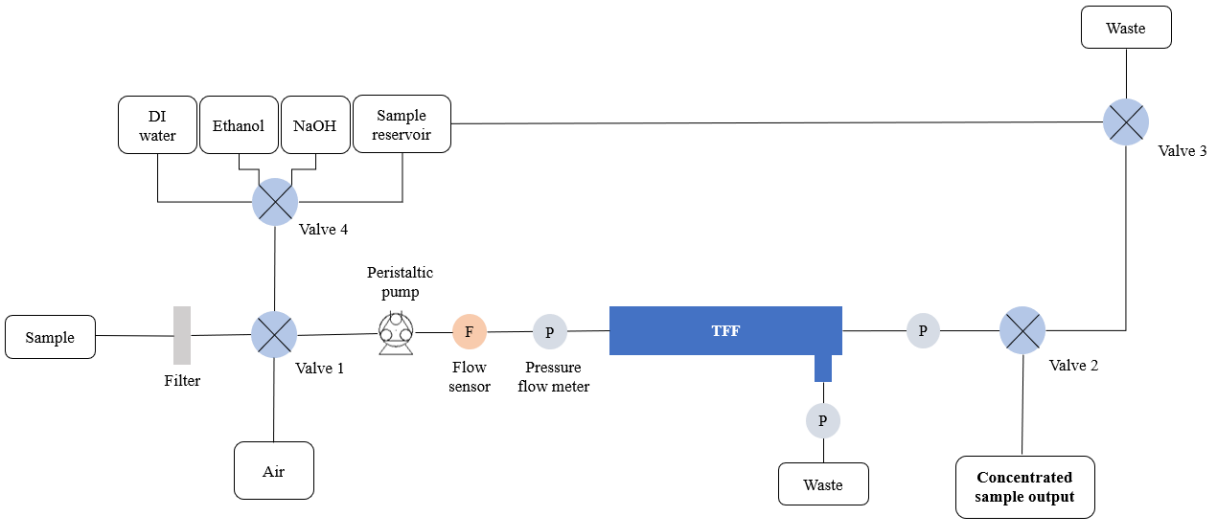

Figure 49. The automated TFF device schematic consisting of a peristaltic pump, valves, and the TFF device.

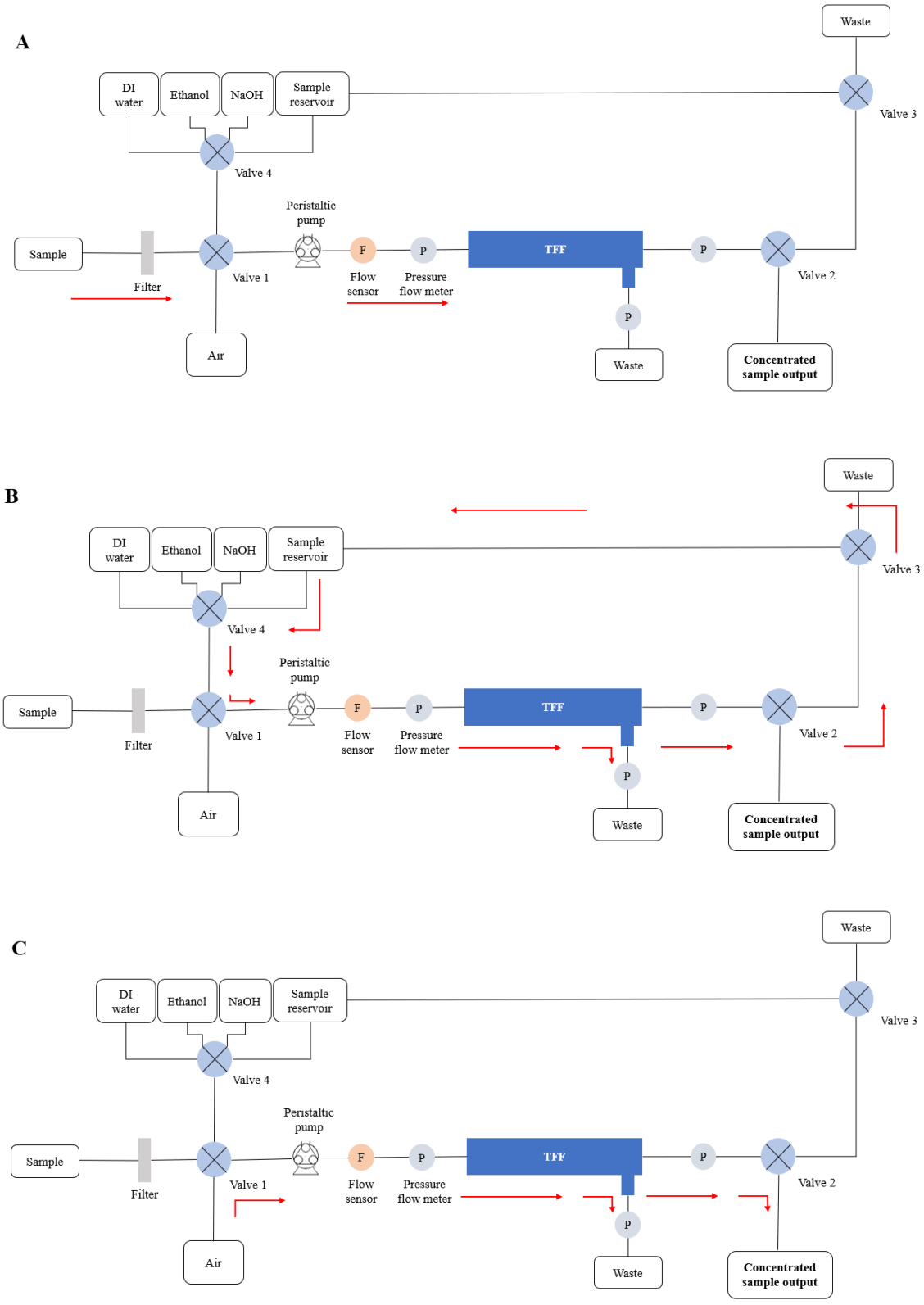

Figure 50. Positions A-C showcase the sample being loaded, the sample being recirculated for concentration, and the final concentrated sample being collected, respectively.

3.6 Discussion

The first part of this chapter consisted of evaluating two size-based alternatives for viral purification using syringe filters with varying pore sizes. Both pore sized filters, 0.45 µm and 5 µm, were tested previously in chapter 2 for bacterial filtration and retentate recovery. Here, they were both tested for viral filtration recovery and bead removal. Unlike with bacteria, the viral recovery under both pore sized filters was close to 100% with the 5 µm pore size filter yielding slightly higher virus recoveries, on average, above 100%. Discrepancies in the luminescence reading as well as our assumption of linearity between the luminescence reading and concentration could be contributing the above 100% recovery. However, overall, the results serve to prove that with this purification step we can recover close to 100% of the virus in the sample. As for the interferents present with the virus, the 0.45 µm filter removed both sized beads while the 5 µm filter recovered only around 40% of the 2 µm beads. The 2 µm beads are smaller in size than the pore size by a factor of around 2.5×, but because the pore size on the filter might vary and be bigger or smaller than indicated, this could contribute to the trapping of the 2 µm beads in the filter membrane. Furthermore, because there was not surfactant present in the sample to avoid any impact on the virus, the beads could have agglomerated together into larger sized structures that were removed by the filter. Nevertheless, if treating the 2 µm beads as interferent, then the removal of 60% of this sample is beneficial for our system. When comparing to the experiments conducted using a 5 µm pore size filter with a mix that only contained 2 µm pore sized beads (section 2.2.2), the recovery was on average around 40% as well. Therefore, the larger size beads present in the virus and bead sample didn't interfere with the 2 µm bead removal. Overall, we get an enrichment improvement of

52,257 ± 30,207- fold when using the 0.45 µm pore size filter and 7 ± 2-fold when using a 5 µm pore size filter. Furthermore, these experiments serve to demonstrate the use of the PVDF filters for purification is promising as it recovers close to 100% of virus even when the virus is present in a matrix of interferents at a high concentration with interferents prone to agglomeration.

Shifting our focus to viral concentration method using the TFF device, the luminescence results show we can use the TFF device to decrease the input volume and increase our concentration, as shown by the luminescence concentration factor for all three tests. Yet, a main drawback arises and is worth considering, the modest 1.6× concentration factor. Considering the 7-20× reduction in volume along with the 1.6× concentration increase, it was calculated that 8-24% of the virus was recovered. This represents a significant overall loss of target, and it appears to indicate that the smaller the final volume achieved, the more virus that's lost inside the TFF device or in the waste. This was the case with one of the runs in which the 5 mL input was reduced to a 250 µL final volume resulting in a 20× reduction in volume which yielded the significant virus loss (8% recovery). Thus, this suggest there might be a volume reduction threshold that must be met to avoid having a significant drop-off in virus recovery.

When testing the integrated system containing the syringe filter for purification along with the TFF device for concentration, Table 4 (Appendix C) highlights the final volumes of each run with them ranging from 500 µL to 1.2 mL. These volumes resulted in around the same concentration factor increase for the virus (~1.6×) as in the concentration experiments, yet there was a higher viral recovery ranging from 25% to 40%, depending on the filter pore size. This suggest that reducing the volume greater than 20×, in this case,

reducing the volume to less than 500 µL, could lead to an accelerated loss of virus through sorption of it in the membrane or possible virus loss in the waste. Thus, keeping final volumes to greater than 500 µL would be ideal. The higher recovery could also be attributed to an added air infusion step in the beginning of the procedure to ensure that much of the sample pushed through the filter would enter the TFF device. As for the viral recovery as a function of the final air volume used to collect the sample in the integrated system, it suggests, through the 5 µm pore size data, that the air used might potentially have an influence in the overall recovery of the virus as observed by the luminescence readings, while the 0.45 µm pore size data does not. Therefore, we are not able to reach conclusive results with regards to this relationship.

As a quick side note, the waste of the system was evaluated using the luminescence assay but yielded no significant luminescence readings, indicating that no virus was present in the sample. However, it is worth noting that these samples were highly diluted and from our first luminescence assay results, we know the assay does not yield distinguishable results between highly diluted, lower concentration virus samples. Therefore, it could be that the virus is present in the sample but too diluted for the assay to detect. To determine if this is the case, in future experiments, the sample could be centrifuged, the supernatant removed, and the pellet resuspended to a lower volume to concentrate the sample. We would then test this with the assay to be able to conclusively determine if virus was present in the waste or not and, therefore, if the virus is getting lost there or inside the TFF device.

Now, moving on to observe the results from Table 4 of the integrated system with the use of the 0.45 µm pore size filter and with the 5 µm pore size filter, there is no apparent trend that holds across the two configurations with regards to volume reduction and

luminescence concentration factor. More experiments would need to be conducted to investigate a possible trend. It is observed that for the 5 µm pore size filter configuration, there were slightly higher luminescence concentration factors, while for the 0.45 µm pore size filter configuration, the luminescence concentration factors were similar to that of the concentration experiment. One possible explanation is that the smaller pore size membrane becomes fouled by the high concentration of interferents, not allowing the virus to flow thorugh, versus with the 5 µm pore size filter. The larger pores allow a percentage of the beads to flow through which would cause less caking and a lower probability of the virus entrance being blocked. The results for these sets of integrated system experiments support this theory as in the 0.45 µm pore size filter configuration the interferents were removed while for the 5 µm pore size filter, around 10% of the 2 µm beads were recovered. Of note, this bead recovery is around 4× less than in the purification experiment, suggesting the 2 µm beads are getting stuck inside the hollow fibers of the TFF device. Overall, we get an enrichment factor of 1,916 ± 1,839-fold when using the 0.45 µm pore size filter and 10 ± 3-fold when using a 5 µm pore size filter

Thinking deeper about why the luminescence readings are higher when using the 5 µm pore size filter, a possible second explanation for the variability could be that the fluorescence of the 2 µm size beads remaining in the sample could be slightly interfering with the luminescence reading of the virus and causing the reading to be higher. This would also explain why we observed higher recovery of the virus, around 40%, when using a 5 µm pore size filter, versus ~25% recovery when using a 0.45 µm filter, a trend similar to what was seen in the purification experiments where the larger pore sized filter yielded larger virus recoveries.

This phenomenon has been studied before where a correction could be implemented [118], nevertheless, there is no reason to believe this significantly impacted our results given no statistically significant difference was found between the virus recoveries using the two different filters in the integrated purification and concentration system. Furthermore, a quick test was performed with the beads mixed with the luminescence assay and it yielded no luminescence reading, confirming that there is no reaction between the beads and the substrate in the luminescence assay. Additionally, it is observed that the concentration factors obtained from the integrated system experiments are comparable to the concentration factors obtained for the concentration experiments with just the TFF device. As for the overall virus concentration, it might be that 1.6× is the best this specific TFF device can do for a 5 mL input. Perhaps a smaller surface area TFF device would yield significant concentration improvements by decreasing dead-volume loss inside the device, which for this TFF device, was around 800 µL.

With regards to volume reduction, it is important to note that getting a consistent output volume from the TFF device, especially when done manually, is difficult since it depends on the pressure applied to the device, the sample used, and the usage of the device. As we progressed in runs, it took longer to concentrate the sample down to a desired volume. When the device was first used, it took a single digit number of presses to concentrate the sample down to less than 1 mL, and towards the last few experiments with the integrated system, it took around 20 presses. This could be a factor of the wear of the hollow fibers that comes as a result of usage and debris not removed during washing steps. Nevertheless, the performance of the system didn't diminish, it just took longer to achieve optimal performance. In all, the TFF device was used 9 times for the concentration of samples, not

counting the cleaning steps in between. Per the manufacturer (HansaBioMed), the TFF device can be used up to 20 times depending on the sample it is being used with. Yet, we would have to perform a longevity study to determine at which point the TFF device would need to be replaced.

Continuing to compare the device performance to the parameters provided by the manufacturer, we recover less of our target than what was expected based on the company's provided data. Primarily an extra cellular vesicle concentration device, data provided by the company achieved 83% recovery of extracellular vesicles in their sample. A main reason why this specific device was chosen was because of the similarities between extracellular vesicles and virus, mainly in their size. Extracellular vesicles (EVs) are nanoparticles that can originate in different parts of the cell and can differ in their size and molecular content. There are varying types of EVs including exosomes, shedding microvesicles (MVs), and apoptotic bodies. Exosomes, or small vesicles, are 30 – 120 nm in diameter while large EVs or microvesicles are larger than 150 nm in diameter. [119] Thus, these sizes are comparable to that of a virus which usually range in from tens to hundreds of nanometers in size, and the shape for both can be assumed to be spheres. Furthermore, the chosen TFF is suitable to concentrate samples starting at 5 mL and even greater volumes than that, thus, making it suitable for processing large volumes of fluid. This then made it puzzling to compare our 20-40% bacteria recovery while they're EV recovery data showed 83% recovery.

A possible explanation for the results is that the input and output volumes from our tests were different than that used for the companies experiments. The company concentrated EVs down from a 50 mL volume to 2 mL of volume, versus our 5 mL volume

down to 500 µL – 1 mL. From further discussions with the vendor, it appears that due to the 2 m^2 membrane surface area, the ideal final concentration volume should be no less than 1.5 mL. This volume would not meet the microliter amounts necessary for biosensor sensing, but the device would be useful for greater volume samples we might expect from the upstream collection team. However, despite the extra loss due to the lower recovered volume, we were still able to recover our target an enhance our concentration with this commercially available TFF device. The limit of detection of the downstream sensor would determine if this would be enough.

Work has been done using a TFF device (HansaBioMed) for EV isolation or purification and comparing it against other methods such as ultracentrifugation. It was found that the method used determined what composition of the EV sub-populations was isolated and purified. Translated to this work, it could mean this TFF device might not be most suitable for viral purification much like it does not appear to be suitable for certain subpopulations of EVs. [120] The hollow fiber material could be a potential reason for this discrepancy. As stated in other work that have used TFFs for bacterial and viral purification and concentration from different marine waters, it is essential to select an optimal membrane suitable for the specific filtration application [90], though even then, it has been reported TFF has variable efficiencies. In this same work, they tested two distinct surface area TFF devices, 0.5 m^2 and 50 cm^2 using sample volumes in the order of liters, and found that for viruses, using a 30 kDa cut-off regenerated cellulose (RC) membrane yielded an average recovery of 35.28%, higher than that achieved using two other types of polyethersulfone (19 – 23%). These results were based on the use of the smaller surface area TFF (50 cm^2), but when switching over to the larger surface area, the PES recoveries

were around 40%. Though the studies used samples from different sources, had TFFs with different surface areas, and used higher flow rates and volumes, it still suggests that a different material might be better results for our TFF device approach. Perhaps trying a RC membrane would help us increase our concentration. Nevertheless, comparing our results to theirs, we seemed to have recovery numbers that were close in value. Yet, seeing as TFF recovery can vary with many factors, such as sample characteristics (morphology, charge), sample matrix (contaminants that might be present) and device surface area, we can develop a list of parameters to optimized. TFF device parameters would include device surface area, material type, membrane pore size, and length of the membrane hollow fibers. The target pathogen and sample type would be taken into consideration to guide the choice of some of these parameters.

To help reduce overall labor time and to allow for consistency between runs, such systems have been automated in a similar fashion to the schematic shown in this thesis. One paper sought to use the same hollow fiber material as us (polysulfone) but with a nominal pore size of 0.2 µm, not 5 nm pores such as in our configuration, and a cross surface are of 0.74 mm^2, smaller than ours. Furthermore, they started with a higher sample volume (250 mL) and were able to reduce the volume down to less than 500 µL within 35 to 45 minutes, not counting the cleaning procedure. In all, they were able to recover 70% of viable bacterial cells from their chicken homogeneity samples. [66] Other work also looked at bacterial concentration with an automated TFF device that focused on reducing liters of sample down to 4-5 mL. They implemented backflushing as a way to increase recovery. Though different in many aspects, these works lay out a blueprint for optimization of our system, such as the reduction of the surface area (currently 2 mm^2) of

our TFF device, which, without changing the hollow fiber material, could help increase viral recovery. The material could also be changed, as previously discussed, and some pulsing backflow steps could be incorporated in the automated system to help disrupt any fouling and therefore increase concentration and target pathogen recovery.

Cleaning is a pivotal step in the between runs. This helps clear out debris to provide a constant environment per run and in this way, ensure the repeatability of results. In our work, we looked at the use of sodium hydroxide, ethanol, and water in between samples, as recommended by the vendor. For our integrated system testing involving both the viral purification and concentration, however, we eliminated the sodium hydroxide step and still received consistent results throughout each run, allowing us to conclude that there were no remaining retentate in the TFF from previous runs that was being carried over into the following runs and thus influencing our recovery results. This suggest that a shorter cleaning step could be implemented between runs, and therefore decrease the running time of the procedure, both manually and under automation. Furthermore, cost could be saved on reagents as well with less of them needed for a shorter cleaning protocol. The final cleaning procedure at the end of all runs would include 0.5 N of sodium hydroxide in order to ensure the device is fully clean by using a harsher chemical. However, to ensure a cleaning step of just water and ethanol would be appropriate between runs, more tests would need to be conducted were both the waste and retentate are tested for virus presence.

3.7 Conclusion

Based on the above discussion, the TFF concentration approach integrated with a purification step can help obtain an increase in enrichment that's 1,916 ± 1,839-fold when using the 0.45 µm pore size filter, and 10 ± 3-fold when using a 5 µm pore size filter.

Around a 1.7× concentration increase is observed and anywhere from 20-40% of the virus can be recovered. For the optimal results, a 5 µm pore size filter should be chosen since it yields higher viral recovery as well as a slightly higher concentration factor. Yet, this pore size filter does not entirely remove interferents 2 µm in size present in the sample. For this to be true, a 0.45 µm filter could be implemented instead, but the recovery of the target pathogen won't be as high. Additionally, for this specific size of TFF, final concentrated sample volumes of less than 500 µL can lead to significant sample loss. Therefore, ideally, the system would recover no less than 500 µL, which with a 5 mL input, no more than a 10× volume reduction would be ideal. To determine the optimal configuration to use, a consensus needs to be reached between amount of the target pathogen to recover versus how much of the interferents to remove. Additionally, the state in which we will find our virus will influence the filter chosen for the purification step. For example, if in a saliva sample or an aerosol sample the virus is found to be encapsulated in mucus and therefore be found in a particle much larger than the 0.45 µm pore size filter, the 5 µm pore size filter should be used. If instead it is found that the virus is found freely flowing in our liquid sample, then the 0.45 µm pore size filter could be used.

The integrated filter and TFF device system can lead to the removal of interferents, concentration of the target pathogen, and a reduction of milliliters of volumes to microliters. Manually, this process took anywhere from 2-3 minutes to perform per manual run. The process is amenable to automation, however, and can be optimized for viral recovery by potentially trying a different hollow fiber material and/or decreasing the surface area of the TFF device to reduce volume trapped inside the system to make it easier to recover the target pathogen.

Future Work

To explore a greater increase in concertation factor and recovery, a smaller area TFF should be tested. Additionally, two other materials, such as PES and RC should be considered. Another potential study to perform is to see how different air volumes for the final sample collection step of the system could affect sample recovery. The work done on that here was inconclusive, therefore, it should be further explored to determine if this parameter could be optimized for greater recovery. Furthermore, in order to test the lifetime of supplies, a longevity study on the TFF device should also be studied. The vendor specifies that it could be reused 20 times while literature has stated around 15 times. Of course, the usage rate will vary on the composition of the sample being concentrated, therefore, a test should be performed with our specific sample type. Final future work to consider would be building the designed automated system and performing automated experiments to compare with the manual runs.

Appendix A: Additional quantification methods

A.1 Inactivate SARS-CoV-2 quantification (ELISA)

Prior to using influenza as the surrogate in our virus experiments, Beta-propiolactone (BPL) inactivated SARS-CoV-2, provided by a collaborator (Jeff Hogan, UGA), was the organism of choice for our experiments. This specific type of inactivation process chemically inactivates enveloped viruses by destroying its nucleic acid yet preserving the structure of the virion. It was important to preserve the morphology of the virus since our purification and concentration techniques rely on the physical structure of the organism. Due to the nature of the inactivation process, qPCR was no longer an option for quantification of the sample, therefore, ELISA was tested as an alternate method.

We purchased a human SARS-CoV-2 Spike ELISA kit (# EH491RB; Thermo Fisher) for our inactivated SARS-CoV-2 detection method. This approach, which uses monoclonal antibodies and targets the S2 fragment of the virus, would allow us to evaluate the effectiveness of our purification and concentration approaches. Prior to evaluating experimental samples, we produced a standard curve using our stock virus and a recombinant human SARS-CoV-2 spike protein standard included in the kit. The assay detected recombinant spike protein as expected (Figure 51). However, we observed no response to inactivated SARS-CoV-2 samples (Figure 52). Collaborators has previously used this inactivated virus stock for successfully testing binding to antibodies for both the spike and nucleocapsid proteins, so, the problem seemed to lie in the ELISA kit itself or in a human mistake when performing the procedure.

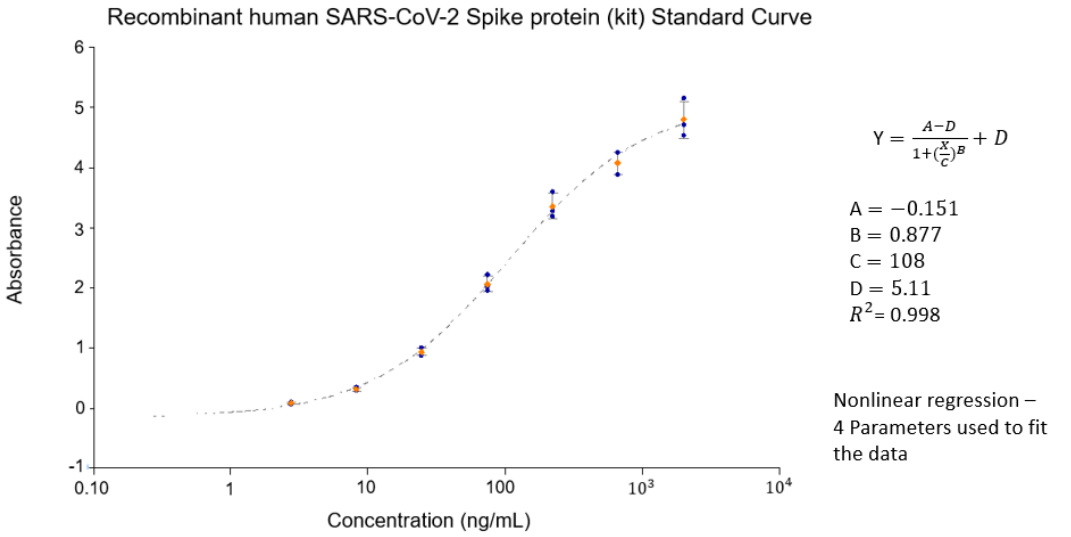

Figure 51. Recombinant human SARS-CoV-2 Spike protein standard curve. If concentration was plated in triplicates.

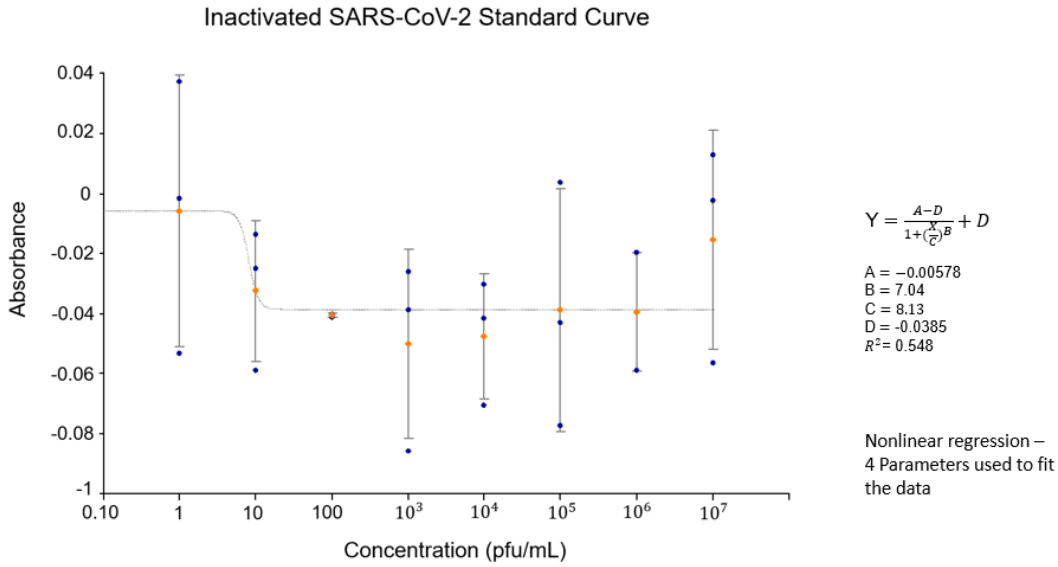

Figure 52. Inactivated SARS-CoV-2 standard curve at varying concentrations. Each sample was plated in triplicates.

A potential reason for the lack of signal obtained when testing our inactivated SARS-CoV-2 is that the sample was not purified. During the inactivation process, the inactivated virus gets mixed with cellular proteins, free spike protein, etc., which could all be interfering with the binding of the virion spike protein. Another explanation could be that the antibody from the manufacturer did not bind well to virus' spike protein. As explained by experts in the field (Dr. Phil Santangelo, Georgia Tech-Emory), commercial antibodies tend to not be as specific as antibodies derived from humans, many of which are only available through research laboratories.

After much troubleshooting, we reached the conclusion that this method would not work for the inactivated SARS-CoV-2 samples. Thus, we explored alternate quantification approaches we will discuss next.

A.2 Surface Plasmon Resonance

Given that the commercially available ELISA did not yield good results for inactivated-SARS-CoV2 quantification, we tested an alternate approach, surface plasmon resonance. In collaboration with Dr. Jie Xu (Food Processing Technology Division, Georgia Tech), we used the mouse antibody GT-3F2 for SPR, previously shown by Dr. Xu and her team to be compatible to the inactivated SARS-COV-2.

To confirm the compatibility of the antibody to our sample and to determine the detection concentration range of the method, we generated a standard curve with a series of dilutions of the virus. Results show in Figure 53 show most diluted samples were indistinguishable with the method, resulting in a small concentration range for accurate viral detection using SPR. Thus, we concluded SPR was not suitable for quantifying samples containing lower levels of virus. It could be a viable method for higher

concentration samples but considerations such as cost, access to and use of specialized equipment, and run-time (hours) should be taken into consideration.

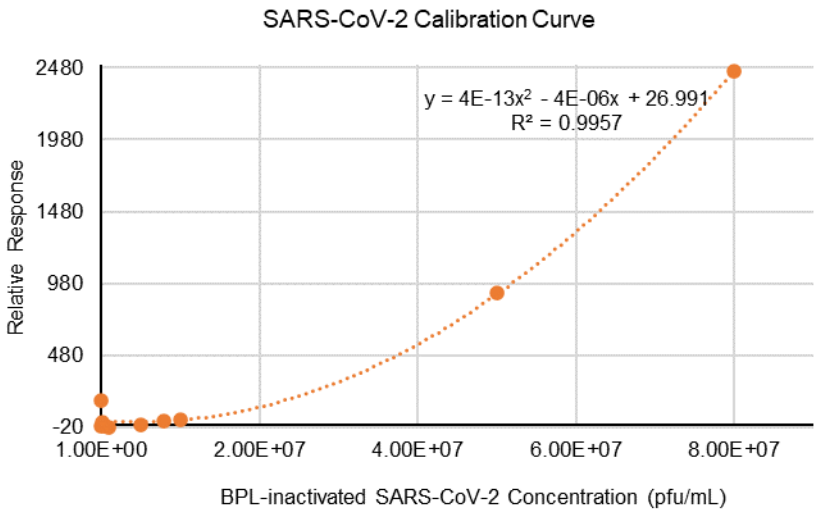

Figure 53. Inactivated SARS-CoV-2 calibration curve. Only concentrations from 10^7 to 10^8 pfu/mL yielded a detectable response on the SPR machine. The experimental samples' concentrations were below the limit of detection.

A.3 Waveguide interferometer sensor

We tested a third approach for inactivated SARS-CoV-2 quantification with Dr. Jie Xu and her team at GTRI, a waveguide interferometer sensor.

For the interferometer sensor experiments, we developed a calibration curve (Figure 54) from stock of BPL inactivated SARS-CoV-2. The concentration range tested was from $1x10^4$ pfu/mL to $5.5x10^6$ pfu/mL. The curve relates the sample concentrations to the phase angle change observed on the sensor; the higher the concentration, the higher the phase angle change. With the developed curve, the region for most reliable quantification appeared to be concentrations $1x10^5$ pfu/mL samples and above.

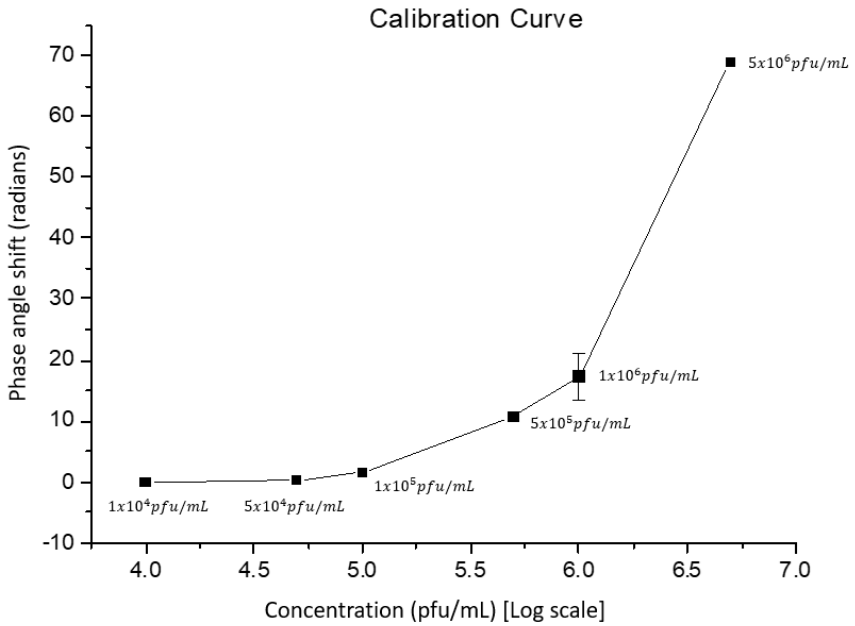

Figure 54. Calibration curve developed for the BPL inactivated SARS-CoV-2 virus. The point for the $5x10^5 pfu/mL$ concentration and the $1x10^6 pfu/mL$ concentration was an average of 2 and 3 data points, respectively with standard deviations of 0.68 and 3.65, respectively as well. All other points consist of one point, ad this is because there was a limitation in sample volume and accuracy of the sensor for those specific samples.

We tested an additional sample, one concentrated using an ultrafiltration procedure, a procedure not previously discussed. Briefly, ultrafiltration is another type of filtration method reliant on a membrane. Membranes come in different molecular weight cut-offs. For ultrafiltration, the specific membrane chosen needs to be smaller than the organism of interest in order for the membrane to capture it. We used the commercially available Amicon Ultra-30K device (Millipore Sigma) with a 30K molecular weight cut-off membrane contained inside 1.5-2 mL tubes suitable for microcentrifugation. The step-by-step process is shown below.

1. Insert the Amicon ultra device into the microcentrifuge tube and add 500 µL of the sample
2. Spin at 14,000 × g for 10 min in a microcentrifuge

3. Weigh and record the weight of each tube after the first spin time
4. Take the Amicon ultra device and place it upside down in a clean microcentrifuge tube (previously labeled)
5. Spin for 2 min at 1,000 × g to transfer the concentrated sample from the device to the tube
6. Weigh the post-spin 2 tube to determine the volume inside

*A spreadsheet calculator is used to record the weights and calculate the volumes using the density of water (1 g/mL).

The procedure took around 12 minutes to run not counting the manual time. With the manual time considered, the entire procedure can take aroun15-20 minutes depending on the number of samples being processed.

The samples prepared consisted of one run (due to limited stock) of an input of $1x10^6$ pfu/mL processed through our ultrafiltration procedure using a 10-minute initial spin time. This procedure concentrated the sample by approximately 18× where the concentration factor is calculated as the input volume (500 µl) over the output volume (27.6 µl in this specific sample).

The recovery of the virus from the output compared to the input sample was difficult to assess using the interferometer. The averaged phase angle change over two technical runs of the same input sample ($1x10^6$ pfu/mL) was approximately 7 radians. When observing the calibration curve, the approximate concentration for this input sample would then be a round $3x10^5$ pfu/mL, only 30% of $1x10^6$ pfu/mL. The output of the ultrafiltration procedure measured using the interferometer yielded a response, but inconclusive results given low concentrations. These low concentrations were caused by a dilution step required

post ultrafiltration to achieve the minimum volume required for the sensor to run (5mL). Furthermore, there were inadequate runs per sample done due to limited sample availability.

To use this method, we would have to generate a more robust standard curve since the limited data does suggest that moving forward, the waveguide interferometer could be a back-up plan. Yet, for it to be an efficient quantification method, we must, once again, operate with high concentrations of the inactivated SARS-CoV-2 virus. Aside from the need of high concentration samples, the method also provided unstable results due to variability in chips used, difficulty in consistency between sample, and long run time between samples. For these reasons, the technique was not pursued further.

A.4 Biotin quantitation kit

A final method tested involved the use of virus-sized biotinylated nanobeads as virus surrogate. We obtained biotin-conjugated nanobeads (100 nm, red fluorescent nanodiamond with biotin, Sigma) and a biotin quantification kit to enumerate the beads before and after filtration (Pierce Biotin Quantification Kit, ThermoFisher).

We firstly focused on characterizing and testing the kit to ensure its usability. Using a standard from the kit (biotinylated-Horseradish Peroxide (HRP)), we investigated the optimal concentration range of the assay while having its limit of detection of 2-2.5 nmol/L in mind. Due to the HABA/Avidin mechanism of the assay, the higher the amount of biotin present in the sample, the lower the absorbance value (500 nm) we should observe when the sample, placed in a 96-well, black plate with a flat bottom (Corning), is placed inside a plate reader for analysis. Figure 55 shows the results of the test where we performed 2-fold dilutions of the sample and tested each dilution in triplicates. In the graph, the absorbance

baseline, i.e., the assay reading with no HRP present in the sample, is included. Overall, the trend is as expected, with an increase in concentration, the absorbance reading decreased. The same trend was observed when reading the absorbance using spectrophotometry (results not shown).

Based on the limit of detection provided by the manufacturer (2-2.5 nmol/L) and the HRP stock concentration ($2.7x10^{-4}$ mol/L), we get a detection range of $2.5x10^{-6}$ – $2.7x10^{-4}$ mol/L that when using Avogrado's number to get an estimate of the particle count to volume concentration, we get that the range is $1.51x10^{15}$ – $1.63x10^{17}$ biotin/mL.

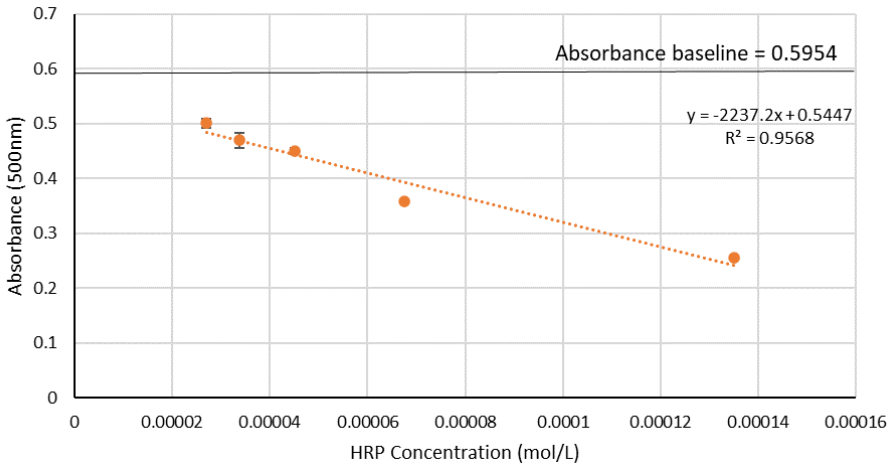

Figure 55. A standard curve was generated for HRP by performing two-fold dilutions from the stock solution. The absorbance baseline is the value for the well under no reaction. Absorbance readings obtained using a plate reader.

There were a series of constraints with the method. The first is that the kit allows you to calculate the number of biotins in a sample, and the number of biotins do not correlate 1:1 with the number of beads in the sample, which is the number we want to quantify. For this reason, an assumption would have to be made of a ratio of 1:200 of bead to biotin (per vendor recommendation). The second is that the bead material (diamonds) at the nanoscale

appears to have unpredictable properties that make them highly absorb light and fluoresce which could interfere with the assay reading [121]. The third constraint was, again, the tight detection range of the assay. Using the 1:200 assumption previously discussed with the starting concentration of the nanodiamond beads, $5.44x10^{11}$ beads/mL, we calculate a starting concentration of $1.09x10^{14}$ biotin/mL for the beads. This value falls outside the detection range for the assay. Thus, in order to use the beads, we would need to concentrate them prior to running any test which would further complicate the overall testing procedure. Thus, the method was no longer pursued.

Appendix B: Flow cytometer vs Fluorescent microscope comparison

As stated in earlier text, literature recalls that flow cytometry and fluorescent microscope yield similar results when used to quantify beads. Here, we looked to validate that was true for our flow cytometry and fluorescent microscope approach.

Beads were quantified for each method as previously discussed. To assess whether these methods were comparable, we tested how each method quantification method compared per bead size. The data analyzed came from the viral purification experiments in section 3.2. For each of the three runs (biological triplicates), the pre-purification samples were sampled for bead quantification both through flow cytometry and fluorescent microscopy, and a concentration was calculated. The results of these tests can be observed in Figure 56, where the dotted, black line is the concentration beads were approximately diluted down to.

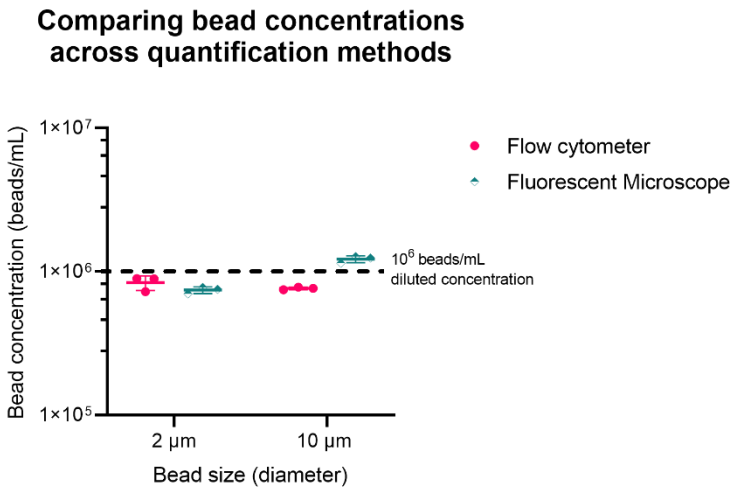

Figure 56. Per bead size, flow cytometer and fluorescent microscope concentration calculations for triplicate runs are shown, i.e., each run was analyzed for bead concentration using both methods. The dotted line represents the starting concentration beads had been approximately diluted to. Data comes from the viral purification experiments (section 3.2). Log10 y-axis.

Per bead size, the concentration values for each run and each method were checked for the assumption of normal distribution and homogeneity of variances. The 2 µm bead values did not meet the normal distribution assumption but did meet the homogeneity of variance assumption, therefore, a nonparametric, paired t-test, the Mann Whitney test, was conducted. Results yielded a non-significant test ($p = 0.275$), and therefore, the concentration values calculated per quantification method were comparable.

For the 10 µm bead, both assumptions previously stated were met, therefore, a paired t-test was performed. Results were significant ($p = 0.005$). However, though this is true, for the purification steps we are using, the 10 µm beads get eliminated since they are at least 2× larger than the filter pore size, therefore, the reading is often 0 concentration post-experiment for them. Thus, the starting concentration of the bead often doesn't matter for final recovery calculation.

The difference in the readings observed for the 10 µm bead could be due to inadequate mixing of the sample prior to bead fluorescent microscope quantification. Because these beads are larger, they tend to settle on the bottom of tubes. Therefore, they must be properly mixed to ensure they are monodispersed prior to taking a sample. For the 2 µm beads, which are never fully removed, we observed results are comparable per quantitation method. Therefore, we conclude the methods are comparable. Preferably, the flow cytometry data might be more reliable since it can quantify a larger volume of the sample and more accurately count the beads and distinguish between singlets and doublets present in the sample. Therefore, when possible, the flow cytometry data was used for bead recovery calculations.

Appendix C: Viral experiments data

C.1 Integrated system results

Table 4. The tables show the results of the system using the 0.45 µm pore size filter or the 5 µm pore size filters. Highlighted are the final volumes the samples were concentrated to for each run and the subsequent volume concentration factor determined by the input volume as compared to the post-filtration volume. The concentration factor based on the luminescence reading is also shown.

0.45 µm filter	Run 1	Run 2	Run 3
Input volume	5 mL	5 mL	5 mL
Number of presses through TFF device	8	10	14
Concentrated volume	515 µL	1.3 mL	1.18 mL
Volume concentration factor	9.7-fold	3.8-fold	4.2-fold
Luminescence concentration factor	1.7	1.5	1.6
5 µm filter	**Run 1**	**Run 2**	**Run 3**
Input volume	5 mL	5 mL	5 mL
Number of presses through TFF device	27	22	22
Concentrated volume	1.2 mL	900 µL	550 µL
Volume concentration factor	4.2-fold	5.6-fold	9-fold
Luminescence concentration factor	2	1.7	1.9

References

[1] "PCR Test for COVID-19: What It Is, How Its Done, What The Results Mean," *Cleveland Clinic*. https://my.clevelandclinic.org/health/diagnostics/21462-covid-19-and-pcr-testing (accessed Nov. 04, 2021).

[2] "COVID Live Update: 248,824,610 Cases and 5,037,026 Deaths from the Coronavirus - Worldometer." https://www.worldometers.info/coronavirus/ (accessed Nov. 04, 2021).

[3] CDC, "COVID-19 and Your Health," *Centers for Disease Control and Prevention*, Feb. 11, 2020. https://www.cdc.gov/coronavirus/2019-ncov/symptoms-testing/testing.html (accessed Nov. 04, 2021).

[4] R. Xu, B. Cui, X. Duan, P. Zhang, X. Zhou, and Q. Yuan, "Saliva: potential diagnostic value and transmission of 2019-nCoV," *Int. J. Oral Sci.*, vol. 12, no. 1, pp. 1–6, Apr. 2020, doi: 10.1038/s41368-020-0080-z.

[5] "Coronavirus disease (COVID-19) Pandemic — Emergency Use Listing Procedure (EUL) open for IVDs," *WHO - Prequalification of Medical Products (IVDs, Medicines, Vaccines and Immunization Devices, Vector Control)*, Oct. 05, 2020. https://extranet.who.int/pqweb/vitro-diagnostics/coronavirus-disease-covid-19-pandemic-%E2%80%94-emergency-use-listing-procedure-eul-open (accessed Nov. 04, 2021).

[6] O. of the Commissioner, "Coronavirus Disease 2019 Testing Basics," *FDA*, Sep. 2021, Accessed: Nov. 04, 2021. [Online]. Available: https://www.fda.gov/consumers/consumer-updates/coronavirus-disease-2019-testing-basics

[7] "Asymptomatic Surveillance Testing | Stamps Health Services | Georgia Tech | Atlanta, GA." https://health.gatech.edu/coronavirus/testing/surveillance (accessed Nov. 04, 2021).

[8] "How does the COVID-19 antigen test work? | MIT Medical." https://medical.mit.edu/covid-19-updates/2020/06/how-does-covid-19-antigen-test-work (accessed Nov. 04, 2021).

[9] Y. Wang, G. Xu, and Y.-W. Huang, "Modeling the load of SARS-CoV-2 virus in human expelled particles during coughing and speaking," *PloS One*, vol. 15, no. 10, p. e0241539, 2020, doi: 10.1371/journal.pone.0241539.

[10] "NUS, NTU scientists and doctors develop new way to detect COVID-19 viral RNA in the air," *CNA*. https://www.channelnewsasia.com/singapore/ntu-nus-detect-covid-19-viral-rna-air-2230126 (accessed Nov. 05, 2021).

[11] E. Anthes, "The Next Trick: Pulling Coronavirus Out of Thin Air," *The New York Times*, Mar. 24, 2021. Accessed: Nov. 04, 2021. [Online]. Available: https://www.nytimes.com/2021/03/24/health/coronavirus-testing-airborne-aerosol-indoor.html

[12] F. Shen *et al.*, "Integrating Silicon Nanowire Field Effect Transistor, Microfluidics and Air Sampling Techniques For Real-Time Monitoring Biological Aerosols," *Environ. Sci. Technol.*, vol. 45, no. 17, pp. 7473–7480, Sep. 2011, doi: 10.1021/es1043547.

[13] W. Jing *et al.*, "Microfluidic Device for Efficient Airborne Bacteria Capture and Enrichment," *Anal. Chem.*, vol. 85, no. 10, pp. 5255–5262, May 2013, doi: 10.1021/ac400590c.

[14] A. R. McFarland *et al.*, "Wetted Wall Cyclones for Bioaerosol Sampling," *Aerosol Sci. Technol.*, vol. 44, no. 4, pp. 241–252, Feb. 2010, doi: 10.1080/02786820903555552.

[15] "The BioWatch Program: Detection of Bioterrorism." https://sgp.fas.org/crs/terror/RL32152.html (accessed Nov. 04, 2021).

[16] J. F. Regan *et al.*, "Environmental Monitoring for Biological Threat Agents Using the Autonomous Pathogen Detection System with Multiplexed Polymerase Chain Reaction," *Anal. Chem.*, vol. 80, no. 19, pp. 7422–7429, Oct. 2008, doi: 10.1021/ac801125x.

[17] "The Next Generation of Sensor Technology for the BioWatch Program," *The Nuclear Threat Initiative*. https://www.nti.org/analysis/articles/sensor-technology-biowatch/ (accessed Nov. 04, 2021).

[18] "Research International, Inc. | CBRNe Identification Instruments." https://www.resrchintl.com/Identify.html (accessed Nov. 04, 2021).

[19] Y. Zhang, C. Xu, T. Guo, and L. Hong, "An automated bacterial concentration and recovery system for pre-enrichment required in rapid Escherichia coli detection," *Sci. Rep.*, vol. 8, no. 1, p. 17808, Dec. 2018, doi: 10.1038/s41598-018-35970-8.

[20] “Graphene Field Effect Transistors for Biological and Chemical Sensors.” https://www.sigmaaldrich.com/US/en/technical-documents/technical-article/materials-science-and-engineering/organic-electronics/graphene-field-effect-transistors (accessed Nov. 04, 2021).

[21] A. Purwidyantri *et al.*, “Sensing performance of fibronectin-functionalized Au-EGFET on the detection of S. epidermidis biofilm and 16S rRNA of infection-related bacteria in peritoneal dialysis,” *Sens. Actuators B Chem.*, vol. 217, pp. 92–99, Oct. 2015, doi: 10.1016/j.snb.2014.11.017.

[22] B. Thakur *et al.*, “Rapid detection of single E. coli bacteria using a graphene-based field-effect transistor device,” *Biosens. Bioelectron.*, vol. 110, pp. 16–22, Jul. 2018, doi: 10.1016/j.bios.2018.03.014.

[23] J. Chang *et al.*, “Ultrasonic-assisted self-assembly of monolayer graphene oxide for rapid detection of Escherichia coli bacteria,” *Nanoscale*, vol. 5, no. 9, p. 3620, 2013, doi: 10.1039/c3nr00141e.

[24] A. Béraud, M. Sauvage, C. M. Bazán, M. Tie, A. Bencherif, and D. Bouilly, “Graphene field-effect transistors as bioanalytical sensors: design, operation and performance,” *Analyst*, vol. 146, no. 2, pp. 403–428, 2021, doi: 10.1039/D0AN01661F.

[25] “Field-effect transistor,” *Wikipedia*. Oct. 06, 2021. Accessed: Nov. 04, 2021. [Online]. Available: https://en.wikipedia.org/w/index.php?title=Field-effect_transistor&oldid=1048502323

[26] N. Formisano *et al.*, “Inexpensive and fast pathogenic bacteria screening using field-effect transistors,” *Biosens. Bioelectron.*, vol. 85, pp. 103–109, Nov. 2016, doi: 10.1016/j.bios.2016.04.063.

[27] A. Tarasov *et al.*, “A potentiometric biosensor for rapid on-site disease diagnostics,” *Biosens. Bioelectron.*, vol. 79, pp. 669–678, May 2016, doi: 10.1016/j.bios.2015.12.086.

[28] S. A. Walper *et al.*, “Detecting Biothreat Agents: From Current Diagnostics to Developing Sensor Technologies,” *ACS Sens.*, vol. 3, no. 10, pp. 1894–2024, Oct. 2018, doi: 10.1021/acssensors.8b00420.

[29] “Saliva,” *Wikipedia*. Oct. 13, 2021. Accessed: Nov. 04, 2021. [Online]. Available: https://en.wikipedia.org/w/index.php?title=Saliva&oldid=1049755622

[30] S. P. Humphrey and R. T. Williamson, “A review of saliva: Normal composition, flow, and function,” *J. Prosthet. Dent.*, vol. 85, no. 2, pp. 162–169, Feb. 2001, doi: 10.1067/mpr.2001.113778.

[31] C. Theda, S. H. Hwang, A. Czajko, Y. J. Loke, P. Leong, and J. M. Craig, “Quantitation of the cellular content of saliva and buccal swab samples,” *Sci. Rep.*, vol. 8, no. 1, p. 6944, May 2018, doi: 10.1038/s41598-018-25311-0.

[32] E. Kaufman and I. B. Lamster, “The Diagnostic Applications of Saliva— A Review,” *Crit. Rev. Oral Biol. Med.*, vol. 13, no. 2, pp. 197–212, Mar. 2002, doi: 10.1177/154411130201300209.

[33] S. Paxton, M. Peckham, and A. Knibbs, “The Leeds Histology Guide,” 2003, Accessed: Nov. 04, 2021. [Online]. Available: https://www.histology.leeds.ac.uk/blood/blood_wbc.php

[34] M. Romeo, B. Mohlenhoff, M. Jennings, and M. Diem, “Infrared micro-spectroscopic studies of epithelial cells,” *Biochim. Biophys. Acta BBA - Biomembr.*, vol. 1758, no. 7, pp. 915–922, Jul. 2006, doi: 10.1016/j.bbamem.2006.05.010.

[35] M.-F. D. Hoebler A. Karinthi, C. Belleville, J. L. Barry, C., “Particle size of solid food after human mastication and in vitro simulation of oral breakdown,” *Int. J. Food Sci. Nutr.*, vol. 51, no. 5, pp. 353–366, Jan. 2000, doi: 10.1080/096374800426948.

[36] O. US EPA, “Particulate Matter (PM) Basics,” Apr. 19, 2016. https://www.epa.gov/pm-pollution/particulate-matter-pm-basics (accessed Nov. 04, 2021).

[37] “How to Understand Particle Size and Distribution for Cleaner Air - Oransi.” https://oransi.com/blogs/blog/particle-size (accessed Nov. 04, 2021).

[38] “Particulates,” *Wikipedia*. Oct. 09, 2021. Accessed: Nov. 04, 2021. [Online]. Available: https://en.wikipedia.org/w/index.php?title=Particulates&oldid=1049005093; CC-BY SA 3.0

[39] X. Niu, B. Guinot, J. Cao, H. Xu, and J. Sun, “Particle size distribution and air pollution patterns in three urban environments in Xi’an, China,” *Environ. Geochem. Health*, vol. 37, no. 5, pp. 801–812, Oct. 2015, doi: 10.1007/s10653-014-9661-0.

[40] L. M. Kurth, M. McCawley, M. Hendryx, and S. Lusk, “Atmospheric particulate matter size distribution and concentration in West Virginia coal mining and non-mining areas,” *J. Expo. Sci. Environ. Epidemiol.*, vol. 24, no. 4, pp. 405–411, Jul. 2014, doi: 10.1038/jes.2014.2.

[41] J. H. Seinfeld and S. N. Pandis, *Atmospheric Chemistry and Physics: From Air Pollution to Climate Change*. John Wiley & Sons, 2016.

[42] J. J. Ezenarro, J. Mas, X. Muñoz-Berbel, and N. Uria, “Advances in bacterial concentration methods and their integration in portable detection platforms: A review,” *Anal. Chim. Acta*, p. 339079, Sep. 2021, doi: 10.1016/j.aca.2021.339079.

[43] K. A. Stevens and L.-A. Jaykus, “Bacterial Separation and Concentration from Complex Sample Matrices: A Review,” *Crit. Rev. Microbiol.*, vol. 30, no. 1, pp. 7–24, Jan. 2004, doi: 10.1080/10408410490266410.

[44] “What is Anthrax? | CDC,” Nov. 19, 2020. https://www.cdc.gov/anthrax/basics/index.html (accessed Nov. 04, 2021).

[45] R. C. Spencer, “Bacillus anthracis,” *J. Clin. Pathol.*, vol. 56, no. 3, pp. 182–187, Mar. 2003.

[46] B. Rathish, R. Pillay, A. Wilson, and V. V. Pillay, “Comprehensive Review Of Bioterrorism,” *StatPearls*, Apr. 2021, Accessed: Sep. 14, 2021. [Online]. Available: https://www.statpearls.com/articlelibrary/viewarticle/131243

[47] N. R. C. (US) S. G. for the W. on S. L. of V. S. Microorganisms, *Correlates of Smallest Sizes for Microorganisms*. National Academies Press (US), 1999. Accessed: Nov. 04, 2021. [Online]. Available: https://www.ncbi.nlm.nih.gov/books/NBK224751/

[48] “E. coli (Escherichia coli) | E. coli | CDC,” Sep. 15, 2021. https://www.cdc.gov/ecoli/index.html (accessed Nov. 04, 2021).

[49] J. Chang *et al.*, “Ultrasonic-assisted self-assembly of monolayer graphene oxide for rapid detection of Escherichia coli bacteria,” *Nanoscale*, vol. 5, no. 9, pp. 3620–3626, 2013, doi: 10.1039/C3NR00141E.

[50] J. Vajda, D. Weber, D. Brekel, B. Hundt, and E. Müller, “Size distribution analysis of influenza virus particles using size exclusion chromatography,” *J. Chromatogr. A*, vol. 1465, pp. 117–125, Sep. 2016, doi: 10.1016/j.chroma.2016.08.056.

[51] “Difference Between Separation and Purification | Compare the Difference Between Similar Terms.” https://www.differencebetween.com/difference-between-separation-and-purification/ (accessed Nov. 04, 2021).

[52] “Purify Definition & Meaning | Dictionary.com.” https://www.dictionary.com/browse/purification (accessed Nov. 04, 2021).

[53] “Isolation, separation and purification - Latest research and news | Nature.” https://www.nature.com/subjects/isolation-separation-purification (accessed Nov. 04, 2021).

[54] “List of purification methods in chemistry,” *Wikipedia*. Jun. 18, 2020. Accessed: Nov. 04, 2021. [Online]. Available: https://en.wikipedia.org/w/index.php?title=List_of_purification_methods_in_chemistry&oldid=963137992

[55] “Concentration,” *Wikipedia*. Aug. 01, 2021. Accessed: Nov. 04, 2021. [Online]. Available: https://en.wikipedia.org/w/index.php?title=Concentration&oldid=1036623825

[56] “Food Pathogen Concentration Techniques.” https://www.rapidmicrobiology.com/test-method/separation-and-concentration-of-microorganisms-from-food-matrices (accessed Nov. 04, 2021).

[57] “7.6: Classifying Separation Techniques - Chemistry LibreTexts.” https://chem.libretexts.org/Bookshelves/Analytical_Chemistry/Analytical_Chemistry_2.1_(Harvey)/07%3A_Obtaining_and_Preparing_Samples_for_Analysis/7.06%3A_Classifying_Separation_Techniques (accessed Nov. 04, 2021).

[58] R. A. Killington, A. Stokes, and J. C. Hierholzer, “4 - Virus purification,” in *Virology Methods Manual*, B. W. Mahy and H. O. Kangro, Eds. London: Academic Press, 1996, pp. 71–89. doi: 10.1016/B978-012465330-6/50005-1.

[59] R. J. Hall *et al.*, “Evaluation of rapid and simple techniques for the enrichment of viruses prior to metagenomic virus discovery,” *J. Virol. Methods*, vol. 195, pp. 194–204, Jan. 2014, doi: 10.1016/j.jviromet.2013.08.035.

[60] K. Vijayaragavan, “Virus purification, detection and removal,” *Diss. Masters Theses Masters Rep. - Open*, Jan. 2014, doi: 10.37099/mtu.dc.etds/850.

[61] “Centrifugation,” *Wikipedia*. Oct. 10, 2021. Accessed: Nov. 04, 2021. [Online]. Available: https://en.wikipedia.org/w/index.php?title=Centrifugation&oldid=1049213069

[62] J. Y. Park *et al.*, “Detection of E. coli O157:H7 in Food Using Automated Immunomagnetic Separation Combined with Real-Time PCR,” *Processes*, vol. 8, no. 8, Art. no. 8, Aug. 2020, doi: 10.3390/pr8080908.

[63] W. Yang, A. Z. Gu, S. Zeng, D. Li, M. He, and H. Shi, “Development of a combined immunomagnetic separation and quantitative reverse transcription-PCR assay for sensitive detection of infectious rotavirus in water samples,” *J. Microbiol. Methods*, vol. 84, no. 3, pp. 447–453, Mar. 2011, doi: 10.1016/j.mimet.2011.01.011.

[64] World Health Organization, *Guidelines for drinking-water quality: fourth edition incorporating first addendum*, 4th ed + 1st add. Geneva: World Health Organization, 2017. Accessed: Nov. 04, 2021. [Online]. Available: https://apps.who.int/iris/handle/10665/254637

[65] “Chapter 2 - WATER QUALITY MONITORING, STANDARDS AND TREATMENT.” https://www.fao.org/3/x5624e/x5624e05.htm (accessed Nov. 04, 2021).

[66] X. Li *et al.*, “Rapid Sample Processing for Detection of Food-Borne Pathogens via Cross-Flow Microfiltration,” *Appl. Environ. Microbiol.*, vol. 79, no. 22, pp. 7048–7054, Nov. 2013, doi: 10.1128/AEM.02587-13.

[67] GEA Process Engineering, “Membrane Filtration in the Dairy Industry.” https://www.lenntech.com/Data-sheets/GE-Osmonics-membrane-filtration-dairy-industry-L.pdf

[68] M. Antfolk, P. B. Muller, P. Augustsson, H. Bruus, and T. Laurell, “Focusing of sub-micrometer particles and bacteria enabled by two-dimensional acoustophoresis,” *Lab. Chip*, vol. 14, no. 15, pp. 2791–2799, 2014, doi: 10.1039/C4LC00202D.

[69] N. Tottori and T. Nisisako, “Editorial for the Special Issue on Particles Separation in Microfluidic Devices,” *Micromachines*, vol. 11, no. 6, Art. no. 6, Jun. 2020, doi: 10.3390/mi11060602.

[70] R. Nasiri *et al.*, "Microfluidic-Based Approaches in Targeted Cell/Particle Separation Based on Physical Properties: Fundamentals and Applications," *Small*, vol. 16, no. 29, p. 2000171, 2020, doi: 10.1002/smll.202000171.

[71] C. Chiam and R. Sarbatly, "Purification of Aquacultural Water: Conventional and New Membrane-based Techniques," *Sep. Purif. Rev.*, vol. 40, no. 2, pp. 126–160, Feb. 2011, doi: 10.1080/15422119.2010.549766.

[72] C. Charcosset, "3 - Microfiltration," in *Membrane Processes in Biotechnology and Pharmaceutics*, C. Charcosset, Ed. Amsterdam: Elsevier, 2012, pp. 101–141. doi: 10.1016/B978-0-444-56334-7.00003-4.

[73] P. Pal, "Chapter 2 - Introduction to membrane-based technology applications," in *Membrane-Based Technologies for Environmental Pollution Control*, P. Pal, Ed. Butterworth-Heinemann, 2020, pp. 71–100. doi: 10.1016/B978-0-12-819455-3.00002-9.

[74] R. W. Baker, *Membrane technology and applications*, 2nd ed. Chichester ; New York: J. Wiley, 2004.

[75] D. W. Green and R. H. Perry, *Perry's Chemical Engineers' Handbook, Eighth Edition*. McGraw-Hill Education, 2008. Accessed: Nov. 04, 2021. [Online]. Available: https://www.accessengineeringlibrary.com/content/book/9780071422949

[76] J. Smith, J. George, T. Nadler, and V. Joshi, "Filters in Dissolution Testing: Evaluation and Selection," *Dissolution Technol.*, vol. 27, no. 4, pp. 6–13, 2020, doi: 10.14227/DT270420P6.

[77] "Syringe Filters for Cell Culture," *Support*, Nov. 14, 2017. https://scientificfilters.com/syringe-filters-cell-culture/ (accessed Nov. 04, 2021).

[78] "Low Cost Polypropylene Membrane Filters - Samples Available- Ships Next Day, Material: Polypropylene," *Tisch Scientific*. https://scientificfilters.com/membrane-filters/polypropylene_ (accessed Nov. 04, 2021).

[79] "Filtration Media Selection Guide," *Support*, Mar. 22, 2016. https://scientificfilters.com/filter-media-selector/ (accessed Nov. 04, 2021).

[80] D. Ariono and A. K. Wardani, “Modification and Applications of Hydrophilic Polypropylene Membrane,” *IOP Conf. Ser.: Mater. Sci. Eng.*, vol. 214, p. 012014, Jul. 2017, doi: 10.1088/1757-899X/214/1/012014.

[81] “How to Select a Syringe Filter and How to Use it? (2020 Guide).” https://airekacells.com/blog/syringe-filter (accessed Nov. 04, 2021).

[82] “Syringe Filters for Aqueous Solutions,” *Support*, Nov. 14, 2017. https://scientificfilters.com/syringe-filters-aqueous-solutions/ (accessed Nov. 05, 2021).

[83] Interchim Innovation, “KrosFlo Hollow Fibers Ultra/Filtration Modules.” [Online]. Available: https://www.interchim.fr/ft/K/KROFIL.pdf

[84] A. C. Enten, M. P. I. Leipner, M. C. Bellavia, L. E. King, and T. A. Sulchek, “Optimizing Flux Capacity of Dead-end Filtration Membranes by Controlling Flow with Pulse Width Modulated Periodic Backflush,” *Sci. Rep.*, vol. 10, no. 1, p. 896, Jan. 2020, doi: 10.1038/s41598-020-57649-9.

[85] P. Zhang, A. M. Kaushik, K. E. Mach, K. Hsieh, J. C. Liao, and T.-H. Wang, “Facile syringe filter-enabled bacteria separation, enrichment, and buffer exchange for clinical isolation-free digital detection and characterization of bacterial pathogens in urine,” *Analyst*, vol. 146, no. 8, pp. 2475–2483, Apr. 2021, doi: 10.1039/D1AN00039J.

[86] S. Isabel *et al.*, “Rapid Filtration Separation-Based Sample Preparation Method for Bacillus Spores in Powdery and Environmental Matrices,” *Appl. Environ. Microbiol.*, vol. 78, no. 5, pp. 1505–1512, Mar. 2012, doi: 10.1128/AEM.06696-11.

[87] Andy Connelly, “Understanding syringe filters,” *Andy Connelly*, Sep. 28, 2016. https://andyjconnelly.wordpress.com/2016/09/28/syringe-filters/ (accessed Nov. 04, 2021).

[88] Corning, “Corning Filtration Guide.” https://www.corning.com/catalog/cls/documents/selection-guides/t_filterselectionguide.pdf;

[89] “Millex-GV Filter, 0.22 µm | SLGVV255F.” https://www.emdmillipore.com/US/en/product/Millex-GV-Filter-0.22m,MM_NF-SLGVV255F (accessed Nov. 05, 2021).

[90] L. Cai, Y. Yang, N. Jiao, and R. Zhang, “Evaluation of Tangential Flow Filtration for the Concentration and Separation of Bacteria and Viruses in Contrasting Marine Environments,” *PLOS ONE*, vol. 10, no. 8, p. e0136741, Aug. 2015, doi: 10.1371/journal.pone.0136741.

[91] Larry Schwartz and Kevin Seeley, “Introduction to Tangential Flow Filtration for Laboratory and Process Development Applications.” Pall Corporation. [Online]. Available: https://www.pall.com/content/dam/pall/laboratory/obsolete-marketing/previous-pall-page/Introduction%20to%20Tangential%20Flow%20Filtration%20for%20Laboratory%20and%20Process%20Development%20Applications%20.pdf

[92] “Thermo Scientific Fluoro-Max Dyed Blue Aqueous Fluorescent Particles - Cell Analysis Products, Microspheres.” https://www.fishersci.com/shop/products/fluoro-max-dyed-blue-aqueous-fluorescent-particles/09980508 (accessed Nov. 05, 2021).

[93] “Particles for Filter and Membrane Challenge Testing | Bangs Laboratories, Inc.” https://www.bangslabs.com/particles-filter-and-membrane-challenge-testing (accessed Nov. 05, 2021).

[94] D. Spettmann, S. Eppmann, H.-C. Flemming, and J. Wingender, “Simultaneous visualisation of biofouling, organic and inorganic particle fouling on separation membranes,” *Water Sci. Technol.*, vol. 55, no. 8–9, pp. 207–210, Apr. 2007, doi: 10.2166/wst.2007.260.

[95] T. Y. Ling, J. Wang, and D. Y. H. Pui, “Measurement of filtration efficiency of Nuclepore filters challenged with polystyrene latex nanoparticles: experiments and modeling,” *J. Nanoparticle Res.*, vol. 13, no. 10, p. 5415, Aug. 2011, doi: 10.1007/s11051-011-0529-2.

[96] Tania Nolan, Jim Huggett, and Elena Sanchez, “Good practice guide for the application of quantitative PCR (qPCR) First Edition 2013.” National Measurement System.

[97] K. Mullis, F. Faloona, S. Scharf, R. Saiki, G. Horn, and H. Erlich, “Specific Enzymatic Amplification of DNA In Vitro: The Polymerase Chain Reaction,” *Cold Spring Harb. Symp. Quant. Biol.*, vol. 51, pp. 263–273, Jan. 1986, doi: 10.1101/SQB.1986.051.01.032.

[98] Bio-Rad Laboratories, “Real Time PCR Applications Guide.” [Online]. Available: https://www.bio-rad.com/webroot/web/pdf/lsr/literature/Bulletin_5279.pdf

[99] F. Watzinger, K. Ebner, and T. Lion, “Detection and monitoring of virus infections by real-time PCR,” *Mol. Aspects Med.*, vol. 27, no. 2, pp. 254–298, Apr. 2006, doi: 10.1016/j.mam.2005.12.001.

[100] K. Greisen, M. Loeffelholz, A. Purohit, and D. Leong, “PCR primers and probes for the 16S rRNA gene of most species of pathogenic bacteria, including bacteria found in cerebrospinal fluid,” *J. Clin. Microbiol.*, vol. 32, no. 2, pp. 335–351, Feb. 1994, doi: 10.1128/jcm.32.2.335-351.1994.

[101] X.-S. Wang *et al.*, “Quantitively Analyzing the Variation of Micrometer-Sized Microplastic during Water Treatment with the Flow Cytometry-Fluorescent Beads Method,” *ACS EST Eng.*, Oct. 2021, doi: 10.1021/acsestengg.1c00253.

[102] K. M. McKinnon, “Flow Cytometry: An Overview,” *Curr. Protoc. Immunol.*, vol. 120, no. 1, Jan. 2018, doi: 10.1002/cpim.40.

[103] M. J. Sanderson, I. Smith, I. Parker, and M. D. Bootman, “Fluorescence Microscopy,” *Cold Spring Harb. Protoc.*, vol. 2014, no. 10, p. pdb.top071795-pdb.top071795, Oct. 2014, doi: 10.1101/pdb.top071795.

[104] “Introduction to Fluorescence Microscopy,” *Nikon’s MicroscopyU*. https://www.microscopyu.com/techniques/fluorescence/introduction-to-fluorescence-microscopy (accessed Nov. 05, 2021).

[105] S. G. Knoll, M. Y. Ali, and M. T. A. Saif, “A Novel Method for Localizing Reporter Fluorescent Beads Near the Cell Culture Surface for Traction Force Microscopy,” *JoVE J. Vis. Exp.*, no. 91, p. e51873, Sep. 2014, doi: 10.3791/51873.

[106] L. J. Hawkins and K. B. Storey, “Improved high-throughput quantification of luminescent microplate assays using a common Western-blot imaging system,” *MethodsX*, vol. 4, pp. 413–422, Oct. 2017, doi: 10.1016/j.mex.2017.10.006.

[107] T. Azad, A. Tashakor, and S. Hosseinkhani, “Split-luciferase complementary assay: applications, recent developments, and future perspectives,” *Anal. Bioanal. Chem.*, vol. 406, no. 23, pp. 5541–5560, Sep. 2014, doi: 10.1007/s00216-014-7980-8.

[108] A. L. Kyriakides and P. D. Patel, “Luminescence techniques for microbiological analysis of foods,” in *Rapid Analysis Techniques in Food Microbiology*, P. D. Patel, Ed. Boston, MA: Springer US, 1995, pp. 196–231. doi: 10.1007/978-1-4615-2662-9_7.

[109] "Overview of ELISA - US." //www.thermofisher.com/us/en/home/life-science/protein-biology/protein-biology-learning-center/protein-biology-resource-library/pierce-protein-methods/overview-elisa.html (accessed Nov. 05, 2021).

[110] R. B. M. Schasfoort, "Chapter 1. Introduction to Surface Plasmon Resonance," in *Handbook of Surface Plasmon Resonance*, 2nd ed., R. B. M. Schasfoort, Ed. Cambridge: Royal Society of Chemistry, 2017, pp. 1–26. doi: 10.1039/9781788010283-00001.

[111] M. Hiltunen *et al.*, "Polymeric slot waveguide interferometer for sensor applications," *Opt. Express*, vol. 22, no. 6, pp. 7229–7237, Mar. 2014, doi: 10.1364/OE.22.007229.

[112] "Pierce™ Biotin Quantitation Kit." https://www.thermofisher.com/order/catalog/product/28005 (accessed Nov. 05, 2021).

[113] X. W. Huijsdens, R. K. Linskens, M. Mak, S. G. M. Meuwissen, C. M. J. E. Vandenbroucke-Grauls, and P. H. M. Savelkoul, "Quantification of Bacteria Adherent to Gastrointestinal Mucosa by Real-Time PCR," *J. Clin. Microbiol.*, vol. 40, no. 12, pp. 4423–4427, Dec. 2002, doi: 10.1128/JCM.40.12.4423-4427.2002.

[114] M. Smati *et al.*, "Real-Time PCR for Quantitative Analysis of Human Commensal Escherichia coli Populations Reveals a High Frequency of Subdominant Phylogroups," *Appl. Environ. Microbiol.*, vol. 79, no. 16, pp. 5005–5012, Aug. 2013, doi: 10.1128/AEM.01423-13.

[115] J. L. Love, P. Scholes, B. Gilpin, M. Savill, S. Lin, and L. Samuel, "Evaluation of uncertainty in quantitative real-time PCR," *J. Microbiol. Methods*, vol. 67, no. 2, pp. 349–356, Nov. 2006, doi: 10.1016/j.mimet.2006.04.005.

[116] "triton-x-100-sigma.pdf." Accessed: Nov. 18, 2021. [Online]. Available: https://www.snowpure.com/docs/triton-x-100-sigma.pdf

[117] P. A. Dunn and H. W. Tyrer, "Quantitation of neutrophil phagocytosis, using fluorescent latex beads: Correlation of microscopy and flow cytometry," *J. Lab. Clin. Med.*, vol. 98, no. 3, pp. 374–381, Sep. 1981, doi: 10.5555/uri:pii:0022214381900433.

[118] A. B. Shapiro, G. K. Walkup, and T. A. Keating, “Correction for Interference by Test Samples in High-Throughput Assays,” *J. Biomol. Screen.*, vol. 14, no. 8, pp. 1008–1016, Sep. 2009, doi: 10.1177/1087057109341768.

[119] “Catalog2021.pdf.” Accessed: Nov. 17, 2021. [Online]. Available: https://www.hansabiomed.eu/shop/image/catalog/Catalog2021/Catalog2021.pdf

[120] T. H. Phan *et al.*, “New Multiscale Characterization Methodology for Effective Determination of Isolation–Structure–Function Relationship of Extracellular Vesicles,” *Front. Bioeng. Biotechnol.*, vol. 9, p. 358, 2021, doi: 10.3389/fbioe.2021.669537.

[121] L. O. Usoltseva, D. S. Volkov, D. A. Nedosekin, M. V. Korobov, M. A. Proskurnin, and V. P. Zharov, “Absorption spectra of nanodiamond aqueous dispersions by optical absorption and optoacoustic spectroscopies,” *Photoacoustics*, vol. 12, pp. 55–66, Dec. 2018, doi: 10.1016/j.pacs.2018.10.003.